1-1-2014

Modeling Breast Cancer Dormancy and Recurrence Following Oncogenic Pathway Inhibition

Jason Robert Ruth
University of Pennsylvania, jasonrruth@gmail.com

Modeling Breast Cancer Dormancy and Recurrence Following Oncogenic Pathway Inhibition

Abstract
Breast cancer recurrence is the primary cause of mortality in breast cancer, and although advances have been made in the treatment of primary breast cancer, recurrent breast cancer remains uncurable. Targeted therapy has had a major impact on survival across multiple cancer types, including breast cancer, however patients who respond to targeted therapy ultimately relapse. Residual disease, the tumor cells that survive initial therapy, represent an attractive therapeutic target, however little is known about the biology of these cells. We use mouse models of breast cancer to investigate the phenotype of residual disease that survives targeted therapy, and to explore approaches to inhibit tumor recurrence. Residual disease exhibits cellular dormancy in models driven by distinct oncogenic pathways. Gene expression profiling reveals that residual tumor cells are enriched for a phenotype associated with normal and neoplastic stem-like cells, but are not enriched for tumor initiative cells. Interventions that inhibit inflammatory signaling inhibit tumor recurrence, however increasing inflammation promotes tumor recurrence. Inflammatory macrophages may be leukocytes that promote inflammation and drive recurrence in these models. Together, our findings present a more comprehensive picture of residual tumor cells surviving targeted therapy, and suggest possible therapeutic strategies for targeting residual disease that gives rise to cancer recurrence.

Degree Type
Dissertation

Degree Name
Doctor of Philosophy (PhD)

Graduate Group
Bioengineering

First Advisor
Lewis A. Chodosh

Second Advisor
Andrew Tsourkas

Keywords
Cancer, Immunology, Model, Mouse, Recurrence, Resistance

Subject Categories
Biology | Biomedical | Oncology

MODELING BREAST CANCER DORMANCY AND RECURRENCE

FOLLOWING ONCOGENIC PATHWAY INHIBITION

Jason R. Ruth

A DISSERTATION

in

Bioengineering

Presented to the Faculties of the University of Pennsylvania

in

Partial Fulfillment of the Requirements for the

Degree of Doctor of Philosophy

2014

Supervisor of Dissertation

_____

Lewis A. Chodosh, MD., PhD.

Professor of Cancer Biology

Graduate Group Chairperson

_____

Jason Burdick, PhD., Professor of Bioengineering

Dissertation Committee

Andrew Tsourkas, PhD., Associate Professor of Bioengineering (Committee Chair)

Robert H. Vonderheide, MD., DPhil., Professor of Medicine

Warren S. Pear, MD., PhD., Professor of Pathology and Laboratory Medicine

MODELING BREAST CANCER DORMANCY AND RECURRENCE FOLLOWING ONCOGENIC PATHWAY INHIBITION

This work is dedicated to cancer patients,

the friends and family members who love them,

and the health care professionals that care for them.

ACKNOWLEDGMENT

This dissertation ultimately reflects the outstanding opportunities that I've been given, and the countless hours of help I've received from mentors and loved ones. By their example, I strive to live a life where I am similarly able to help others, with the ultimate goal of using our collective resources and abilities to improve the lives of future generations. We plant trees so that our children will have shade.

Thank you to my fiancé Tanya Keenan, who has been an immutable light for me throughout graduate school. She is my greatest love, my inspiration, and my steadfast partner in life.

Thank you to my family, particularly my parents, sister, and grandfather 'Grampee.' I am grateful to my mother for her unending kindness, and for the deep value that she places on education. I am grateful to my father for the example of his passion, and his sense of humor. Together, my parents provided me with everything I needed to succeed. Along with my parents, my maternal grandfather inculcated me with the key values that drive my major decisions, and their steadfast love and support have allowed me to overcome all of the obstacles that I have faced. Similarly, my sister's unwavering support, creative and adventurous spirit, and constant love have given my life a harmonic resonance that keeps me grounded in the important things.

Thank you to my mentors, Brian Crawford, Bruce Tromberg, and especially Lewis Chodosh. I have always admired Lewis' spirit, determination, and particularly his zeal for good science. It was a great honor to train in his lab for my PhD, and I will always keep close the lessons that he taught me.

ABSTRACT

MODELING BREAST CANCER DORMANCY AND RECURRENCE FOLLOWING ONCOGENIC PATHWAY INHIBITION

Jason R. Ruth

Lewis A. Chodosh, MD, PhD

Breast cancer recurrence is the primary cause of mortality in breast cancer, and although advances have been made in the treatment of primary breast cancer, recurrent breast cancer remains uncurable. Targeted therapy has had a major impact on survival across multiple cancer types, including breast cancer, however patients who respond to targeted therapy ultimately relapse. Residual disease, the tumor cells that survive initial therapy, represent an attractive therapeutic target, however little is known about the biology of these cells. We use mouse models of breast cancer to investigate the phenotype of residual disease that survives targeted therapy, and to explore approaches to inhibit tumor recurrence. Residual disease exhibits cellular dormancy in models driven by distinct oncogenic pathways. Gene expression profiling reveals that residual tumor cells are enriched for a phenotype associated with normal and neoplastic stem-like cells, but are not enriched for tumor initiative cells. Interventions that inhibit inflammatory signaling inhibit tumor recurrence, however increasing inflammation promotes tumor recurrence. Inflammatory macrophages may be leukocytes that promote inflammation and drive recurrence in these models. Together, our findings present a more comprehensive picture of residual tumor cells surviving targeted therapy, and suggest possible therapeutic strategies for targeting residual disease that gives rise to cancer recurrence.

TABLE OF CONTENTS

LIST OF TABLES

LIST OF ILLUSTRATIONS

CHAPTER 1

Breast Cancer Dormancy and Recurrence Following Oncogenic Pathway Inhibition

Breast cancer

Breast cancer is the most prevalent cancer among women worldwide [1]. Almost 40,000 women in the United States will succumb to this disease in 2013, and it is the second most frequent cause of cancer-related deaths among women in the developed world [1, 2]. Improvements in diagnosis and treatment of breast cancer have led to a dramatic increase in the survival of breast cancer patients since the 1970s [2], however these gains have primarily come from successful resection of early stage breast cancers that have not spread [3]. As a result of improved treatment of early breast cancer, nearly three million women in the United States are breast cancer survivors, and these women are at risk of breast cancer recurrence [4]. In contrast to primary breast cancer, recurrent breast cancer is incurable, and consequently represents the primary cause of mortality among breast cancer patients.

A broad understanding of breast cancer can be achieved by identifying epidemiological and clinical parameters that impact incidence and survival. Disease incidence and outcome are each functions of a large number of parameters. Various epidemiological factors impact both breast cancer risk and clinical prognosis, including sex, age, and genetic background, among many others [2, 5-8]. Females have a greater than 100-fold higher risk of developing breast cancer than men [5]. Age also has a major impact, as the probability of developing breast cancer before the age of 40 years old is almost one eighth of the risk of developing breast cancer between the ages 60-69 years old [2]. Genetic background may impact breast cancer risk as the combination of many germline variations with a small impact on cancer incidence [9], or the presence of germline mutations that confer a major increase in the risk of developing breast cancer, such as mutations in *BRCA1* or *BRCA2* [10].

Additionally, certain clinical, histopathological, and molecular qualities of the cancer itself are major determinants of a patient's prognosis. For example, tumor grade is a number given by a pathologist analyzing a hematoxylin and eosin-stained section, which incorporates tubule formation, nuclear grade, and mitotic rate, in order to provide prognostic information about a patients' particular tumor [11]. Tumor stage is determined by the TNM staging system, wherein tumor size and local invasion (T), lymph node involvement (N), and presence of metastatic disease (M) are synthesized to evaluate tumor stage [12]. Higher tumor grade or tumor stage are each associated with a poor prognosis. Both grade and stage are critical components to determining the proper clinical management for a particular breast cancer patient.

Beyond the use of epidemiological and clinical parameters, stratifying breast cancer by its molecular etiology provides an indispensable approach for understanding and treating this malignancy. Like all cancers, breast cancer is driven by alterations in several key cellular processes, resulting from genomic alterations that activate oncogenic pathways driving tumorigenesis [13]. Whereas qualities such as tumor size and extent of dissemination are determined largely by the length of time a tumor has developed within a patient prior to presentation, tumor subtypes largely reflect the oncogenic pathways driving the tumor. One can broadly define breast cancer using either histopathological subtypes, molecular subtypes defined through gene expression profiling, or genomic subtypes using genomic mutation data.

Histopathological subtype is broadly defined by expression of the hormone receptors estrogen receptor (ER) and progesterone receptor (PR), and expression of the human epidermal growth factor receptor 2 (HER2). Using expression of these receptors, breast cancer can be classified into three major types, hormone receptor positive, HER2 positive, or triple negative breast cancer (TNBC), wherein a tumor does not express sufficient levels of either hormone receptor or HER2 in order to qualify as one of those subtypes. Targeted therapy against hormone receptor positive tumors includes selective estrogen receptor modulators and aromatase inhibitors, both of which ultimately decrease signaling through the estrogen receptor in order to treat cancer. Analogously, patients with HER2-positive breast cancer receive treatments that block signaling through HER2,

such as the tyrosine kinase inhibitor (TKI) lapatinib, or a combination of the anti-HER2 antibodies trastuzumab and pertuzumab.

In the early 2000s, recurrent molecular subtypes of breast cancer were identified in a landmark study that used unsupervised hierarchical clustering to identify breast cancer subtypes based on gene expression profiles [14]. Tumors in these subtypes respond differently to chemotherapy [15]. A general role for gene expression profiles in clinical management manifests through a gene expression profile that is used as a predictive test to drive treatment decisions in early stage ER-positive breast cancer [16].

An alternative method of identifying molecular drivers behind breast cancer has recently emerged in profiling genomic alterations in tumors. Early profiling efforts revealed that breast cancer has a greater degree of heterogeneity than may have been expected prior to genomic profiling [17]. Recent studies across multiple cancer types indicate that genetic heterogeneity may underlie resistance, and genomic profiling is a critical component in the identification of therapies suitable for specifically targeting a patient's cancer, generally referred to as targeted therapies. Wide recognition for the potentially transformative role of genomic profiling and targeted therapy is evidenced by the success of Foundation Medicine, a company whose primary product platform is targeted deep sequencing of a panel of cancer-related genes. Less than two years after raising Series A funding, Foundation Medicine went public with a one billion dollar initial public offering in September 2013.

Oncogenic pathway inhibition – Clinical impact and disease resistance

Cancer researchers have long sought to develop anti-cancer compounds with progressively greater specificity and sensitivity, in hopes of prolonging both survival and quality of life in cancer patients. This tenet was present even in Sydney Farber's use of anti-folates to treat acute lymphoblastic leukemia (ALL) in 1948 [18], however chemotherapies such as anti-folates generally have broader side effect profiles than targeted therapies. Recent years have seen a dramatic shift away from the development of novel chemotherapeutics in favor of targeted therapies developed against specific molecular targets critical to oncogenic pathway activity.

Reflecting this shift towards an increased use of targeted therapies, the number of new molecular entity (NME) approvals by the FDA for targeted therapies has increased dramatically in recent years. Whereas only three targeted therapies (rituximab, trastuzumab, and imatinib) were given the NME designation over the span of 1997 – 2002, a total of seventeen targeted therapies were approved as NMEs from 2011 – 2013 (Figure 1.1). These targeted therapies have a major positive impact on overall survival (OS) for cancer patients. The anti-HER2 antibody trastuzumab can result in greater than 30% improvement in five year OS compared to chemotherapy alone [19]. Despite the significant gains to recurrence-free survival (RFS) and OS afforded by the first targeted therapies, many patients ultimately developed recurrent disease [20, 21]. Unfortunately, recurrent disease is frequently refractory to previous therapies that had been used in a particular patient, and thereby is frequently fatal.

As a consequence of the frequency of recurrent disease, the increase in NME approvals from 2011 – 2013 reflects in part the development of drugs intended to be administered in conjunction with, or after treatment failure of, the targeted therapies that first appeared over a decade ago. Examples of these new drugs include pertuzumab and ponatinib. Trastuzumab works in part through inhibition of HER2:HER2 homodimers [22]. In contrast, pertuzumab inhibits HER2:HER3 heterodimerization, and administration of pertuzumab in combination with trastuzumab and docetaxel in the neoadjuvant setting improved median progression-free survival (PFS) by 6.1 months vs trastuzumab-docetaxel alone (12.4 months PFS with trastuzumab-docetaxel vs. 18.5 months PFS with pertuzumab-trastuzumab-docetaxel, $p<0.001$) [23]. While pertuzumab is intended to be administered in conjunction with trastuzumab to inhibit HER2 signaling in patients with breast cancer, ponatinib is intended to be given as a single agent after treatment failure with a tyrosine kinase inhibitor, such as imatinib, in order to block signaling through the Philadelphia chromosome in patients with Philadelphia chromosome-positive ALL [24]. Administration of ponatinib resulted in a 54 percent major hematologic response when administered to patients with Philadelphia chromosome-positive chronic phase-ALL who were previously intolerant or resistant to treatment with imatinib [24]. Despite the improvement in survival that these newer targeted therapies provide, many patients develop recurrent disease.

To develop therapies that can prevent disease relapse, researchers have investigated both the biology of recurrent tumors, as well as the biology of residual disease.

A major challenge in treating recurrent disease is the diversity of mechanisms that can underlie treatment resistance, suggesting that although targeted therapies inhibiting single pathways may be sufficient to treat a specific molecular subtype of cancer, many different strategies will be required to treat the address the many molecular subtypes associated with resistance. Examples of mechanisms that recurrent tumors exploit to resume growth following targeted therapy include mutation or amplification of the drug target, increasing signaling through bypass pathways, defects in growth arrest or survival, or cell state alterations such as an epithelial-to-mesenchymal transition (EMT) [25]. p95-HER2, a truncated 95kDa isoform of HER2 that lacks the trastuzumab binding region, is associated with resistance to trastuzumab therapy, but remains susceptible to treatment with the anti-HER2 TKI lapatinib [27, 28]. Other mutations to HER2 exist as well [25]. Bypass signaling has been reported in the setting of trastuzumab resistance, by receptor tyrosine kinases (RTKs) signaling through EGFR, HER3, IGF-1R, or MET, and by mutations in downstream signaling components such as PI3K/AKT or loss of PTEN [29-32]. Alternatively, alterations that promote cell cycle entry, such as Cyclin E amplification and down-regulation of cyclin-dependent kinase inhibitor p27 may also underlie trastuzumab resistance [33-34]. Reports in non-small cell lung cancer (NSCLC) reveal that recurrent tumors may also exhibit tumor cells with an alteration in cell state, such as EMT, or alternatively NSCLC may also recur as small cell lung cancer [35].

Given the pleiotropic mechanisms underlying tumor recurrence, it would be desirable to define a single biological phenotype that generally describes all tumor cells responsible for resistance, such that inhibition of this phenotype or state may have a broad impact on cancer progression. One such general endpoint is represented by the idea of ‘cancer stem cells’ a broad term generally used to describe a rare subpopulation of tumor cells that both give rise to other tumor cells, and are more resistant to therapy than the bulk population of tumor cells. Perhaps because the idea of a single cell type that underlies all resistance is such an appealing Achilles’ heel of

cancer, a plurality of studies assume residual breast cancer is likely comprised of tumor cells with stem cell-like properties [36], whereas it actually remains unclear whether residual disease in breast cancer is maintained by such a population. In the case of breast cancer patients treated with neoadjuvant therapy targeted against the estrogen receptor, residual tumor cells have been identified locally within breast tissue upon surgical resection [37]. These residual tumor cells are identified by expression of CK8, and express phenotypic markers correlated with both a mesenchymal and a stem cell phenotype. While this study supports a role for a stem cell-like population in disease resistance, a recent study using alternative methodology of isolating residual tumor cells arrives at a different conclusion. Microfluidic chips coated with antibodies to capture cells in the blood expressing EpCAM, EGFR, and HER2, were used to identify circulating tumor cells in patients undergoing therapy, and assessed epithelial or mesenchymal phenotype of captured cells from mRNA in situ immunohistochemistry [38]. In this study, the authors they find that residual breast cancer cells may either be enriched for an epithelial phenotype, or a mesenchymal phenotype. Consequently, it is clear that residual disease can't generally be described as consistently either mesenchymal or epithelial, but instead that the result may be context dependent.

Taken together, these reports reveal that the use of targeted therapies has dramatically improved outcomes in cancer patients, and newer generation therapies will continue to strengthen these gains. In spite of this progress, patients frequently relapse. Analysis of tumor recurrence reveals a breadth of resistance mechanisms, posing a challenge for the development of therapeutic strategies that will impact large percentages of patients. However, it is possible that residual disease across different cancer types may harbor unifying characteristics, although residual disease is challenging to identify and isolate in vivo. Thus, targeting residual disease is an attractive strategy to prevent tumor recurrence, but more investigation is required to describe the phenotype of residual disease.

Immunity and inflammation in recurrence

A role for the immune system and inflammation in cancer progression is well established, and several clinical studies have demonstrated that therapeutically targeting either specific components of the immune system, or inflammation in general, can improve survival for cancer patients. Clinical trials using checkpoint blockade inhibitors targeting PD-1 and CTLA-4 have resulted in major improvements in the OS of patients with melanoma, NSCLC, and renal cell carcinoma [39, 40]. In breast cancer, trastuzumab works in part through antibody-dependent cell-mediated cytotoxicity [41]. Anti-inflammatory drugs may also have a major impact on cancer progression, as evidenced by a greater than 50% reduction in relative risk of breast cancer recurrence identified in the Nurse's Health Study for breast cancer patients taking daily aspirin following initial therapy [42]. Together, these data support increased research into the mechanisms underlying the relationship between immunity, inflammation, and cancer progression, and suggest that therapies targeting the immune system may have a major impact on breast cancer recurrence.

Breast cancer recurrence

For patients with breast cancer, following initial diagnosis, early stage breast cancers are locally resected, whereas patients with locally advanced breast cancers may receive neoadjuvant chemotherapy prior to surgery, in order to permit surgical resection of their cancer. Metastatic breast cancer is unlikely to be cured, and therefore goals of treatment in this setting are prolongation of survival and quality of life [43]. Patients whose primary tumors have been surgically removed may then undergo adjuvant therapy, in order to delay or prevent disease recurrence by eliminating subclinical disseminated disease. At this point, patients may receive targeted therapies based on their tumor's histopathological subtype, such as tamoxifen to inhibit ER or trastuzumab and pertuzumab to inhibit HER2. For patients who are not candidates for one of these therapies, they may have their tumors sequenced, in order to identify targeted therapies that would provide the maximum efficacy. Despite efforts to choose targeted therapies with the

maximum efficacy for any particular patient, many patients treated with targeted therapies ultimately recur, and succumb to their recurrent disease.

Breast cancer recurrence can be categorized as either locoregional recurrence, or distant recurrence. Survival following locoregional recurrence is generally superior to survival following distant recurrence. Following breast conservation therapy, local recurrence usually occurs within the breast, whereas following mastectomy, local recurrence occurs in the chest wall. Regional recurrence indicates a recurrence in regional lymph nodes. Ten-year overall survival rates following local recurrence after breast conservation therapy is as high as 80%, however five-year overall survival rates for patients with recurrence in the chest wall or regional lymph nodes are up to 52% or 28%, respectively [44]. Patients with distant recurrence are not likely to be cured. Although targeted therapies have led to improvements in OS for these patients [45, 46], the five-year OS for breast cancer patients with metastatic disease is only 22% [47]. Factors that are prognostic for OS at primary tumor presentation are generally prognostic for RFS, given that distant disease recurrence is the primary cause of breast cancer-related mortality in these patients. Residual tumor cells that survive therapy are termed minimal residual disease (MRD), and are responsible for cancer recurrence.

Different breast cancer subtypes exhibit different recurrence kinetics. While TNBC and HER2-positive breast cancer predominantly recur within 5 years of initial therapy, hormone receptor-positive breast cancer has a nearly-constant rate of cancer recurrence for 20 years [48]. As recurrent disease arises from residual disease that survives initial therapy, disease relapse up to 20 years after initial treatment is consistent with reports detecting MRD in patients decades after initial therapy [48].

Given that recurrent breast cancer is generally incurable, therapies that eliminate residual breast cancer prior to acquisition of a recurrent phenotype may decrease the rate of recurrence and thereby improve OS for breast cancer patients. Given the heterogeneity of oncogenic pathways driving tumor progression, and the diversity of resistance mechanisms that have been described, it would be useful to identify biological qualities shared by residual disease in different settings.

Considering clinical evidence suggesting MRD may be dormant prior to tumor recurrence in patients with a long recurrence latency, dormancy may offer a therapeutic target in these patients. However it is unclear whether dormancy plays a role in tumor recurrence where the latency period is not decades long.

Residual disease and cancer dormancy – Incidence and relevance to recurrence

To develop approaches for preventing tumor recurrence, recent clinical efforts have aimed to better understand the incidence and biology of residual disease. Residual disease can be detected as circulating tumor cells (CTCs) in the blood, or disseminated tumor cells (DTCs) in the bone marrow, by identifying cells expressing tumor-specific markers. Indeed, the 2008 FDA approval of the CELLSEARCH platform for detecting CTCs, using the epithelial marker EpCAM, represents both the widespread acceptance of the clinical importance of detecting residual disease as well as a general reliance on epithelial markers for this process [49]. The ability to detect MRD has revealed that dissemination can occur early in tumorigenesis, such that up to 40% of early-stage breast cancer patients harbor DTCs [50]. Studies have found that the presence of MRD following treatment is an independent prognostic indicator for poor RFS in breast cancer [51], suggesting that this residual disease may give rise to recurrent tumors. This finding may apply outside of breast cancer as well, as subsequent studies have demonstrated a connection between detectable MRD and outcome in other cancer types as well [52-59]. In spite of the paramount clinical importance of understanding the biology of residual disease in order to develop approaches to prevent recurrence, the biology of MRD remains largely unknown.

Growth rates of breast cancers that recur after a long period of latency are inconsistent with a Gompertzian growth model following initial therapy, and therefore a period of tumor dormancy has been proposed to explain long recurrence latency of breast cancer [60, 61]. The idea that residual disease is dormant is supported by analyses showing that DTC in the bone marrow of breast cancer patients are frequently Ki67 negative [62-65]. More recently, long recurrence latencies have been identified for patients with melanoma [66], renal cell carcinoma [67], and

other cancer types as well [68, 69], suggesting that dormancy may occur in these malignancies as well.

In spite of the large number of patients with MRD, the association between MRD and recurrence, and clinical evidence that MRD is dormant, it remains unclear whether dormancy offers an attractive therapeutic target. First, growing tumors may be comprised predominantly of tumor cells that are Ki67 negative [70, 71]. Hence, analysis of Ki67 alone may be insufficient to prove that DTCs are dormant. These cells may instead represent the non-proliferative fraction of a tumor, or alternatively exhibit cell cycle arrest for a reason other than dormancy, such as senescence. Further, while patients with hormone receptor positive breast cancer may exhibit a latency period of more than two decades prior to recurrence, many breast cancer patients recur within the first few years after treatment, and thus it remains unclear whether residual disease in these patients undergoes dormancy prior to recurrence. Indeed, as tumors with a diameter smaller than 1 cm are below the detection limits for modern imaging modalities [72], and the efficacy of adjuvant chemotherapy is predicated on the idea that subclinical disseminated disease is actively growing, it is likely that many patients harbor proliferative residual disease at the time they initially receive therapy. Thus, demonstrating the relevance of cancer dormancy to cancer recurrence in a broader population of cancer patients remains a critical task.

Residual disease and cancer dormancy – Biology

If a large fraction of the residual disease that gives rise to recurrent tumors is dormant, and thus dormancy offers an attractive therapeutic target, the next task – developing therapeutic approaches to eliminate dormant tumor cells or maintain them in a dormant state in order to prevent recurrence – remains challenging due to the paucity of information on the in vivo biology of dormancy. Dormancy can be divided into two categories, tumor mass dormancy and cellular dormancy or quiescence [73]. Tumor mass dormancy occurs when a proliferating population of tumor cells is unable to grow at a Gompertzian rate due to a countervailing level of cell death caused by a lack of vasculature (angiogenic dormancy), or an anti-tumor immune response (immunological dormancy). Cellular dormancy occurs when tumor cells have exited the cell cycle

for a prolonged period of time, and thus the tumor does not grow. Clinical identification of DTCs that lack the proliferation marker Ki67 supports a role for cellular dormancy in MRD and tumor progression. The following section will focus on the biology of cellular dormancy in order to provide a background necessary for contextualizing subsequent findings in this thesis.

Recent studies have begun to elucidate microenvironmental factors that can contribute to dormancy of solitary disseminated breast cancer cells in various microenvironments, including the bone marrow. Mesenchymal stem cells (MSCs) within the bone marrow reside in a quiescent state within their niche, and can lead to cell cycle arrest of nearby immune cells that had previously been activated, similar mechanisms may contribute to dormancy of tumor cell in the bone marrow [74]. Indeed, recent data from in vitro co-culture studies demonstrate that, in an analogous manner, bone marrow MSCs may induce a dormant state in breast cancer cells by signaling through exosomal miR-23b [75]. A separate publication recently found that stable vasculature can promote tumor cell dormancy through secretion of thrombospondin-1, whereas sprouting neovasculature triggers dormant tumor cell proliferation through periostin and TGF-β1 [76]. While these studies support their in vitro findings by correlating in vivo expression of components of the molecular pathways identified in vitro with the presence of disseminate tumor cells, it remains a possibility that the molecular mechanisms identified in these studies that are able to regulate dormancy in vitro are not the exact same as those that actually regulate dormancy in vivo. Thus, studies that systematically examine pathways activated or inactivated in dormant tumor cells in vivo may provide a more accurate understanding of the biology of dormancy.

Outside of the bone marrow, several studies have identified dormant isolated breast cancer DTCs in lungs or liver [77, 78]. In an attempt to identify molecular mechanisms underlying dormancy of DTCs in the lung, a recent study indicates that bone morphogenic protein (BMP) signaling may promote dormancy, whereas the inhibitor of BMP signaling Coco may allow dormant tumor cells to resume growth [79]. Additional studies of breast cancer DTCs in cortical bone indicate that recruiting monocytes to sites of micrometastases may trigger outgrowth of bone metastases from

previously indolent disease [80]. These studies suggest that a wide variety of mechanisms may regulate escape from dormancy.

Beyond studies in models of breast cancer, other models have also contributed towards a more thorough understanding of cellular dormancy. A series of experiments with human head and neck squamous cell carcinoma (HNSCC) cells in chicken chorioallantoic membranes revealed a role for urokinase plasminogen activator receptor (uPAR) in cellular dormancy. When expressed at high levels, uPAR activates the fibronectin receptor integrin α5β1, which binds to fibronectin in order to organize complexes with focal adhesion kinase or EGFR that up-regulate the ratio of activated ERK to activated p38, maintaining tumor cells in a proliferative state [81-83]. In contrast, when low levels of uPAR are present in tumor cells, the disorganized fibronectin fibrils cannot bind to integrin α5β1, leading to a low ratio of activated ERK to activated p38, thus promoting tumor cell dormancy [81-82]. Following with the line of reasoning that a low ratio of active ERK to active p38 can induce dormancy, recent work with dormant HNSCC cells in mouse bonne marrow suggests that TGF-β2 signaling through a TGF-β3 complex can promote dormancy by activating p38, which leads to dormancy by up-regulating the transcriptional repressor DEC2 and repressing the transcription factor FOXM1 [84].

These studies are predicated on a model wherein dormancy occurs when individual tumor cells metastasize to new sites, but fail to give rise to macrometastases because they undergo cellular dormancy. The above models do not show, however, that isolated dormant tumor cells that become dormant at metastatic sites subsequently give rise to recurrences in vivo, as they usually rely on ex vivo manipulation to switch dormant cells to a proliferative state. As dormancy is primarily of interest because it may represent a state that tumor cells pass through prior to recurrence, it is critical that studies investigating residual disease use models that demonstrate spontaneous recurrence following a period of dormancy in vivo.

The breadth of mechanisms that may underlie dormancy across these different settings raises the possibility that different therapeutic strategies would be required to target dormancy in different

settings. From a therapeutic development perspective, this is less attractive than the idea of a single mechanism or pathway common to all dormant tumor cells.

Towards the end of identifying a single conserved mechanism describing residual disease across multiple settings, the 'cancer stem cell' theory posits the existence of cancer stem cells (CSCs), which suggests that a single population of tumor cells is responsible both for primary tumor development, metastatic outgrowth, and resistance to therapy, and further that this tumor cell population typically exhibits extremely low levels of proliferation consistent with dormancy [85]. As the CSC theory proposes that CSCs are the only cells capable of giving rise to tumors, the identification of tumor cell populations enriched for tumor initiating cells (TICs) is a means to identify tumor cell populations enriched for putative CSCs. This assay has identified CD44+CD24- breast cancer cells as a putative breast cancer stem cell population [86]. Recent reports demonstrate that breast cancer cells that have undergone an EMT exhibit a CD44+CD24- surface phenotype, and are enriched for TICs [87]. Taking these ideas together in the context of the aforementioned clinical findings, it is appealing to conceive that dormant tumor cells exhibit a mesenchymal morphology, survive therapy, and give rise to tumors at metastatic sites. Indeed, it has been proposed that EMT may be associated with dormancy due to its association with stem-like cancer cells [88, 89]. Some clinical reports support the idea that residual disease may have either a phenotype associated with TICs, such as CD44+CD24- breast cancer cells [90], or be enriched for tumor cells with a mesenchymal phenotype [37]. However, alternate studies indicate that residual disease may not necessarily acquire a mesenchymal phenotype [38], and thus the phenotype of residual disease remains unclear. This may reflect in part the challenge of unambiguously identifying residual tumor cells that survive therapy and have completely lost expression of epithelial markers after complete EMT, however methods for detecting residual disease in humans still rely on markers present in primary tumor cell populations that may no longer be expressed by residual tumor cells.

Separate studies using inducible transgenic mouse models suggest that residual disease may be enriched for dormant tumor cells that express markers associated with a stem cell phenotype,

however these studies fail to use markers that unambiguously identify residual tumor cells, and consequently it is difficult to determine whether they provide an unbiased picture of residual disease [91, 92]. Further, these studies do not investigate angiogenic insufficiency or senescence, so it remains unclear whether residual disease in these models is truly dormant. Additionally, as neither of these models is reported to demonstrate spontaneous tumor recurrence, it is unclear whether the findings from these models can be applied to residual disease that gives rise to recurrent tumors. Interestingly, the report of Ki67 negative residual disease in models driven by two distinct oncogenes expressed in two different cells of origin together suggest that exit from the cell cycle may be a general quality of residual tumor cells that survive targeted therapy.

Together, the above studies demonstrate that a wide variety of mechanisms may control tumor cell dormancy. Critically, none of the above studies investigating dormancy demonstrate the presence of a dormant tumor cell population that subsequently gives rise to recurrence in vivo. Additionally, while some evidence supports the idea that residual disease may be enriched for a stem cell-like phenotype following oncogenic pathway inhibition, previous studies have not used unambiguous markers such as fluorescent proteins to identify residual tumor cells, and thus it remains unclear whether they represent an analysis of all residual tumor cells, or only those that express markers present on tumor cells in the primary tumors. Thus, models that allow unambiguous identification of dormant residual tumor cells that give rise to recurrence could significantly improve our understanding of residual disease that survives oncogenic pathway inhibition.

Residual disease and cancer dormancy – Therapeutically targeting dormant disease

Although the best strategy to eliminate dormant tumor cells or prevent dormant tumor cells from re-entering the cell cycle is unclear, a wide array of approaches have emerged. Strategies to kill residual tumor cells include targeting the cytoskeleton of dormant tumor cells [93], reactivation of metabolic demand in residual cells unable to increase biosynthetic capability [94], inhibition of the limited transcriptional machinery [95], or using high throughput screening methods to

systematically identify methods to kill dormant tumor cells. Alternatively, therapies that maintain dormant tumor cells in a quiescent state may also prevent tumor recurrence. Towards this end, strategies that target the pathways maintaining tumor cells in a dormant state, or epigenetic drugs that can induce a dormancy-like state, have been proposed as another type of dormant-targeted therapy [96]. A strategy that is less clearly dormancy-specific is targeting kinases involved in recurrent tumor growth [97], although referring to this as a dormancy-targeting therapy may be technically incorrect as the therapy's efficacy is predicated on preventing growth of recurrent tumors, and as such can't be distinguished from therapies targeting escape pathways active in recurrent tumors.

As approaches to therapeutically target dormant disease continue to emerge and mature, models that exhibit dormancy prior to recurrence in vivo will be critical to their preclinical testing. Consequently, characterizing the biology of dormant residual disease that gives rise to recurrence in vivo may provide important insights into such therapies.

Dissertation objectives

Residual disease gives rise to recurrence, however little is known about the generalizable qualities of residual disease in vivo, thus making it difficult to detect and target. Clinical data suggest that isolated DTCs unable to give rise to metastases may generally exhibit a dormant phenotype, however whether residual disease that gives rise to recurrent tumors exhibits dormancy remains unknown, thus the potential efficacy of targeting dormancy remains unclear. Further, the molecular profile of dormant residual disease that gives rise to recurrence in vivo remains unknown, limiting our ability to target residual disease. The goals of this dissertation are to provide insight into the relevance and biology of cellular dormancy as a general characteristic of MRD, to identify generalizable qualities associated with residual disease, and to test therapeutic strategies that prevent the recurrence of residual disease.

Objective 1: Identify generalizable qualities of residual disease across two models of breast cancer driven by different oncogenes

Using fluorescent protein to track tumor cells, we identified dormant residual disease present at sites that previously harbored tumors. Immunofluorescence (IF) staining and intravital labeling demonstrated that outgrowth of residual disease is not limited by angiogenic insufficiency. Dormant tumor cells located in minimal residual lesions can be identified both at local sites in HER2/neu and Wnt1-driven murine models of breast cancer, and also at metastatic sites in these models. Additionally, we demonstrate that human breast cancer displays a dormant phenotype following oncogenic pathway inhibition in vivo. Thus, we identify dormancy as a candidate generalizable quality of residual disease.

We also use gene expression profiling of residual tumor cells in the HER2/neu and Wnt1 models in order to determine similarities between the molecular profiles of dormant residual disease in models driven by different oncogenes. This analysis revels a dramatic overlap between the profile of residual disease in these two different models, including enrichment for gene expression profiles associated with normal and neoplastic stem-like cells. In spite of previous reports indicating that an EMT is associated with a dormant stem-like population of tumor cells, we find that only residual tumor cells in the HER2/neu model exhibit EMT. Surprisingly, we find that residual disease is not enriched for primary TICs but may be enriched for recurrent tumor TICs, thereby suggesting an evolution of TIC populations in response to targeted therapy.

Objective 2: Elucidate the role of the immune system and inflammation in dormancy and recurrence

Our investigation into the generalizable qualities of residual disease revealed that macrophages are recruited to local HER2/neu residual disease. Macrophages may promote cancer growth and resistance to therapy, however their impact on dormant residual disease remains unknown. We hypothesized that macrophages promote breast cancer recurrence through local inflammatory signaling, and thus that either abrogating inflammatory signaling or ablating macrophages within residual disease would inhibit tumor recurrence. We investigated the impact of both modulating inflammation and macrophage ablation on tumor recurrence latency to test our hypothesis.

We identified strategies that promote both inflammation and tumor recurrence, and found that dexamethasone administration inhibited tumor recurrence at doses that also ablated macrophages. Methods targeting *c-fms*-based signaling were able to ablate the majority of macrophages within residual disease, however their impact on tumor recurrence was very small in comparison to the impact of dexamethasone. We found that dexamethasone ablated pro-inflammatory CD11c+ macrophages, whereas *c-fms*-targeted therapy did not ablate this macrophage population, thus providing a tenable explanation for the different efficacy of dexamethasone and *c-fms*-targeted therapy.

Figure Legend

Figure 1.1. Cumulative Number of Targeted Therapy New Medical Entity (NME) Approvals by the FDA

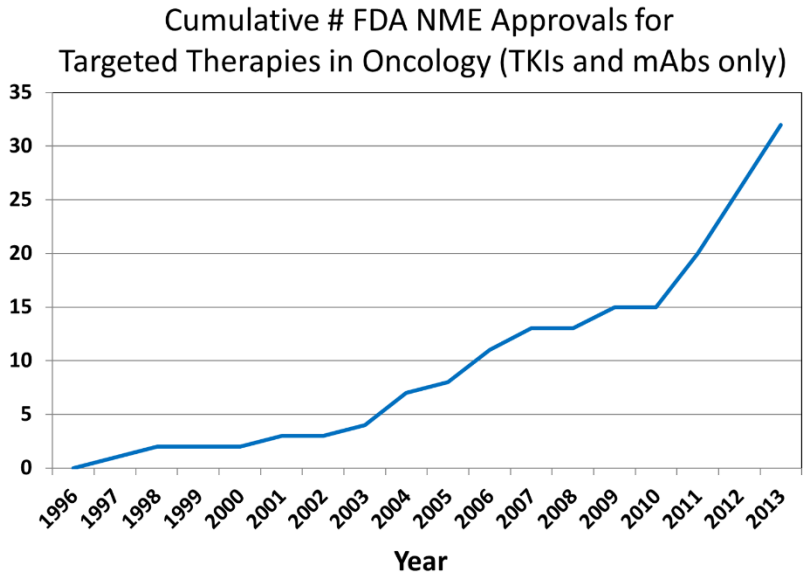

Figure showing the cumulative number of FDA NME approvals from 1996 – 2013.

CHAPTER 2

Modeling Cancer in Mice

Introduction to cancer models

Cancer models are a primary tool in the cancer researcher's armamentarium, as they allow systematic manipulation of known parameters in order to test specific hypotheses related to cancer. Ideally, these models faithfully recapitulate the molecular and cellular mechanisms driving cancer progression in humans, can be experimentally manipulated to precisely answer questions about these mechanisms, and provide reproducible results either between investigators or over a period of time. In practice, generating cancer models that meet these ideals is challenging for several reasons, including the biologically heterogeneity of cancer, and the complexity of performing experiments in the incompletely-understood multiparametric space defining biological systems. This can limit the applicability of models, and thus in order to model various elements of cancer progression, a variety of cancer models have been developed, including *in vitro* cell culture, *in vivo* animal models, and *in silico* computational representations.

While all of these models have strengths and weaknesses, animal models are uniquely capable of recapitulating all the major stages of cancer progression on a cellular level within a single system. Given that 99% of proteins in humans have homologs in mice, the housing and maintenance cost per animal are lower for mice than for larger animals, and the wide variety of tools available to genetically manipulate mice, mice represent the most widely adopted animal model for studying cancer. Various types of mouse models exist, including genetically engineered mouse models of human cancer (hereafter referred to as GEMMs, although broadly defined GEMMs may also refer to non-cancer models), xenograft models, and allograft models. Whereas we will discuss xenograft and allograft mouse models later in this text, we will first focus on genetically engineered mouse models, due to their central role in this work. As this thesis focuses predominantly on in vivo work in mouse models, we will not discuss the use of non-mouse animal models, or non-animal models of cancer such as in vitro systems.

Genetically engineered mouse models (GEMMs)

The first report of a GEMM was published in 1984 [98], and from that time, scientists have used GEMMs for various applications including validating oncogenes or tumor suppressors, and studying tumorigenesis *in situ* [99]. The ability of GEMMs to provide important insights into human cancer is highlighted by recent efforts using these models in co-clinical trials to investigate mechanisms underlying drug efficacy, and to discover clinically relevant biomarkers [99].

GEMMs currently used in research have been optimized to recapitulate human tumorigenesis by using spatial and temporal control of gene expression to recapitulate phenotypes of cancers driven by a plethora of clinically relevant oncogenic drivers, resulting in models that closely recapitulate human tumorigenesis. The tools used to develop transgenic mouse models of cancer have been examined extensively elsewhere [99], but will be briefly reviewed here. Techniques to control gene expression spatially include both driving oncogene expression through a tissue-specific promoter and viral gene delivery, the latter of which can also temporally control gene expression. Additional methods to temporally control gene expression include the use of tetracycline-regulated promoters, and the estrogen receptor fusion system. For example, a model where expression of the reverse tetracycline transactivator (rtTA) is controlled by the mouse mammary tumor virus long terminal repeat (MMTV) allows doxycycline-dependent expression of downstream oncogenes specifically in mammary epithelial cells [100]. Transgenic models also permit inclusion of reporters that allow monitoring of gene expression, such as firefly luciferase downstream of an oncogene to monitor oncogene activity, or tracking of individual tumor cells through expression of fluorescent proteins such as green fluorescent protein (GFP), yellow fluorescent protein (YFP) or tdTomato. Newer efforts to develop transgenic models include using RNAi in lieu of knockouts [101], chimeric organ transplantation models [102], and humanized knock-in mouse models [103].

In spite of efforts made to optimize the similarities between GEMMs and human cancer, GEMMs differ from human cancer in several key metrics. Differences in the size of mice compared to people result in difficulty when modeling many parameters related to size, such as the size of a

tumor relative to the organ from which it arises or a tumor's growth rate, and thereby latency and spread prior to detection. While approximately 99% of mouse proteins have human homologs, sequence differences in these proteins, as well as different molecular circuitry regulating the expression of these proteins, makes molecular findings in mice difficult to systematically extrapolate to humans [104]. The mutational background of tumors that arise in GEMMs may not reflect that of human cancer, and given that resistance in human cancer can arise from genomic alterations, this represents a critical hurdle to the use of GEMMs to predict biology of resistance in humans. The germline background of mice is also constrained to homogenous inbred strains that fail to reflect the massive genetic diversity of germline variations defining the human genomes from which human cancers arise. While GEMMs are not always predictive, work is underway to 'further improve the predictive potential of GEMMs in clinical studies.'

In spite of differences between GEMMs and human cancer, a wide range of studies indicate that GEMMs will remain an important tool for studying clinically relevant questions in cancer progression. The cure for acute promyelocytic leukemia (APL) was developed in part through experimentation in GEMMs, due to the ability of these models to recapitulate response to therapy of the human disease [104, 105]. Putative mechanisms underlying the efficacy of several immune therapies have been identified in GEMMs [106, 107]. GEMMs were used to identify a role for both the loss of HER2 in previously HER2-positive breast cancer, as well as EMT, in cancer recurrence several years prior to when these phenomenon were observed in recurrent cancer in humans [108]. Additional studies reveal a critical role of GEMMs for studying the biological roles of drug targets and identifying alternative mechanisms underlying resistance to therapy [103], for identifying mechanisms underlying tumor resistance to therapy [99, 105, 109-113]. Thus, GEMMs may be useful models to study both the role of the immune system in cancer, as well as mechanisms underlying resistance to targeted therapy.

Non-GEMM animal models

Mouse models other than GEMMS, such as xenograft and allograft models, provide alternative approaches to modeling cancer in mice, and are associated with unique strengths and

drawbacks. These models involve implantation of tumor cells into host mice. Orthotopic implantation of tumors cells, wherein tumor tissue is implanted into the organ associated with that tumor type, is preferred because the microenvironmental signals impacting the implanted tumor cells are more likely to be analogous to those impacting an autochthonous tumor. An example of orthotopic implantation is implantation of breast cancer cells into the mammary gland of a mouse. A less desirable alternate approach is ectopic implantation, wherein tumor cells are implanted into a site not normally associated with the normal growth of those tumor cells. An example of an ectopic implantation is subcutaneous implantation of breast cancer cells. Other mouse models for cancer, including carcinogen-induced and spontaneous cancer models, are discussed in detail elsewhere but their discussion is not pertinent to this thesis [99].

Xenograft models involve the use of human cancer cells to grow cancer in mice, and extremely immunocompromised mice are often used in order to minimize the mouse host's anticancer immune response to the implanted cells. Human cancer cells in mice can contain the same genetic mutations and express the same proteins present in cancers in patients, and thus the efficacy of therapeutics targeting human proteins may be more faithfully recapitulated when generating orthotopic tumors using human tumor cells than mouse tumor cells. The term 'xenograft' model used in isolation frequently refers to the use of a human cancer cell line cultured in plastic prior to injection in mice. In vitro culture acts as a bottleneck that can skew the phenotype of tumor cells away from the phenotype they demonstrate in humans. In contrast, a newer method of establishing xenografts, implanting complete human cancer – including stroma – directly into mice, can result in both faithful recapitulation of the genotype of the donor tumor, as well as generation of a human stroma derived from the donor tumor stroma. This approach allows investigators to generate biological replicates of the same donor tumor, and thus perform controlled experiments in order to test hypotheses about the donor tumor. While GEMMs and human cancer cell lines may exhibit genomic alterations that do not reflect precisely the mutations found in cancer patients, patient-derived xenograft (PDX) models are thought to more faithfully recapitulate these mutations, and thus may be useful for identifying genomic alterations that underlie resistance in vivo. A significant disadvantage to the use of PDX models is that it can

be challenging to manipulate the tumor cells in order to test experimental hypotheses, as methods for tumor cell manipulation – such as overexpression or knockout of target proteins – are typically designed for in vitro culture. Another disadvantage to xenograft models is that dramatically immunocompromised mice such as *NOD/scid/Il2γnull* (*NSG*) mice are more likely to allow engraftment and growth of tumor cells than mildly immunocompromised mice such as *nu/nu* mice, which dramatically curtails the potential for studying immunity in cancer progression in these models.

In contrast to xenograft models, allograft models involve implantation of cancer cells arising from a mouse into a separate host mouse. The host mouse may either be immunocompromised, or alternatively may be from the same strain and genotype, called a syngeneic allograft. While these models may not recapitulate the specific mutational aberrations present in human cancers, and mouse proteins may lack exact homology to their closest human homologs thereby inaccurately representing the efficacy of therapeutics developed to target human cancer cells, these models have several advantages over xenograft models. The ligands and receptors on the implanted tumor cells will be from the same species as the microenvironmental factors that support the growth of the implanted tumor cells, thus the impact of the microenvironment on tumor cells will more accurately represent what would be present in an autochthonous tumor than would be the case for a xenograft tumor. Further, the use of syngeneic hosts enables investigators to produce syngeneic tumors in multiple animals with a fully intact immune system, thereby providing a system well-suited to test hypotheses about the role of immunity in cancer.

Disadvantages of allograft models and GEMMs relative to xenograft models can be partially overcome. Using therapeutics developed against mouse proteins, homologous to therapeutics developed against human proteins, allows one to perform preclinical testing in GEMM and allograft mouse models with intact immune systems. There are also circumstances in which therapeutics used in humans have pharmacodynamic profiles in mice analogous to those in humans, which further permits preclinical testing in mouse models.

CHAPTER 3

Modeling Dormant Residual Disease and Breast Cancer Recurrence

The vast majority of breast cancer deaths are due to disease relapse following a period of clinical remission after treatment. In this regard, a cardinal feature of human breast cancers is the survival and persistence of residual tumor cells in a latent state despite treatment of the primary tumor. These surviving tumor cells, termed MRD, serve as the reservoir from which recurrent breast cancers arise. At present, little is known about the biology of MRD or the nature of the latent state in which they reside. Using conditional transgenic mouse models for human breast cancer driven by either HER2/neu or Wnt1, we demonstrate that residual tumor cells surviving oncogenic pathway inhibition exhibit cellular dormancy at local as well as metastatic sites. In an analogous manner, we find that human breast cancer cells are quiescent following targeted therapy in vivo. Residual tumor cells from both HER2/neu and Wnt1-induced tumors exhibit a gene expression program characteristic of normal and neoplastic mammary stem cells and cellular quiescence, whereas EMT transition occurred in HER2/neu, but not Wnt1, residual disease. Surprisingly, while both HER2/neu and Wnt1 residual tumor cells displayed phenotypic properties associated with tumor initiating cells (TICs), functional assays revealed that residual tumor cells were not enriched for primary tumor TICs , but were instead enriched for TICs capable of giving rise to recurrent tumors. Together, our data reveal that targeted therapies predicated on oncogene addiction give rise to a small population of dormant tumor cells that are capable of re-entering the cell cycle and giving rise to recurrent tumors, and suggest that cellular dormancy represents a potential therapeutic target for preventing recurrent breast cancer.

Modeling oncogenic pathway inhibition

The recent increase in the clinical adoption of targeted therapies, in combination with the dramatic rate of relapse following targeted therapy, have spurred investigation into the biology of residual disease that survives therapy and gives rise to tumor recurrence. Importantly, while primary breast cancers can be cured, recurrent breast cancers cannot. Thus, therapeutic

targeting of MRD could represent an attractive approach to reducing breast cancer recurrence by depleting the reservoir of residual tumor cells that persists following therapy, or otherwise preventing them from giving rise to recurrent cancers. Unfortunately, little is known about the biology of MRD or the pathways that govern the behavior of these cells.

Mounting clinical evidence suggests that tumor dormancy may offer a therapeutic window through which to target MRD and thereby prevent tumor recurrence [114-117]. For example, DTCs in the bone marrow or circulating tumor cells (CTCs) in the blood of cancer patients have been reported to be quiescent and to persist throughout treatment, suggesting that recurrent cancers may arise from dormant tumor cells [118-120]. Nevertheless, it is also possible that tumor relapse in patients results from proliferative, yet subclinical, micrometastases that survive therapy. If true, this would suggest that dormancy is unlikely to constitute a useful therapeutic target. In light of this uncertainty, determining whether dormancy plays a role in tumor cell survival and recurrence is essential for understanding whether MRD represents a stage of neoplastic progression that would be vulnerable to therapies targeting cellular dormancy.

At present, remarkably little is known about the biology of dormancy. This reflects difficulties in identifying and isolating dormant tumor cells in humans, as well as the general lack of animal models for studying dormancy in vivo. To this end, we previously described doxycycline-dependent conditional transgenic mouse models for breast cancer in which HER2/neu, Wnt1, or c-MYC pathway inhibition results in the regression of primary mammary tumors to a non-palpable state, persistent MRD, and eventual relapse following a latent period of remission [108, 121, 122]. Notably, recurrent tumors arising in the HER2/neu-induced tumor model were frequently HER2-negative and had undergone an EMT. In an analogous manner, clinical observations have subsequently revealed that recurrent cancers, as well as MRD, can exhibit phenotypes distinct from the primary tumors from which they arose, both with respect to EMT and to the loss of HER2 expression in breast cancers that were previously HER2+ [37, 123, 124]. These findings highlight the plasticity of neoplastic progression and suggest that conditional transgenic mouse models

may provide a tractable approach to identifying residual tumor cells and elucidating mechanisms of cancer progression following therapy [108, 125, 126].

The biological properties of residual tumor cells that give rise to recurrent cancers following a variable latency period have not, as yet, been described in vivo. In principle, at least three types of tumor dormancy have been described that could potentially contribute to the latent period of MRD prior to tumor recurrence: angiogenic dormancy, cellular dormancy and immunological dormancy. At present, however, the nature of the latent state in which residual tumor cells reside following oncogenic pathway inhibition are unknown. As such, an improved understanding of tumor dormancy will be required to enable the rational design of strategies for detecting and eliminating MRD.

To address this critical gap in knowledge, we now report the use of conditional transgenic mouse models for HER2/neu and Wnt1-induced breast cancers to identify features of MRD in vivo that are shared for tumors driven by different oncogenes. By combining cell sorting with gene expression profiling, we demonstrate that residual tumor cells that survive oncogenic pathway inhibition in vivo exhibit cellular dormancy and express markers characteristic of mammary stem cells. We further demonstrate cellular dormancy at metastatic sites in tumor-bearing mice, and in human breast cancer xenografts treated with anti-HER2 therapies. Contrary to expectation, however, limiting dilution assays revealed that residual tumor cells are not enriched for primary TICs. In aggregate, our observations suggest that cellular dormancy may be a general feature of residual tumor cells surviving oncogenic pathway inhibition and provide new insights into biological properties of MRD relevant to their detection and elimination.

The kinetics of tumor recurrence following oncogene inhibition suggest dormant residual disease

We previously described conditional bitransgenic mouse models for HER2/neu and Wnt1-induced mammary tumorigenesis that recapitulate key features of breast cancer progression as it occurs in patients, including primary tumor formation, response to therapy, and a variable latency period prior to spontaneous tumor recurrence [108, 121, 127]. In these models, doxycycline

administration induces oncogene expression in the mammary epithelium resulting in the formation of primary mammary adenocarcinomas. Analogous to the treatment of human cancers with targeted therapies, doxycycline withdrawal in tumor-bearing mice results in oncogenic pathway inhibition followed by primary tumor regression due to oncogene addiction [121, 127]. However, similar to the phenomena of resistance and relapse in patients treated with targeted therapies, most mice develop spontaneous recurrent tumors following a variable period of latency. As such, these models provide an opportunity to study the phenotype of residual tumor cells that survive targeted therapy and are capable of giving rise to tumor recurrence.

To identify characteristics of residual tumor cells that are shared between HER2/neu and Wnt-1-driven tumor models, we first wished to determine whether the kinetics of tumor recurrence are similar in these models. Therefore, we monitored tumor-bearing *MMTV-rtTA;TetO-HER2/neu* (*MTB;TetO-HER2/neu*) and *MMTV-rtTA;TetO-Wnt1* (*MTB;TetO-Wnt1*) bitransgenic mice in which primary tumors had regressed to a non-palpable state following oncogenic pathway inhibition. Consistent with previous observations, tumors recurred with stochastic kinetics following oncogenic pathway inhibition in both the HER2/neu and Wnt1 models (Figure 3.1A, C).

A recent study using inducible mouse models for lymphoma and leukemia suggested that long-term tumor regression following oncogenic pathway inhibition may require the adaptive immune system [128]. To determine whether adaptive immunity is required for sustained regression of mammary adenocarcinomas in the HER2/neu or Wnt1 models, we injected limited passage tumor cells generated from primary mammary tumors arising in *MTB;TetO-HER2/neu (HER2/neu-Prim1)* and *MTB;TetO-Wnt1* (*Wnt1-Prim1*) mice into the mammary fat pads of immunocompromised female *nu/nu* mice maintained on doxycycline. Following primary tumor formation, doxycycline was withdrawn to induce oncogene down-regulation and tumor regression. Mice bearing fully regressed orthotopic tumors were then monitored for tumor recurrence.

Orthotopic primary tumors recurred with stochastic kinetics following a variable latency period, paralleling our findings in intact *MTB;TetO-HER2/neu* and *MTB;TetO-Wnt1* mice (Figure 3.1B, D). Notably, orthotopic tumors recurring after either short or long intervals exhibited similar growth

rates – a feature that was also observed for recurrent tumors arising in intact mice (Figure 3.1E). These data demonstrate that the kinetics of tumor recurrence in orthotopic mouse models parallel those in intact mice and further indicate that a competent adaptive immune system is not required for sustained periods of tumor regression of up to 200 d following oncogenic pathway inhibition in genetically engineered mouse models.

Our observation that the growth rates of recurrent tumors – in both intact and orthotopic mouse models – are independent of the length of the latent period that preceded their detection was reminiscent of observations in breast cancer patients suggesting the potential existence of a dormant phase between the treatment of primary tumors and their subsequent recurrence at local or distant sites [115]. Therefore, to address whether mice bearing fully regressed mammary tumors harbor dormant residual disease, we first readministered doxycycline to intact *MTB;TetO-HER2/neu* mice whose primary tumors had regressed to a non-palpable state following doxycycline withdrawal, but had not exhibited spontaneous tumor recurrences when maintained off doxycycline for a period of six months.

Following doxycycline re-administration and re-expression of the *HER2/neu* transgene, all mice developed recurrent tumors at the original sites of their primary tumors within two weeks, but did not develop tumors at other sites (Figure 3.1F). This finding demonstrates that essentially all mice bearing tumors that have regressed to a non-palpable state harbor residual cancer cells that are capable of giving rise to recurrent tumors. Moreover, since the median latency for spontaneous tumor recurrence was 17 wk, and since more than a year was required for 95% of mice to recur, the observation that *HER2/neu* transgene reactivation resulted in the appearance of recurrent tumors within 2 wk strongly suggests that mice bearing fully regressed primary mammary tumors harbor dormant residual disease.

Minimal residual lesions contain residual tumor cells

The molecular analysis of dormant residual tumor cells first requires their identification and isolation. To identify residual cancer cells, doxycycline was withdrawn from tumor-bearing *MTB;TetO-HER2/neu* and *MTB;TetO-Wnt1* mice to induce oncogenic pathway inhibition and

tumor regression. Mice were sacrificed 56 d following doxycycline withdrawal and carmine staining was performed on whole-mounted mammary glands that either did, or did not, harbor tumors prior to doxycycline withdrawal. This analysis revealed the presence of abnormal histological lesions in mammary glands that had previously harbored a primary tumor, but not in mammary glands that had not harbored tumors (Figure 3.2A, B arrows). Hematoxylin and eosin (H&E) staining of tissue sections from previously tumor-bearing glands revealed that residual foci were densely cellular (Figure 3.2C, D).

To determine whether abnormal foci observed in whole mounts and histological sections contained residual tumor cells that had survived oncogenic pathway inhibition, or were instead composed of host stromal cells or residual scar tissue, doxycycline-dependent primary tumor cells derived from *HER2/neu* and *Wnt1* primary tumors were stably transduced to express H2B-eGFP and injected orthotopically into the mammary glands of female *nu/nu* mice maintained on doxycycline. Following primary tumor formation, doxycycline was withdrawn to induce tumor regression and mice were sacrificed 56 d later.

H&E staining of histological sections from residual lesion-bearing mammary glands revealed cellular foci within a dense eosinophilic extracellular matrix (ECM) similar to those identified in intact mice (Figure 3.2E). Fluorescence microscopy confirmed the presence of eGFP-labeled tumor cells within these residual foci, which we term minimal residual lesions (MRLs) (Figure 3.2F).

As metastatic breast cancer is the primary cause of mortality for this disease, we also wanted to establish models for systemic metastases. Towards this end, we performed intracardiac injection of *HER2/neu-Prim1* tumor cells into the left ventricle of *nu/nu* mice on doxycycline. Injection into the left ventricle allows tumor cells to bypass the lungs, which otherwise serve as the primary metastatic site for the majority of tumor cells injected intravenously. Using this system, we were able to generate systemic metastases in the *nu/nu* mice, which we observed both with bioluminescence firefly luciferase imaging (Figure 3.3A) and with GFP fluorescence upon gross dissection (Figure 3.3C). Consistent with our previous observations of metastatic disease [127],

luciferase activity was completely diminished following doxycycline withdrawal, indicating that the oncogene can be turned off at metastatic sites following doxycycline withdrawal (Figure 3.3B).

To develop a model of systemic metastases in which tumor cells specifically express fluorescent proteins, but that had been minimally manipulated in vitro, we crossed *MTB;TetO-HER2/neu* mice with *TetO-TurboCre (TTC);Rosa26-lox-stop-lox-YFP (rYFP)* mice to generate *MTB;TetO-HER2/neu;TTC;rYFP* mice in which doxycycline administration results in the inducible expression of both HER2/neu and cre recombinase specifically in mammary epithelial cells. Consequently, doxycycline treated mice harbor fluorescent mammary epithelial cells, due to Cre-mediated excision of the stop cassette preceding *YFP*, that HER2/neu-induced mammary adenocarcinomas with yield fluorescently-labeled tumor cells. Alternatively, the fluorophore *tdTomato* was used in place of the fluorophore *YFP* in some mice, as tdTomato is dramatically brighter than YFP. Enzymatically digested primary doxycycline-dependent tumors from these quadtransgenic reporter mice were injected orthotopically into *nu/nu* mice to generate 'no culture' orthotopic models, i.e. orthotopic models that had not been cultured, analogous to an allograft version of a PDX model.

Mice bearing no culture orthotopic tumors developed systemic metastases (Figure 3.4). There was a wide range of tumor growth rates across all tumors injected from the same donor, and the orthotopic tumors that grew the slowest on doxycycline gave rise to the greatest number of metastases in locations other than the lung. In general, 1 out of 5 mice would have primary orthotopic tumors that grew sufficiently slow to generate liver metastases, and bone marrow metastases. While primary metastases formed in mice on doxycycline (Figure 3.4A), upon doxycycline withdrawal, metastases regressed and left disseminated residual lesions in different organs, including lung, liver, and bone marrow (Figure 3.4B, C).

Given our observations that these mice can develop systemic disease, we next wanted to know whether we could use these mouse models to study CTCs and DTCs, due to the fact that there is a large clinical interest in these populations but the biology connecting these populations to residual disease that gives rise to recurrence is poorly understood. We first investigated whether

MTB/TAN/TTC/rYFP mice could be used to study these populations. Flow cytometry revealed that peripheral blood leukocytes from *MTB/TAN/TTC/rYFP* mice expressed YFP (Figure 3.5). This occurred only in mice that had both the *MTB*, *TTC*, and *rYFP* transgenes (Figure 3.5A, data not shown). Presumably this occurred due to promiscuous activity from the *MMTV-LTR* promoter in the *MTB* transgene, as previous studies have indicated that MMTV-*LTR* may be active in leukocyte populations. *MTB*/*oncogene* mice do not develop hematological malignancies, because the expression of oncogenes in leukocytes is vanishingly small even in the presence of doxycycline. Thus we were surprised that YFP fluorescence occurs in the absence of doxycycline in leukocytes. This speaks in part to the strength of the Cre-based reporter system, and suggests that even low level MMTV activation of Cre is sufficient to lead to excision of the stop locus upstream of YFP. This phenomenon did not occur in all *MTB/TAN/TTC/rYFP* mice, and some mice exhibited YFP expression in only a fraction of their peripheral blood leukocytes (data not shown). Upon establishing orthotopic no culture tumors with this system, the extreme rarity of CTC and DTCs combined made it challenging to reliably distinguish fluorescent reporter tumor cells from leukocyte doublets in vivo (data not shown).

As an alternative approach to identify CTC and DTCs, we established orthotopic H2BeGFP-labeled *HER2/neu-Prim1* tumors in *nu/nu* mice. Upon generation of primary doxycycline-dependent bilateral tumors with a mean diameter of 4cm, we were able to use flow cytometry of blood drawn from a right ventricle cardiac puncture to identify a large number of CTCs in some of these mice (Figure 3.6A, B). Fluorescence imaging for Hoechst and GFP on sections of frozen decalcified bone revealed DTCs (Figure 3.6 C-F). We then performed flow cytometry for GFP+ events on additional *nu/nu* mice with smaller tumor burdens (‘small tumor’ = 5mm diameter, ‘large tumor’ = 15mm diameter), and found a small number of GFP+ events in the blood and bone marrow (Figure 3.6 G). We also identified events in the blood and bone marrow at various stages of dormancy and tumor recurrence. Due to the small number of events identified in these studies, it was not possible to definitively say that these events were indeed tumor cells and were not simply rare events with high levels of autofluorescence.

Residual tumor cells exhibit cellular dormancy

Based on the stochastic kinetics of mammary tumor recurrence that we observed in *MTB;TetO-HER2/neu* and *MTB;TetO-Wnt1* mice, as well as the similar growth rates exhibited by recurrent tumors irrespective of their latency to recurrence, we hypothesized that residual tumor cells surviving oncogene down-regulation exhibit cellular dormancy. To test this hypothesis, we generated orthotopic primary tumors from H2B-eGFP-labeled *HER2/neu-Prim1* cells and sacrificed mice bearing primary tumors at 0, 28 d or 56 d following oncogene down-regulation.

IF for Ki67 performed on tissue sections from primary tumors and MRLs revealed Ki67 expression in 0.25% and 0.17% of residual tumor cells at 28 d and 56 d following HER2/neu down-regulation, respectively (Figure 3.7A, D). In contrast, primary tumor cells exhibited rates of Ki67 positivity that were greater than 40-fold higher (p-value primary tumor: vs. 28 d MRL = 0.011; primary tumor vs. 56 d MRL = 0.029). This finding indicates that residual tumor cells are quiescent following oncogene down-regulation.

In order to distinguish slow cycling cells from tumor cells undergoing prolonged cell cycle arrest, as would be anticipated for dormant tumor cells, we evaluated tumor cell proliferation rates over extended periods of time. Orthotopic primary tumors and MRLs were generated, as above, from H2B-eGFP-labeled *HER2/neu-Prim1* or *Wnt1-Prim1* tumor cells in *nu/nu* mice and osmotic pumps were then employed to deliver bromodeoxyuridine (BrdU) for 2 wk to label cells that underwent DNA synthesis during that period.

Whereas greater than 90% of *HER2/neu-Prim1* tumor cells were labeled with BrdU over the 2 wk period prior to sacrifice, fewer than 9% of *HER2/neu-Prim1* residual tumor cells incorporated BrdU over the same time period (Figure 3.7B, E). In an analogous manner, greater than 95% of *Wnt1-Prim1* tumor cells were labeled with BrdU over a 2 wk period, while fewer than 8% of *Wnt1-Prim1* residual tumor cells incorporated BrdU during this same period (Figure 3.7C, F). These findings suggest that residual tumor cells from either HER2/neu or Wnt1-induced mammary tumors reside in a latent G_0-like state following oncogene down-regulation, or are extremely slow cycling.

The finding that the vast majority of residual tumor cells fail to incorporate BrdU over extended periods of time did not distinguish between the possibility that residual tumor cells were dormant – existing in a reversible state of cell cycle arrest – and the possibility that these cells had irreversibly exited the cell cycle as might occur if cells had undergone senescence or terminal differentiation. To address this question, we generated orthotopic primary tumors and MRLs from H2B-eGFP-labeled *HER2/neu-Prim1* or *Wnt1-Prim1* tumor cells and then re-administered doxycycline to mice for 72 hr. Mice were then injected with BrdU 2 hr prior to sacrifice in order to label proliferating cells.

In both the *HER2/neu-Prim1* and *Wnt1-Prim1* models, residual tumor cells in MRLs in which oncogene expression had been reactivated incorporated BrdU at rates similar to primary tumor cells. In contrast, residual tumor cells within MRLs in which oncogene expression had not been reactivated incorporated BrdU at ~20-fold lower rates (Figure 3.7G-J; p-value <0.001 for dormant residual tumor cells vs. primary tumor cells or vs. reinduced residual tumor cells in both *HER2/neu* and *Wnt1* models). Together, these findings demonstrate that residual tumor cells exist in a reversible state of cell cycle arrest following oncogenic pathway inhibition, suggesting that these cells exhibit cellular dormancy.

As cellular dormancy is also associated with a low rate of apoptosis, we used IF to quantify the number of tumor cells in the *HER2/neu* model that expressed the apoptosis marker cleaved caspase-3 (CC-3). While primary tumor cells exhibited more than 2% CC-3 expression, dormant residual tumor cells rarely expressed CC-3 at 28d after doxycycline withdrawal, and no residual tumor cells expressed CC-3 56 days after doxycycline withdrawal (Figure 3.7 K, L). This finding further supports the possibility that residual tumor cells are dormant.

Residual disease is well vascularized and is not hypoxic

Our findings to this point suggested that the latent period between primary tumor regression and spontaneous tumor recurrence might be explained if residual tumor cells existed in a state of cellular dormancy. In contrast, prior reports have suggested that sustained tumor regression following oncogenic pathway inhibition may be attributable to a lack of functional vascularization

[129, 130]. Angiogenic dormancy refers to the state in which ongoing cellular proliferation is counterbalanced by hypoxia-induced apoptosis resulting from inadequate vascularization [131]. Although the extremely low rates of proliferation that we observed in residual tumor cells within MRLs suggested a model other than angiogenic dormancy, this finding did not exclude the possibility that hypoxia due to a limiting blood supply might contribute to the dormant state of residual tumor cells.

To assess the state of vascularization within MRLs, we first performed IF for the endothelial cell marker CD31 on tissue sections from MRLs harvested from orthotopic *HER2/neu-Prim1* and intact *MTB;TetO-Wnt1* mouse tumor models. This analysis demonstrated that both *HER2/neu* and *Wnt1* residual lesions are densely vascularized (Figure 3.8A, B). Indeed, CD31 staining revealed that the density of blood vessels within MRLs is similar to, or greater than, that present within actively growing primary tumors (Figure 3.8B).

The pattern of CD31 staining that we observed in MRLs was consistent with the maintenance of a competent microvasculature following tumor regression. However, CD31 staining could not definitively demonstrate that blood vessels within MRLs were functional. To address this, mice bearing orthotopic MRLs generated from H2B-eGFP-labeled *HER2/neu-Prim1* tumor cells 28 d following HER2/neu down-regulation were intravenously (i.v.) injected with Lectin-Streptavidin-AlexaFluor647 (Lectin-AF647) to label patent blood vessels. Virtually all CD31 staining co-localized with Lectin-AF647, demonstrating that blood vessels within MRLs are well perfused (Figure 3.9).

Though the above data suggested that MRLs contain a patent and robust vasculature, we could not exclude the possibility that regions of hypoxia existed within MRLs. To address this, we generated mice bearing orthotopic MRLs from H2B-eGFP-labeled *HER2/neu-Prim1* tumor cells and intravenously injected those mice with Lectin-AF647, Hoechst 33342 and pimonidazole prior to sacrifice. Pimonidazole forms covalent adducts with proteins in hypoxic microenvironments ($pO_2<10$mmHg) and is sufficiently sensitive to detect physiological hypoxia surrounding hepatic veins [132].

IF to detect pimonidazole adducts in control experiments revealed that, as anticipated, such adducts were present within low-oxygen tension regions of the liver adjacent to hepatic veins (Figure 3.8C, arrowhead), but absent from well-oxygenated regions adjacent to the hepatic arterial vasculature (Figure 3.8C, arrow). Strikingly, virtually no pimonidazole staining was observed in MRLs examined from multiple animals, indicating that residual tumor cells within the MRL are not present within a hypoxic microenvironment (Figure 3.8C).

As some prior reports have suggested that diffusion of small molecules out of blood vessels may be limited within a desmoplastic environment [133], Hoechst 33342 was injected into MRL-bearing mice to assess whether the absence of pimonidazole staining might be due to restricted diffusion of pimonidazole within MRLs. Specifically, the distribution of i.v. injected Hoechst 33342 was evaluated by fluorescence microscopy in order to visualize the ability of small molecules to diffuse within the MRL. Livers from mice bearing MRLs served as positive controls. Intravenously injected Hoechst 33342 efficiently labeled the nuclei of cells in both livers and MRLs, indicating that small molecules within the circulation can diffuse out of the vasculature and gain access to residual tumor cells within MRLs (Figure 3.8C).

In aggregate, data from both *HER2/neu* and *Wnt1* tumor models support the hypothesis that MRLs are well-vascularized with a patent vasculature, and that dormant residual tumor cells within MRLs are not hypoxic. Accordingly, these findings suggest that the dormant state of residual tumor cells observed following oncogenic pathway inhibition is not due to the limited delivery of oxygen or nutrients resulting from an inadequate blood supply.

Residual metastatic tumor cells recapitulate features of local residual disease

As distant recurrence is the primary cause of mortality from breast cancer, we wished to determine whether our findings were also true for micrometastatic disease. We therefore asked whether, following oncogenic pathway inhibition, residual lung metastases demonstrated cellular dormancy in the context of a well-vascularized microenvironment.

Fluorescent primary tumors from doxycycline-induced *MTB;TetO-HER2/neu;TTC;rYFP* mice were

enzymatically dissociated and injected orthotopically into *nu/nu* mice. Mice that developed orthotopic primary tumors also harbored lung metastases. Doxycycline was withdrawn from a cohort of these mice to induce regression of lung metastases, as previously reported [127], and lung metastases in mice on doxycycline were compared to residual metastatic foci 28 d following doxycycline withdrawal.

Lung metastases in tumor-bearing mice maintained on doxycycline were histopathologically similar to primary tumors and were composed of well-delineated epithelial and stromal compartments (Figure 3.10A). In contrast, residual YFP+ tumor cells were scattered throughout an eosinophilic stroma within metastatic foci that had regressed in the lungs of mice in which HER2/neu had been down-regulated. IF for Ki67 revealed that the majority of tumor cells within metastases were Ki67+ in mice on doxycycline, whereas metastatic tumor cells within residual foci were uniformly Ki67-negative (Figure 3.10B).

Consistent with our observations in local residual disease, staining for CD31 revealed that residual metastatic foci in the lungs of tumor-bearing mice were well-vascularized (Figure 3.10C).

Human breast cancer cells exhibit quiescence following targeted therapy

Given that murine mammary tumor cells exhibit cellular dormancy following oncogene pathway inhibition, we reasoned that residual human breast cancer cells that survive targeted oncogenic pathway inhibition might also be dormant. To address this possibility, we generated orthotopic xenografts from GFP-labeled BT474M1 breast cancer cells in *NOD/scid/Il2γnull* (*NSG*) mice that had been oophorectomized and implanted subcutaneously with 17β-estradiol pellets. All mice developed orthotopic tumors at sites of injection. Consistent with the identity of BT474M1 tumor cells as a HER2-dependent breast cancer cell line, IF revealed that tumor cells in the primary tumor expressed HER2 (Figure 3.11A). Tumors also gave rise to a large number of micrometastases, comprised of individual GFP+ tumor cells seeding the lungs of these mice (Figure 3.11B). In spite of analyzing a large number of tissue sections, metastases with more than 1 or 2 cells in isolation were not observed, suggesting that these tumor cells were not able to grow in the lung. Following the development of 1cm tumors, HER2 signaling was inhibited by

triplet anti-HER2 therapy comprised of Trastuzumab, Pertuzumab, and Lapatinib, and estrogen receptor (ER) signaling was down-regulated by removal of 17β-estradiol pellets (Figure 3.12A). Tumors treated with combination anti-HER2 and anti-ER therapy rapidly regressed to a non-palpable state, whereas untreated tumors continued to grow (Figure 3.12B). Mice were sacrificed 72 hr after treated tumors had regressed to a non-palpable state

Fluorescence microscopy performed on sections from mammary glands that had previously harbored tumors revealed scattered GFP^+ residual tumor cells (Figure 3.12C-D). In light of our observations of cellular dormancy in residual *HER2/neu-Prim1* tumor cells, we next asked whether residual BT474M1 tumor cells that survived targeted therapy are quiescent. IF for Ki67 revealed that scattered residual tumor cells were predominantly quiescent, with only ~2% expressing Ki67 (Figure 3.12C, E). In contrast, greater than 25% of untreated primary tumor cells were Ki67+. These findings suggest that residual human breast cancer cells that survive targeted therapy are quiescent, and provide a conceptual link between murine residual disease following oncogene down-regulation and residual human breast cancer cells following targeted therapy.

We next asked whether the microenvironment of quiescent residual human breast cancer xenografts was similar to that seen in dormant residual disease in the mouse. IF staining for CD31 in BT474M1 residual lesions revealed a rich vasculature (Figure 3.12D). Together, our findings suggest that quiescent residual tumor cells residing in a well-vascularized microenvironment may be a general feature of residual disease following oncogenic pathway inhibition.

Residual disease juxtaposed with normal mammary ducts is not dormant

While observing residual disease, labeled for 2 weeks with BrdU, 56d after doxycycline withdrawal in *HER2/neu-Prim1* orthotopic residual lesions in *nu/nu* mice, we identified a small number of residual lesions with regions of GFP+ tumor cells that were uniformly BrdU+ (Figure 3.13). We found that these tumor cells surrounded normal mouse mammary ducts, identified as cells that did not express GFP but expressed epithelial cytokeratins as stained by a pan-cytokeratin antibody (Figure 3.13). Staining for the mesenchymal tumor cell marker PDGFR-β

revealed that these tumor cells exhibited a mesenchymal phenotype (Figure 3.14A-C). To determine whether this phenomenon was an event that promoted tumor recurrence, we performed a recurrence assay using *HER2/neu-Prim1* orthotopic tumors in syngeneic *TAN* monotransgenic mice that either had the normal mammary epithelium surgically removed (fat pad clearing surgery) prior to puberty, or that had a sham surgery (Figure 3.14D). The mammary fat pads in mice that underwent fat pad clearing surgery would presumably not contain the normal mammary ducts that gave rise to these duct-juxtaposed proliferative foci, and thus allowed us to test whether this phenomenon promoted tumor recurrence. Mammary fat pad clearing did not delay the time to recurrence in this model, instead there was a trend towards an increased rate of recurrence in mice with fat pad clearing, although this result was not statistically significant (Figure 3.14E).

We then looked at local residual disease in the BT474M1-GFP model, and identified a similar phenomenon, wherein residual BT474M1-GFP tumor cells that were encapsulated inside of normal mouse mammary ducts (between red arrows) expressed much higher levels of Ki67 (white arrows) than the scattered BT474M1-GFP residual tumor cells that were not juxtaposed with normal mouse mammary duct (Figure 3.14 F-I).

Together, these findings suggest that signaling from normal parenchymal or stromal tissue may allow residual cells to enter the cell cycle. This may occur through signaling of growth factors (e.g. PDGF) through RTKs on the surface of residual tumor cells (e.g. PDGFR-β). This finding is consonant with a previously published role for microenvironmental signaling in impacting residual disease following targeted therapy [134].

Gene expression profiling of residual tumor cells reveals enrichment for genes associated with dormancy

Our finding that tumor cells surviving oncogenic pathway down-regulation are quiescent within a richly vascularized, non-hypoxic microenvironment suggested that these cells exist in a state of cellular, rather than angiogenic, dormancy. The in vivo molecular profile of dormant tumor cells that survive treatment and give rise to recurrent tumors has not been reported, and the

mechanisms maintaining these cells in a quiescent state are largely unknown. While disparate mechanisms that promote quiescence have been identified in some model systems, it is unclear whether these mechanisms are relevant to dormant tumor cells that survive therapy and give rise to recurrent tumors in vivo.

To assess the molecular phenotype of residual tumor cells and to identify candidate mechanisms potentiating cellular dormancy in the context of oncogenic pathway inhibition, we performed gene expression profiling on purified dormant residual tumor cells that were isolated using fluorescence-assisted cell sorting (FACS). Using no culture orthotopic *MTB/TAN/TTC/rYFP* residual lesions, we found that approximately 618 residual tumor cells were required in order to obtain the minimum 500pg RNA, with RNA integrity number >7.0, necessary for whole transcriptome amplification prior to genome expression profiling (Figure 3.15, Table 3.1). H2B-eGFP-labeled *HER2/neu-Prim1* or *Wnt1-Prim1* tumor cells were injected into the mammary fat pads of *nu/nu* mice and the resulting orthotopic primary tumors, MRLs at 28 d post HER2/neu down-regulation, and recurrent tumors were harvested, enzymatically digested, and GFP+ tumor cells were FACS-isolated. RNA isolated from GFP+ tumor cells, as well as GFP- stromal cells isolated from recurrent tumors, was used to perform microarray expression profiling (Figure 3.16A).

Principal component analysis revealed tight clustering between biological replicates from each FACS-isolated cell population, and further indicated that residual tumor cells exhibit a gene expression pattern that is unique compared to either primary or recurrent tumor cells (Figure 3.16B). To identify functionally related groups of genes that were differentially expressed within residual tumor cells compared to either primary or recurrent tumors, DAVID gene ontology analysis was performed on genes differentially up- or down-regulated in residual tumor cells compared to all other tumor cell types for both the *HER2/neu* and *Wnt1* models. Genes down-regulated in residual tumor cells in each of these data sets were dramatically enriched for ribosomal- and cell cycle-related gene sets (Table 3.2). Indeed, consistent with our observation that residual tumor cells are quiescent, transcripts for cyclins and cyclin-dependent kinases were

down-regulated as much as 90% in residual tumor cells (Figures 3.16C). As ribosomal biogenesis can be regulated by mTOR activity [135], we quantified mTOR pathway activity using a previously described method [136]. This revealed significant down-regulation of mTOR pathway activity in both HER2/neu and Wnt1 residual tumor cells compared to their corresponding primary or recurrent tumors (Figure 3.16D, E). Conversely, differentially up-regulated transcripts in residual tumor cells were enriched for secretory and ECM gene sets, including genes such as *fibronectin* (Table 3.3). Consistent with this, IF for collagen type-I and fibronectin revealed an abundant desmoplastic stroma within MRLs, whereas collagen type-IV expression was restricted to blood vessels (Figure 3.17A-F). Performing the same staining on tissue sections of residual no culture *MTB/TAN/TTC/rYFP* metastases and on BT474M1-GFP residual disease, we observed strikingly similar findings in both of these models to what was observed in local dormant HER2/neu residual disease (3.17G-O). Interestingly, while collagen type-IV was localized to blood vessels in BT474M1-GFP residual disease (Figure 3.17O), it was located throughout the whole ECM of residual metastases (Figure 3.17L).

In light of our observation that proliferation-related transcripts are markedly down-regulated in residual tumor cells, we sought to identify candidate mechanisms that might potentiate cellular dormancy. In this regard, the transcriptional repressor Dec2 exhibited the greatest up-regulation amongst all transcription factors, and the transcription factor Foxm1 was significantly down-regulated, in residual tumor cells in both the *HER2/neu* and *Wnt1* models. Previous in vitro analyses of dormant squamous carcinoma cell lines have suggested uPAR down-regulation, or up-regulation of TGFβ-II/TGFβR-III signaling, as a cause of a low ERK:p38 signaling ratio that up-regulates DEC and down-regulates FOXM1 [137, 138]. Consistent with these in vitro observations, we found that residual tumor cells in vivo up-regulated *Tgfbr3* (TGFβR-III), as well as its ligand *Tgfb2* (TGFβ-II), and markedly down-regulated *Plaur* (uPar) compared to either primary or recurrent tumor cells (Figure 3.16G).

Additionally, we found that Thrombospondin-1 (*Thsb1*) was up-regulated ~3-fold in residual tumor cells in both the *HER2/neu* and *Wnt1* models (p-values <0.01). Thsb1 has been implicated in

promoting dormancy of isolated breast cancer cells unable to form metastases upon seeding metastatic sites in xenograft models [137], however data supporting a role in dormant residual disease that survives therapy and gives rise to recurrence has not been reported.

Our finding – that molecular mechanisms mediating dormancy in disparate models intended to replicate the conditions of isolated DTCs might contribute to dormancy of residual tumor cells that survive therapy and give rise to recurrent tumors – suggested that quiescent tumor cells may possess similar molecular features in multiple biological contexts. In support of this possibility, we found that a dormancy gene expression signature, derived from a p38-induced in vitro dormancy model in combination with an in vivo angiogenic dormancy model [139], was significantly up-regulated in dormant residual tumor cells compared to all other cell types (Figure 3.16F).

Together, these findings reveal that dormant tumor cells surviving oncogenic pathway inhibition exhibit molecular features analogous to those observed in disparate models of dormant tumor cells. This suggests that the molecular mechanisms regulating dormancy may be conserved across dormant tumor cells derived from distinct cancer types and driven by distinct oncogenic pathways, and in differing biological contexts.

No culture models fail to recapitulate gene expression or genomic alterations of intact tumors

We next wanted to extend our findings to a model that had been minimally manipulated in vitro, so generated no culture orthotopic tumors in *nu/nu* mice using *MTB/TAN/TTC/rYFP* donors' primary tumors. Prior to extending our gene expression analysis findings to this model, we wanted to determine whether these orthotopic tumors faithfully recapitulated their quadtransgenic donor tumors. For mutational analysis, we performed both array comparative genomic hybridization (aCGH) to analyze copy number alterations and deletions, and whole exome sequencing to identify non-synonymous mutations. To analyze gene expression, as we had done before for the H2B-eGFP-labeled *HER2/neu-Prim1* and *Wnt1-Prim1* models, we sorted out YFP+DAPI-CD45- tumor cells from the primary intact donor tumor and from the resulting primary

orthotopic tumors, and performed gene expression analysis with RNA-Seq on the FACS-isolated tumor cells.

Surprisingly, although tumors from intact mice had been injected orthotopically into *nu/nu* mice, including both tumor and stromal cells that had never been cultured in vitro, there were significant and reproducible differences between the no culture orthotopic tumors and the primary intact donor tumors from which they arose. aCGH analysis revealed that orthotopic no culture tumors had up to several thousand-fold more copy number gains, but up to several-hundred fold fewer copy number loses (Table 3.4). Several copy number gains that were exclusively detected in orthotopic primary tumors were identified across all of the orthotopic tumors, independent of the donor tumor, but were not identified in any of the donor tumors (Figure 3.18A). Mutational profiling revealed a loss of non-synonymous mutations in the majority of orthotopic tumors arising from 2 of the 3 donor tumors, and a maintenance of the same number of mutations in orthotopic tumors from a third donor (Figure 3.18B). Unsupervised hierarchical clustering of these mutations revealed that the intact tumors clustered together along with 4 of the 9 orthotopic tumors, but that the remaining 5 orthotopic tumors with few mutations clustered separately (Figure 3.18C). PCA of gene expression analysis on FACS-isolated tumor cells revealed that intact donor tumors clustered together well, however they did not cluster with orthotopic tumors, and orthotopic tumors clustered together with other tumors from the same donor, but not across donors (Figure 3.18D). Gene expression pathway analysis of the pathways up-regulated and down-regulated in orthotopic tumors compared to primary tumors (Figure 3.18E) revealed that several pathways were repeatedly up-regulated in orthotopic tumors compared to intact tumors, including pathways associated with proliferation, Met, Myc, and TGF-β (Figure 13.8F).

Together these data reveal the surprising result that orthotopic tumors generated by injecting whole tumor digest directly from a donor tumor into a *nu/nu* mouse recipient do not recapitulate the mutational or gene expression profiles of their donor tumors. It seems unlikely that these mutations were newly acquired in the time between digestion of the primary tumor and growth of the resulting orthotopic tumors. Thus, a plausible explanation for these findings is the existence

of subclones that are well-suited for growth in the orthotopic model. One possible explanation for the recurrent copy number gains and losses is that these alterations promote tumor cell growth in an orthotopic setting by augmenting growth related pathways that are recurrently up-regulated, including Myc and Met. These may be present in orthotopic tumors and absent from intact tumors because of the particular barriers that need to be overcome for a tumor cell to grown during orthotopic injection, such as surviving digestion into a single cell suspension and surviving the host immune response to orthotopic injection. Given that an analogous strategy – injecting whole tumors from patients into immunocompromised mice - is used to generate PDX mouse models, these results warrant caution in interpreting results found from PDX models, and suggest that further study is necessary to better characterize PDX systems.

Gene expression profiling in the no culture orthotopic model

We next performed gene expression profiling on FACS-isolated tumor cells from primary, residual, and recurrent tumors in order to determine whether results in this model would recapitulate what we had seen in the *HER2/neu-Prim1* and *Wnt1-Prim1* models.

First we wanted to determine whether recurrent tumors in this model displayed a mesenchymal phenotype, as was the case for intact tumors and orthotopic *HER2/neu-Prim1* tumors. We analyzed the phenotype of recurrent tumors in *nu/nu* mice injected orthotopically with *MTB/TAN/TTC/rYFP* tumor cells that had not been cultured in vitro. While practically all recurrent tumors in intact *MTB/TAN* mice display a mesenchymal phenotype, a subset of recurrent tumors in the no culture orthotopic system displayed an epithelial phenotype as identified by IF (Figure 3.19A-C). These epithelial recurrent tumors appear to have reactivated the *HER2/neu* oncogene, as they display staining for HER2 by IF, and also express greater than 500,000-fold more luciferase activity than other recurrent tumors of the same size (Figure 3.19B, D). Thus, all recurrent tumors in subsequent analyses were first determined to have a mesenchymal phenotype prior to analysis.

For each of 8 donor tumors arising in *MTB/TAN/TTC/rYFP* mice, tumor cells from primary doxycycline-dependent tumors were injected orthotopically and bilaterally into 20 *nu/nu* mice on

doxycycline. All 320 injected sites developed primary tumors. 4 *nu/nu* mice with orthotopic primary tumors arising from each of the 8 donor tumors were sacrificed, tumors were enzymatically digested, and RNA was acquired from FACS-isolated primary tumor cells. The remaining 16 mice from each cohort were deinduced. For each cohort, 6 mice were sacrificed with residual lesions 28 days after doxycycline withdrawal, and all 12 residual lesions were digested and tumor cells were FACS-isolated for RNA. Over 80% of residual lesions did not yield a sufficient number of tumor cells necessary to perform WTA and gene expression profiling. Of the remaining 20 tumors (on 10 mice) in each cohort, only 4 cohorts developed at least 3 recurrent tumors with a mesenchymal phenotype. Recurrent tumor cells were FACS-isolated from all recurrent tumors that arose in these mice. From 8 donors, only 1 series of orthotopic primary, residual, and recurrent tumors had at least 3 residual lesion samples with >618 tumor cells, and at least 3 mesenchymal recurrent tumors.

Pathway analysis of FACS-isolated tumor cells revealed that, consistent with our observations in the *HER2/neu-Prim1* and *Wnt1-Prim1* models, mTOR pathway activity was significantly decreased in dormant tumor cells, whereas residual tumor cells also exhibited a high dormancy score (Figure 3.20). Also in line with our observations in the previously analyzed models, DAVID analysis of differentially expressed genes revealed up-regulation of genes associated with disulfide bonds, secreted and signal pathways, and down-regulation gene families associated with proliferation (Table 3.5). Interestingly, extracellular matrix gene groups were not up-regulated in this model, and residual tumor cells did not display enrichment for an EMT signature (Table 3.5). Consistent with our expectation that *Dec2* plays a critical role in dormant tumor cells, we found that it was the most up-regulated transcription factor in dormant tumor cells compared to primary and recurrent tumor cells.

These findings further corroborate several of our earlier observations in the *HER2/neu-Prim1* and *Wnt1-Prim1* models, in particular the down-regulation of biosynthetic activity in dormant tumor cells, and the possibility that *Dec2* plays a key role in regulating dormant residual tumor cells that survive oncogenic pathway inhibition.

Dormant residual *HER2/neu* tumor cells exhibit a mesenchymal phenotype

While residual disease in the setting of neoadjuvant chemotherapy or hormonal therapy in patients has been reported to be enriched for a mesenchymal phenotype [37], whether residual tumor cells are enriched for a mesenchymal phenotype following oncogene pathway inhibition is unknown. To address this, we investigated the expression of transcripts encoding epithelial and mesenchymal proteins in FACS-isolated tumor cells. Transcripts associated with a mesenchymal phenotype, including *Cdh2* (N-Cadherin), were up-regulated in residual *HER2/neu* tumor cells compared to primary tumor cells, whereas transcripts associated with an epithelial phenotype, including *Epcam,* and *Krt8* (Cytokeratin 8) were down-regulated in residual tumor cells (Figure 3.21A). In contrast, residual tumor cells in the *Wnt1* model did not up-regulate the mesenchymal marker *Cdh2*, but did up-regulate the epithelial markers *Epcam* and *Cdh1* (E-Cadherin), as well as the myoepithelial marker *Krt14* (CK14) (Figure 3.21B). Consistent with their expression in both myoepithelial and mesenchymal cells, *Pdgrfb* and *Acta2* were also up-regulated in both *HER2/neu* and *Wnt1* residual disease (Figure 3.21). Together, these data suggest that dormant residual disease in the *HER2/neu* model may be enriched for tumor cells that have undergone EMT, whereas dormant residual disease in the *Wnt1* model may be enriched for tumor cells with a myoepithelial phenotype.

To directly address the mesenchymal versus epithelial phenotype of residual disease in the *HER2/neu* and *Wnt1* models, we generated primary tumors and MRLs from H2B-eGFP labeled *HER2/neu-Prim1* and *Wnt1-Prim1* tumor cells. Sections of primary tumors and MRLs were stained for the luminal epithelial marker CK8 as well as the myoepithelial marker CK14. As anticipated, primary tumor cells in both the *HER2/neu* and *Wnt1* models expressed the epithelial marker CK8, and a subset of tumor cells in the Wnt1 tumor expressed the myoepithelial marker CK14 (Figure 3.22A, B). In contrast, residual *HER2/neu* tumor cells lost expression of epithelial marker CK8, whereas residual *Wnt1* tumor cells expressed CK8 and CK14 (Figure 3.22A, B).

To determine whether residual tumor cells might display a mesenchymal phenotype, we performed IF for the mesenchymal markers PDGFR-β and S100A4 (fibroblast-specific protein-1).

Residual *HER2/neu-Prim1* tumor cells expressed both PDGFR-β (Figure 3.22D) and FSP-1 (Figure 3.23). Tumor cells in the residual lesion that expressed either the mesenchymal marker S100A4 or the epithelial marker CD24 were admixed throughout the residual lesion (Figure 3.23).

To confirm the mesenchymal phenotype of *HER2/neu* residual tumor cells, we performed IF using a pan-cytokeratin antibody as well as 7 additional epithelial markers, including CK5, CK18, CK19, EpCAM, E-Cadherin, P-Cadherin, and p63. Whereas expression of each of these epithelial markers was detectable in normal mammary ducts, their expression was undetectable in the vast majority of residual *HER2/neu* tumor cells (Figure 3.22E-T). These data confirm that residual *HER2/neu* tumor cells have undergone EMT and generally lack expression of epithelial-specific markers.

The presence of tumor cells within HER2/neu residual neoplastic lesions that exhibit some features of EMT raised the possibility that a pre-existing population of mesenchymal-like tumor cells within HER2/neu primary tumors might be enriched in residual disease following oncogene down-regulation. To address this possibility, we performed multicolor flow cytometry on orthotopic H2B-eGFP-labeled *HER2/neu-Prim1* primary tumors and MRLs to evaluate expression of the epithelial marker CD24 in combination with either PDGFR-β or CD49e as markers of the mesenchymal-like phenotype. Flow cytometry identified rare populations of $CD24^{-}PDGFR\text{-}\beta^{+}$ and $CD24^{-}CD49e^{+}$ primary tumor cells that were dramatically enriched in MRLs following HER2/neu down-regulation (Figure 3.24A-D). We were also able to identify epithelial and mesenchymal populations in *HER2/neu-Prim1* tumor cells in vitro (Figure 3.24E), indicating that mesenchymal tumor cells in orthotopic tumors may arise either through EMT in vivo, or from this pre-existing population of mesenchymal tumor cells present in vitro.

Together, these findings demonstrate that HER2/neu-induced primary tumor cells are predominantly epithelial, but contain a small population of mesenchymal-like tumor cells that is dramatically enriched among those tumor cells that survive HER2/neu down-regulation and persist in MRLs in a dormant state. In contrast, both primary and residual tumor cells from Wnt1-induced tumors express epithelial markers characteristic of luminal and myoepithelial cells.

We wanted to determine whether residual tumor cells in intact quadtransgenic *MTB/TAN/TTC/rYFP* mice also exhibited EMT. IF staining for CK5 and CK8 revealed cytokeratin-negative, spindle-shaped tumor cells (Figure 3.25). Flow cytometry on intact residual tumor cells revealed a large population of YFP+CD45-DAPI- tumor cells that were EpCAM-CD24-PDGFRβ+CD49e+, consistent with a mesenchymal phenotype (Figure 3.26B-D).

Finally, we wanted to know whether residual tumor cells at metastatic sites also exhibited EMT in the *HER2/neu* model following doxycycline withdrawal. IF of tissue sections from residual metastases-bearing lungs in *nu/nu* mice with no culture orthotopic *MTB/TAN/TTC/rYFP* tumors revealed that residual tumor cells at metastatic sites had lost expression of CK8 and acquired expression of vimentin, consistent with an EMT phenotype, analogous to our observations for local residual disease (data not shown).

Mesenchymal tumor cell markers CD49e and PDGFR-β are markers of poor recurrence-free survival in HER2+ breast cancer

As tumor cells with mesenchymal features have been associated with treatment resistance and disease progression, we reasoned that elevated expression of CD49e and/or PDGFR-β in $HER2^+$ breast cancers might be associated with an increased risk of relapse in breast cancer patients. First, we asked whether residual human breast cancer showed down-regulation of the epithelial marker EpCAM and up-regulation of the mesenchymal marker CD49e. We found that EpCAM was significantly down-regulated, while CD49e was significantly up-regulated in residual disease (Figure 3.27A). Also, decreased EpCAM was correlated with increased CD49e expression in these samples (Figure 3.27B), consistent with an enrichment for mesenchymal disease following therapy. To test whether enrichment for mesenchymal markers was prognostic for poor RFS, we performed a multivariate meta-analysis across 14 publicly available clinical data sets containing information on HER2 status, gene expression data, clinical outcomes, tumor grade, and tumor size. 10-year RFS analysis was performed as a continuous function of the levels of expression of the mesenchymal markers (CD49e and PDGFR-β) and epithelial markers (EpCAM and CD24) that were previously used to identify epithelial and mesenchymal tumor cells by flow cytometry in

MTB;TetO-HER2/neu;TTC;rYFP mice.

Multivariate Cox hazard ratio analysis was performed on HER2+ breast cancers and was adjusted for tumor grade and tumor size. For patients with HER2+ breast cancer, expression of each of the mesenchymal markers *CD49e* and *PDGFR-β* was associated with a higher probability of recurrence in both 10-year RFS analyses, whereas neither EpCAM nor CD24 was associated with RFS after 10 years of follow-up (Figure 3.27C-F).

These results indicate that expression of *PDGFR-β* and *CD49e* are independent indicators for decreased RFS in patients with $HER2^+$ breast cancer and, when taken together with our findings in mice, raise the possibility that this association may reflect the presence of mesenchymal-like tumor cells that are resistant to treatment.

Dormant residual tumor cells express a mammary stem cell signature

Tumor cells that undergo EMT may acquire properties of normal mammary stem cells in some models [140]. Therefore, we evaluated whether residual tumor cells that survive oncogene down-regulation exhibit a gene expression profile similar to that of normal mammary stem cells. Indeed, in both *Wnt1-Prim1* and *HER2/neu-Prim1* models, genes reported to be enriched in human mammary stem cells were significantly up-regulated in dormant residual tumor cells compared to all other tumor cell types (Figure 3.28A, B, p-value HER2/neu: 2.7E-24, p-value Wnt1: 1.3E-14) [141]. Consistent with this, the normal human mammary stem cell marker CD10 [142] was up-regulated nearly 25-fold in HER2/neu residual tumor cells, and ~7-fold in Wnt1 residual tumor cells, compared to all other FACS-isolated tumor cells (Data not shown).

As stem-like properties of TICs may be distinct from those of normal mammary stem cells, we also investigated the expression of genes associated with neoplastic human mammary stem-like cells [143, 144]. Expression analysis revealed that residual tumor cells in both *HER2/neu* and *Wnt1* models were enriched for genes up-regulated in tumorigenic breast cancer stem-like cells (Figure 3.28C, D, p-value HER2/neu: 0.001, p-value Wnt1: 4.7E-21) [145]. Additionally, the putative breast cancer stem cell marker *Aldh1a3* was up-regulated in residual tumor cells in both

the *HER2/neu* (~2-fold (FDR<0.05) and *Wnt1* models (~5-fold (FDR<10^{-6}) [146] (data not shown). Collectively, these findings indicate that dormant tumor cells that survive HER2/neu or Wnt1 down-regulation exhibit a gene expression profile with similarities to normal mammary stem cells as well as tumorigenic breast cancer cells.

Residual Wnt1 tumor cells are enriched for cells with normal mammary stem cell properties

Our previous observations led us to propose that residual tumor cells may have properties of normal mammary stem cells, such as the ability to give rise to a mammary tree. Consistent with this possibility, we observed YFP+ structures with mammary duct morphology growing out of *MTB/TWNT/TTC/rYFP* no culture orthotopic residual lesions, in many residual lesions less than 10 weeks after doxycycline withdrawal (Figure 3.29A). These structures were not observed in over 30 *MTB/TAN/TTC/rYFP* residual lesions more than 32 weeks after deinduction (Figure 3.29B). A key feature of normal mammary stem cells is their ability to reconstitute a mammary ductal tree when injected into a mammary fat pad that has been cleared of epithelial cells. To determine whether residual tumor cells were enriched for cells with normal mammary stem cell properties, we injected 1,000 tumor cells from either primary tumors or residual lesions into cleared mammary fat pads in syngeneic TAN/TTC/rYFP mice. After 2 months, more than half of the sites injected with residual lesion tumor cells formed mammary epithelial ductal trees, whereas only 2 of 12 sites formed ductal trees when injected with tumor cells from a primary tumor (Figure 3.29 C-D).

Residual HER2/neu tumor cells are not enriched for primary TICs

Our observations that residual tumor cells are capable of giving rise to recurrent tumors, possess mesenchymal features, and are enriched for transcripts associated with normal mammary stem cells as well as tumorigenic breast cancer cells, suggested the possibility that residual tumor cells might be functionally enriched for TICs. To test this hypothesis in a model with minimal ex vivo manipulation, we used *MTB;TetO-HER2/neu;TTC;rYFP* mice to isolate fluorescently labeled tumor cells in autochthonous tumors that had not been cultured in vitro.

To validate this model, we first addressed whether residual tumor cells in *MTB;TetO-HER2/neu;TTC;rYFP* mice were enriched for mesenchymal tumor cells compared to primary tumor cells, as we had observed in *HER2/neu-Prim1* orthotopic tumors. Indeed, primary tumor cells in *MTB;TetO-HER2/neu;TTC;rYFP* mice were predominantly CD24+EpCAM+Cd49e-PDGFRβ- (7.4-fold enrichment vs. residual lesion, p-value <0.001), demonstrating an epithelial phenotype, whereas residual tumor cells were predominantly CD24-EpCAM-CD49e+PDGFRβ+ (3-fold enrichment vs. primary tumor, p-value <0.001), reflecting a mesenchymal phenotype (Figure 3.26B-E). These findings indicate that residual lesions derived from primary tumors arising in *MTB;TetO-HER2/neu;TTC;rYFP* mice, as well as residual lesions derived from *HER2/neu-Prim1* orthotopic tumors tumor cells, are enriched for tumor cells with mesenchymal-like properties.

Next, we asked whether residual tumor cells are functionally enriched for TICs by performing limiting dilution experiments on YFP+CD45-DAPI- tumor cells isolated from primary tumors (n=3) or residual lesions (n=3) arising in *MTB;TetO-HER2/neu;TTC;rYFP* mice. Isolated viable tumor cells were injected into the mammary fat pads of *nu/nu* mice on doxycycline, and mice were monitored for 4 months for tumor development. TIC frequency was calculated based upon the fraction of mice that developed tumors when injected with a given number of tumor cells [147]. Whereas injection of 50,000 tumor cells from each of the 3 primary tumors tested resulted in tumor formation at 100% of injected sites, injection of an equivalent number of tumor cells isolated from 2 of the 3 residual lesions tested failed to give rise to any tumors at any of the 8 sites injected after 4 months (Table 3.6). The remaining residual lesion exhibited a TIC frequency similar to that observed for one of the primary tumors. These findings raise the possibility that residual tumor cells may not be enriched for TICs compared to primary tumor cells.

The extremely wide range of TIC frequencies observed among primary tumors, and among residual lesions, suggested that factors such as somatic genetic heterogeneity between tumors might influence TIC frequency. To control for this possibility, we generated matched pairs of syngeneic orthotopic primary tumors and residual lesions by orthotopically injecting tumor cells

from doxycycline-dependent primary tumors arising in *MTB;TetO-HER2/neu;TTC;rYFP* mice into *nu/nu* mice on doxycycline. We then withdrew doxycycline from a cohort of mice bearing primary tumors to generate syngeneic orthotopic residual lesions from the same donor tumor.

Using these syngeneic pairs of orthotopic primary tumors and residual lesions, we performed limiting dilution experiments to quantify the TIC frequency in primary tumors and residual lesions generated from the same intact donor tumor. As before, while substantial variation was observed in TIC frequencies for different primary tumors, in no case were TICs enriched in tumor cells isolated from residual lesions compared to tumor cells isolated from the corresponding syngeneic primary tumor (Table 3.7). Specifically, for the two donor primary tumors analyzed, the TIC frequencies of primary tumor cells were ~18-fold and 1,000-fold higher than the TIC frequencies in residual tumor cells from the same donor tumor, and these results were statistically significant.

As HER2/neu residual lesions were enriched for mesenchymal tumor cells compared to primary tumors, we considered the possibility that mesenchymal tumor cells within residual lesions might not be enriched for TICs, but that residual epithelial tumor cells – which constitute only a minority of tumor cells in residual lesions – might exhibit an increased TIC frequency. To address this possibility, we isolated epithelial (EpCAM+CD49e-) tumor cells from an intact *MTB;TetO-HER2/neu;TTC;rYFP* primary tumor and residual lesion, and performed limiting dilution experiments to measure the TIC frequency of epithelial tumor cells from primary tumors and residual lesions.

Consistent with our observations above quantifying TIC frequency in HER2/neu primary tumors and residual lesions, we found that epithelial tumor cells from residual lesions were not enriched for TICs compared to epithelial tumor cells from primary tumors (Table 3.8). These findings suggest that the failure to observe TIC enrichment among residual tumor cells is not a consequence of changes in the epithelial vs. mesenchymal composition of primary tumors compared to residual lesions.

When taken together, our observations indicate that residual tumor cells that survive HER2/neu down-regulation in HER2/neu-induced mammary tumors are not enriched for TICs compared to primary tumor cells.

Residual Wnt1 tumor cells are not enriched for primary TICs

We next asked whether the observation that HER2/neu residual tumor cells are not enriched for TICs would also be true for Wnt1-induced mammary tumors using an analogous approach in *MTB;TetO-Wnt1;TTC;rYFP* mice. As CD24+Thy1+ mammary tumor cells from *MMTV-Wnt1* mice have previously been reported to possess TIC properties, we first performed a limiting dilution experiment to ask whether CD24+Thy1+ tumor cells in Wnt1-driven primary tumors were enriched for TICs compared to non-CD24+Thy1+ tumor cell populations [148, 149]. Consistent with prior reports, we found that CD24+Thy1+ tumor cells were enriched ~10-fold for TICs compared to non- CD24+Thy1+ tumor cell subsets (Figure 3.26F).

To assess whether residual Wnt1 tumor cells were enriched for TICs, we next determined whether residual tumor cells that had survived Wnt1 pathway down-regulation were enriched for CD24+Thy1+ tumor cells compared to primary tumor cells. Flow cytometry performed on primary tumors and residual lesions from *MTB;TetO-Wnt1;TTC;rYFP* mice revealed that tumor cells within residual lesions were enriched ~8-fold for CD24+Thy1+ tumor cells compared to primary tumors (Figure 3.26G-H, p-value = 0.002). Indeed, whereas <5% of primary tumor cells were CD24+Thy1+, ~40% of residual tumors cells exhibited a CD24+Thy1+ phenotype.

The above results suggested that residual tumor cells surviving oncogenic pathway inhibition in *MTB;TetO-Wnt1;TTC;rYFP* mice are enriched for cells with a cell surface phenotype that has been associated with TICs in primary tumors. However, these experiments did not address whether residual tumor cells are, in fact, functionally enriched for TICs. To address this question, we performed limiting dilution studies using sorted YFP+CD45-DAPI-tumor cells isolated from primary tumors and residual lesions arising in *MTB;TetO-Wnt1;TTC;rYFP* mice. Contrary to expectations based upon enrichment for CD24+Thy1+ cells in residual lesions, we observed a 4-fold decrease in TIC frequency in residual tumor cells compared to primary tumor cells (Table

3.9). Thus, despite our observations that CD24+Thy1+ primary tumor cells are enriched 10-fold for TICs compared to non-CD24+Thy1+ tumor cells, and that CD24+Thy1+ tumor cells are enriched 8-fold in residual lesions compared to primary tumors, we did not observe functional enrichment for TICs in Wnt1 residual disease.

While this result was consistent with our observation that residual HER2/neu tumor cells are not enriched for TICs, we wished to extend these findings by addressing the possibility that genetic heterogeneity among tumors might result in differing TIC frequencies for different donor tumors. Accordingly, we generated syngeneic pairs of orthotopic primary tumors and residual lesions in *nu/nu* mice from individual tumors arising in *MTB;TetO-Wnt1;TTC;rYFP* mice using an approach analogous to that performed above for *MTB;TetO-HER2/neu;TTC;rYFP* mice. Limiting dilution studies were then performed using YFP+CD45-DAPI- tumor cells isolated from syngeneic orthotopic primary tumors or residual lesions. This analysis revealed that, for each of the donor tumors tested, residual Wnt1 tumor cells exhibited ~ 7- to 11-fold lower TIC frequencies compared to primary tumor cells (Table 3.10). These findings further support the conclusion that residual tumor cells are not enriched for TICs relative to primary tumor cells in Wnt1-induced mammary tumors, and are consistent with the lack of enrichment for TICs that we observed in residual tumor cells in HER2/neu-induced mammary tumors.

In aggregate, our data using tumor cells isolated directly from intact mice, or from syngeneic pairs of orthotopic primary tumors and residual lesions, suggest that residual tumor cells are not enriched for TICs in either the HER2/neu or Wnt1-induced tumor models.

Residual disease may be enriched for recurrent tumor TICs

Despite our finding that residual tumor cells do not appear to be enriched for TICs compared to primary tumor cells in the setting of oncogene activation (i.e. when injected into *nu/nu* mice maintained on doxycycline), we considered the possibility that residual tumor cells might be enriched for TICs in the setting of oncogene inactivation. If true, this would be consistent with our observation that – when maintained off doxycycline for long periods of time – mice bearing fully regressed HER2/neu or Wnt1 mammary tumors eventually develop spontaneous tumor

recurrences that do not express the initiating oncogene (e.g. HER2/neu or Wnt1) [108, 121]. That is, assays for TICs performed in the presence of oncogene activation may detect TICs capable of forming primary tumors, whereas assays for TICs performed in the absence of oncogene activation may detect TICs capable of forming recurrent tumors. In this regard, enrichment for cells in primary tumors capable of giving rise to recurrent tumors (i.e. recurrent tumor TICs) might occur during primary tumor regression induced by doxycycline withdrawal by virtue of the apoptotic elimination of primary tumor cells that could not survive oncogenic pathway down-regulation.

To address this question, we generated orthotopic primary tumors from H2B-eGFP *HER2/neu-Prim1* tumor cells and isolated primary tumor cells from tumor-bearing mice on doxycycline, as well as residual tumor cells from mice bearing fully regressed tumors maintained off doxycycline. Each set of primary or residual tumor cells was injected into cohorts of *nu/nu* mice that were maintained either on or off doxycycline.

Consistent with our observations in intact *MTB;TetO-HER2/neu;TTC;rYFP* mice, we did not observe enrichment for TICs among residual tumor cells when injected into mice on doxycycline. In contrast, when injected into *nu/nu* mice not on doxycycline, we observed a ~7-fold increase in TIC frequency among residual tumor cells compared to primary tumor cells (Table 3.11). These findings raise the intriguing possibility that TICs for primary tumors and recurrent tumors may be distinct and that HER2/neu down-regulation results in enrichment for recurrent tumor TICs, but not primary tumor TICs.

Residual lesion expression of proteins for transcripts up-regulated in residual disease

Identification of dormant tumor cells in humans is challenging in large part due to the lack of positive markers for dormancy. Given our observation that particular transcripts were repeatedly up-regulated in residual tumor cells compared to primary and recurrent tumor cells, we wanted to know whether these might serve as markers of dormancy tumor cells. The majority of proteins whose transcripts were up-regulated in residual disease showed expression in both normal mammary epithelial cells and residual lesion cells (Figure 3.30A). Dec2 was expressed at

various levels in tumor cells in primary tumors, and showed slight enrichment in nuclei (Figure 3.30B, left). In contrast, Dec2 was expressed at high levels in the nucleus of residual lesion tumor cells, consistent with a role for Dec2 in transcriptional regulation of dormant residual tumor cells (Figure 3.30B, left). These findings suggest that nuclear expression of Dec2 may serve as a protein marker for dormant tumor cells in clinical samples.

Discussion

Defining the biology of MRD is an important, but elusive, goal with important implications for the prevention and treatment of recurrent cancers. Using genetically engineered mouse models for human breast cancer driven by two different oncogenic pathways, we report in vivo evidence that tumor cells surviving targeted therapy exhibit cellular dormancy following oncogenic pathway. Residual tumor cells exhibit reversible cell cycle arrest following oncogenic pathway inhibition despite the presence of a robust and functional vasculature, irrespective of the presence or absence of an adaptive immune system, and without exhibiting signs of senescence. Consistent with this, gene expression profiling of residual tumor cells isolated in vivo following oncogenic pathway inhibition revealed clear evidence of cellular quiescence. In an analogous manner, we found evidence for cellular dormancy in mice bearing xenografted human breast cancer cells treated with targeted therapies, and in mice bearing residual metastatic disease following oncogenic pathway inhibition – novel observations of particular clinical interest given that distant recurrence is the primary cause of mortality among breast cancer patients. In aggregate, we conclude that residual tumors cells that survive targeted down-regulation of a dominant oncogenic pathway exist in a state of cellular dormancy, and that recurrent tumor outgrowth in this context is limited neither by angiogenic insufficiency nor by the immune system.

In providing the first expression profiling analysis of purified residual tumor cells and along with matched primary and recurrent tumor cells, one of the most important findings of the present study is its clear demonstration that residual tumor cells represent a distinct tumor cell state that has little resemblance to actively growing primary or recurrent tumors. This has significant implications for both the detection and treatment of residual disease. Given the unique

phenotype of residual tumor cells, it seems likely that phenotypic markers specific to primary or recurrent tumor cells may fail to detect some – or perhaps even many –residual tumor cells. In an analogous manner, therapeutic approaches predicated on the increased proliferative or metabolic activity commonly associated with actively growing tumor cells may fail to impact the long-term survival or regrowth of residual tumor cells that are quiescent. These findings extend in vitro findings that residual tumor cells express a unique phenotype [150], and further indicate a need for strategies to more effectively detect and target residual disease.

Notably, dormant residual tumor cells in both the Wnt1 and HER2/neu models were enriched for expression signatures associated with normal, as well as neoplastic, mammary stem-like cells. Residual tumor cells in each of these models were also enriched for phenotypes reported to be associated with TICs – EMT in the case of HER2/neu, and a CD24+Thy1+ cell surface phenotype in the case of Wnt1. Despite these suggestive phenotypic traits, however, functional studies revealed that residual tumor cells were not enriched for primary tumor TICs, whether isolated directly from transgenic mice or from mice bearing syngeneically paired orthotopic primary tumors and residual disease. These findings suggest that the phenotypes of TICs may differ in primary tumors and MRD, and imply that caution may be indicated in attempting to infer functional properties of residual tumor cells based upon cell surface phenotypes defined in TICs in primary tumors.

Although residual tumor cells failed to show enrichment for TICs relative to primary tumor cells in the setting of oncogene activation, tumor cells isolated from residual lesions were enriched for TICs capable of giving rise to recurrent tumors in the setting of oncogene inhibition. This intriguing finding suggests that the evolution of tumors, from primary to recurrent, may be driven by distinct TIC populations. The possibility that different TIC populations support primary versus recurrent tumor growth is supported by our prior findings that recurrent tumors in *MTB;TetO-HER2/neu* mice exhibit a phenotype distinct from primary tumors [108]. This, in turn, is consistent with clinical reports indicating that recurrent tumors may exhibit a phenotype distinct from primary tumors [37, 123, 124]. In aggregate, our data suggest that the underlying basis for this

phenotypic shift may result from a change in the TIC populations driving primary versus recurrent tumor growth.

Interestingly, while residual disease in both HER2/neu and Wnt1 mouse models exhibited a gene expression profile enriched for features of normal and neoplastic human mammary stem-like cells, we only observed enrichment for tumor cells with an EMT phenotype in HER2/neu residual disease, and not in Wnt1 residual disease, despite the association between EMT and stem-like cells reported in some contexts [140]. While some clinical reports indicate that residual disease may be enriched for tumor cells with a mesenchymal phenotype [37], observations in circulating tumor cells suggest that residual tumor cells with an epithelial phenotype disease may be enriched in certain therapeutic settings [38]. Consequently, our findings that HER2/neu residual disease is enriched for cells exhibiting EMT, whereas Wnt1 residual disease is not, and that neither HER2/neu nor Wnt1 residual disease is enriched for primary tumor TICs, suggests that the properties of TICs, mammary stem cells and EMT may not be tightly linked or, at the very least, are likely to be context-dependent.

Despite the dramatic differences between the HER2/neu and Wnt1 oncogenic pathways, and between the cellular phenotype of tumors driven by each of these oncogenes [121, 127], residual tumor cells in both models exhibited a prolonged, but reversible, cell cycle arrest following oncogenic pathway inhibition. Indeed, in each model greater than 90% of primary tumor cells – but fewer than 10% of residual tumors cells – entered S-phase over a two-week period. Nevertheless, upon oncogene reactivation for as little as 72 h, residual tumor cells in each model re-entered the cell cycle and entered S-phase at rates comparable to primary tumor cells. While prior reports have demonstrated the presence of residual tumor cells that are non-proliferative following oncogenic pathway inhibition, neither senescence nor angiogenic insufficiency have been addressed as contributing factors. This, coupled with the absence of a lineage tracing fluorescent marker to unambiguously label residual tumor cells, as well as the fact that tumors do not recur in these models, has hampered definitive identification of the characteristics of residual disease and the determination of whether cellular dormancy is a significant contributing factor to

preventing tumor outgrowth [92, 93]. Nonetheless, the identification of non-proliferative residual disease following oncogenic pathway inhibition in Myc-driven pancreatic cancers and in Hedgehog-driven basal cell carcinomas highlights the possibility that dormancy is a conserved response to targeted therapy independent of the oncogene or cell of origin.

Remarkably, despite the fact that prior studies investigating dormancy have been conducted in disparate experimental models, including chicken chorioallantoic membrane assays and in vitro cell culture, we find strong evidence for similarities between these previously identified pathways and gene expression signatures and properties of dormant tumor cells that we have identified in two separate genetically engineered mouse models for dormant residual disease capable of giving rise to recurrent tumors. Indeed, the remarkable similarities between the gene expression profiles of residual tumor cells from HER2/neu and Wnt1 mammary tumors, coupled with significant overlap in dormancy-related gene expression profiles between these models and previously described models of X and Y cancers, raises the intriguing possibility that dormancy may be regulated by similar molecular mechanisms independent of the driving oncogene or cancer type.

Importantly, though dormant disseminated tumor cells are often assumed to be the source from which recurrent tumors arise, little preclinical or clinical evidence exists demonstrating a precursor-product relationship between dormant isolated tumor cells and recurrence. In this regard, it is possible that dormant MRD in the bone marrow is correlated with systemic disease burden, but that these cells themselves do not give rise to recurrent tumors. In contrast, the efficacy of adjuvant chemotherapy in delaying recurrence demonstrates that subclinical proliferative metastases may underlie disease recurrence in some patients. As such, our observation that primary tumor cells that survive oncogenic pathway inhibition exist in a dormant state prior to recurrence provides new evidence that dormancy is a potential therapeutic target with direct relevance to preventing tumor recurrence.

Remarkable similarities in findings from Wnt1 and HER2 models and its implications for generalizability

While inter-tumor heterogeneity, due to a plethora of oncogenic drivers within and across tissue types, represents a major obstacle for cancer treatment, the remarkable similarity between gene expression profiles of residual disease in the HER2/neu and Wnt1 models suggests that therapeutic strategies useful for targeting dormant residual disease in tumors driven by one oncogene may apply to dormant residual disease in tumors driven by other oncogenes. Strikingly, in spite of our observation of EMT in only one of two residual disease models, the top 10 clusters of down-regulated genes, and the top 3 clusters of up-regulated genes, ranked by DAVID enrichment score for either HER2/neu or Wnt1 residual disease were also found in the top clusters from the other genotype. Therapeutic strategies suitable for targeting dormant tumor cells may therefore be more productively focused on pathways regulated similarly across models driven by different oncogenes, or arising from different cells of origin. For example, strategies to eliminate dormant residual tumor cells might target secreted proteins or extracellular matrix components that are up-regulated in dormant disease, thereby potentially disrupting pro-survival tumor cell-microenvironment interactions.

Together, our observations indicate that residual cancer cells exhibit a unique phenotype that may underlie resistance to therapy, as well as provide insights into more effective therapeutic strategies.

Figure 3.1. Kinetics of Tumor Recurrence Suggest a Latent Phase

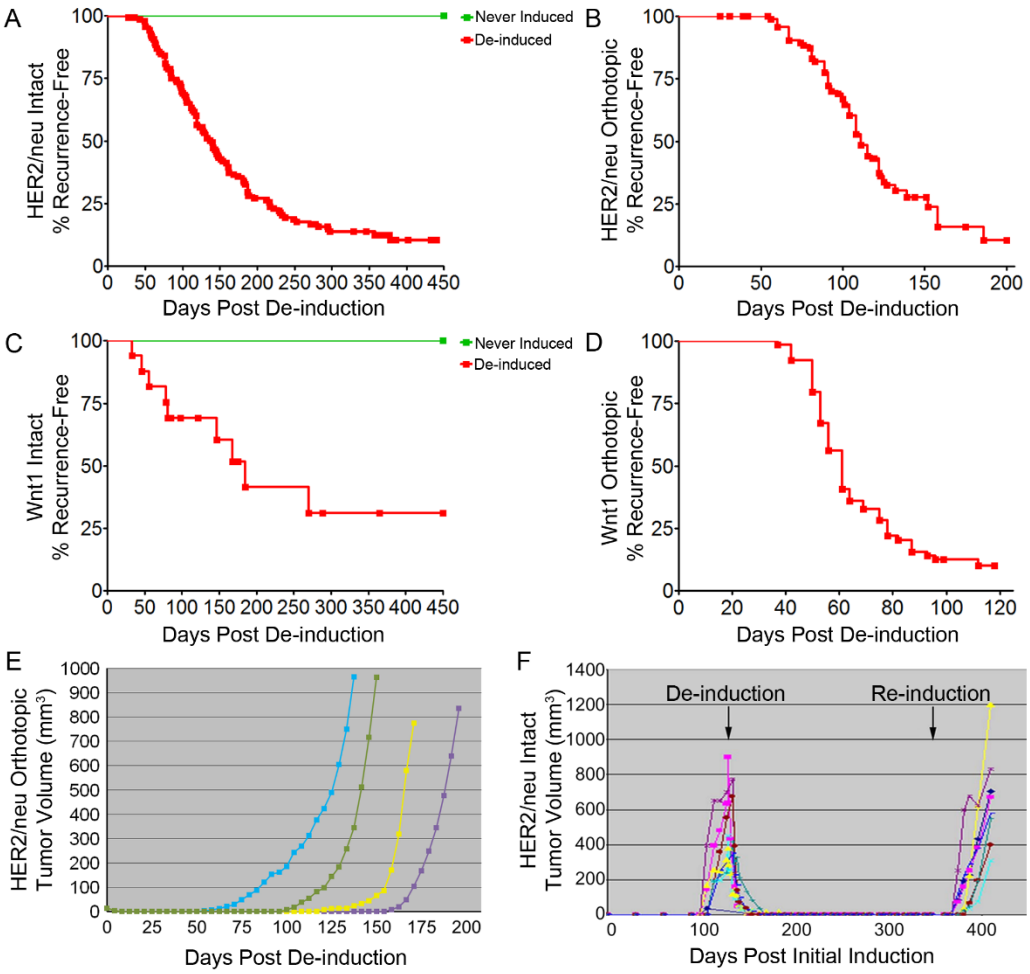

(A-D) Kaplan-Meier curves showing recurrence-free survival (RFS) for (A) *MTB;TetO-HER2/neu* intact, (B) *HER2/neu-Prim1* orthotopic, (C) *MTB;TetO-Wnt1* intact, and (D) *Wnt1-Prim1* orthotopic models. (E) Recurrent tumor growth curves from *MTB;TetO-HER2/neu* orthotopic tumors with different recurrence latencies. (F) Tumor growth curves following doxycycline re-administration to intact *MTB;TetO-HER2/neu* mice that previously harbored primary tumors that had not spontaneously recurred.

Figure 3.2. Identification of Residual Tumor Cells Following Oncogenic Pathway Inhibition

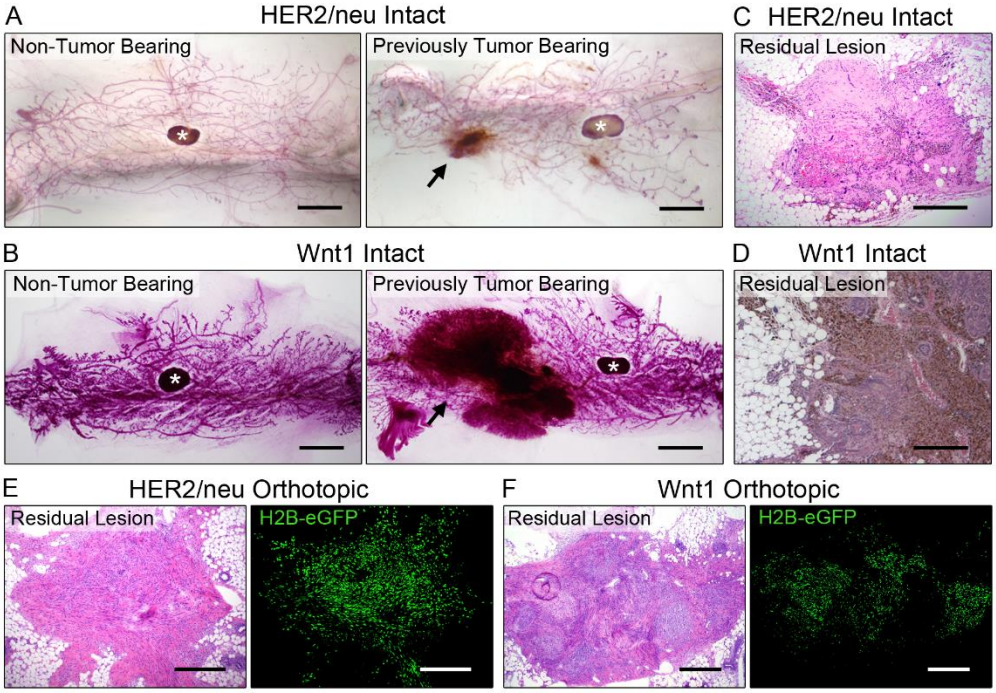

(A, B) Carmine staining of mammary glands following oncogenic pathway inhibition in bitransgenic (A) *MTB;TetO-HER2/neu* and (B) *MTB;TetO-Wnt1* models. Lymph nodes are designated with an asterisk (*). (C, D) Hematoxylin and eosin-stained sections of intact (C) *MTB;TetO-HER2/neu* and (D) *MTB;TetO-Wnt1* MRLs. (E, F) Hematoxylin and eosin-stained sections (left) and fluorescence microscopy of H2B-eGFP-labeled tumor cells (right) in orthotopic (E) *HER2/neu-Prim1* and (F) *Wnt1-Prim1* MRLs. Scale bars (A, B): 750μm, (C-F): 250μm.

Figure 3.3. Systemic Metastases with Intracardiac Injection of *HER2/neu-Prim1* Tumor Cells

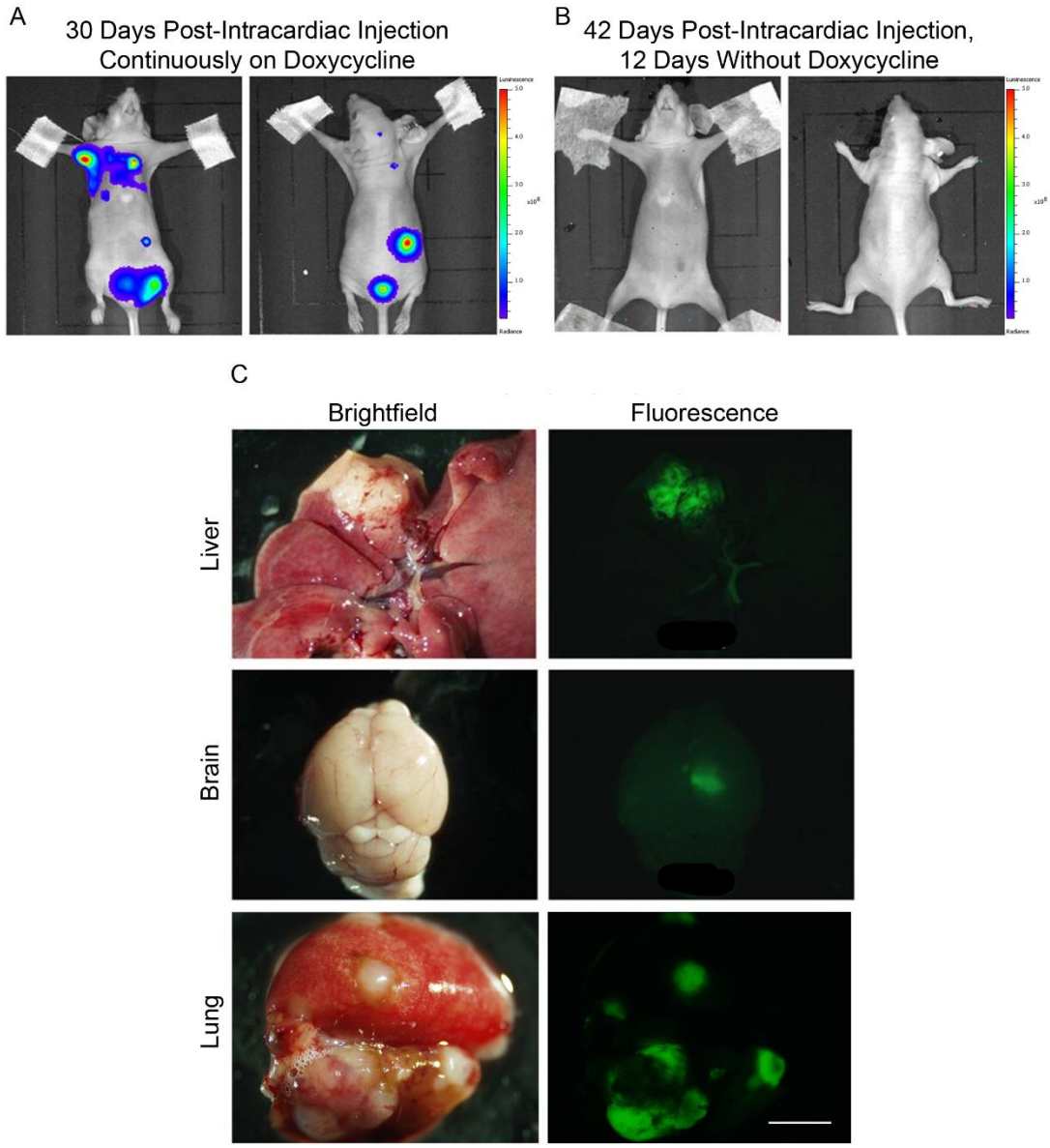

(A, B) Bioluminescence imaging of a *nu/nu* mouse following intarcardiac injection of *HER2/neu-Prim1* tumor cells either (A) on doxycycline continuously for 30 days following injection or (B) 12 days after doxycycline withdrawal. (C) Brightfield (left) and GFP fluorescence (right) imaging of liver (top), brain (center) or lungs (bottom) of a *nu/nu* mouse on doxycycline sacrificed 30 days after intracardiac injection of *HER2/neu-Prim1* tumor cells. Scale bar (C): 750μm

Figure 3.4. Systemic Metastases in Cre-driven YFP and tdTomato Fluorescent Reporter Mice

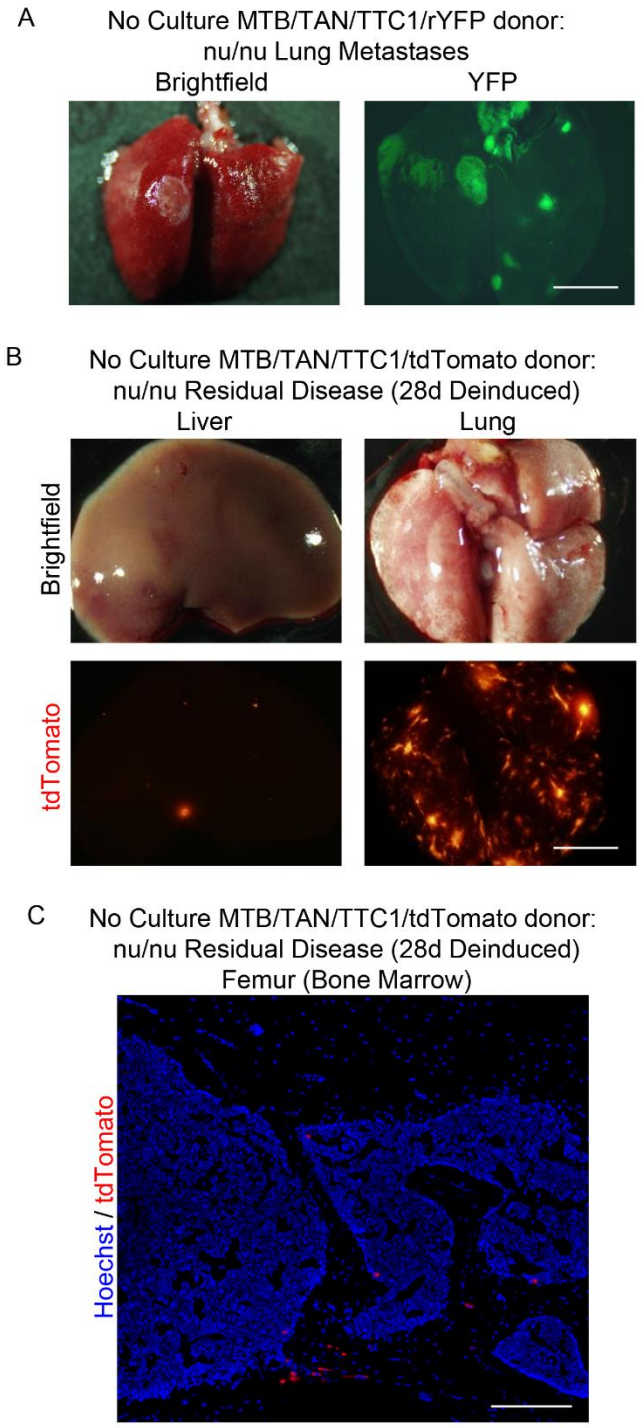

(A) Brightfield (left) and YFP fluorescence (right) images of lungs from an *MTB/TAN/TTC/rYFP*

mouse on doxycycline with lung metastases. (B) Brightfield (top) and tdTomato fluorescence (bottom) images of liver (left) and lung (right) bearing residual metastases 28d after doxycycline withdrawal. (C) Fluorescence microscopy image of Hoechst and tdTomato fluorescence in a tissue section showing residual DTCs 28d after doxycycline withdrawal. Scale bar (A-B): 750μm, (C): 100μm

Figure 3.5. Peripheral Blood Leukocytes in *MTB/TAN/TTC/rYFP* Model Express YFP

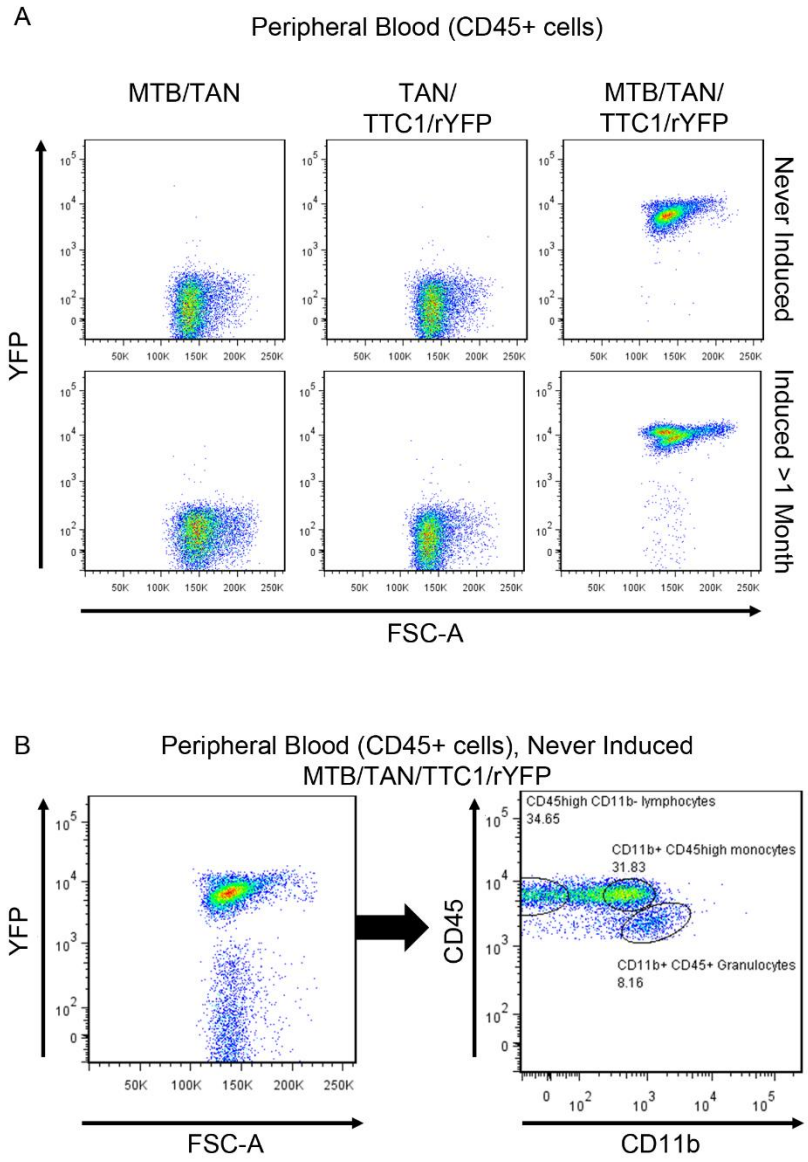

(A) Flow cytometry of unstained FSC-A^{hi} peripheral blood leukocytes from *MTB/TAN* (left), *TAN/TTC/rYFP* (middle), or *MTB/TAN/TTC/rYFP* (right) mice that are either never induced (top) or induced for more than 1 month (bottom). (B) Flow cytometry of FSC-A^{hi} peripheral blood leukocytes from *MTB/TAN/TTC/rYFP* that were never induced and were stained for CD45 and CD11b.

Figure 3.6. CTCs and DTCs in Orthotopic *HER2/neu-Prim1* Model

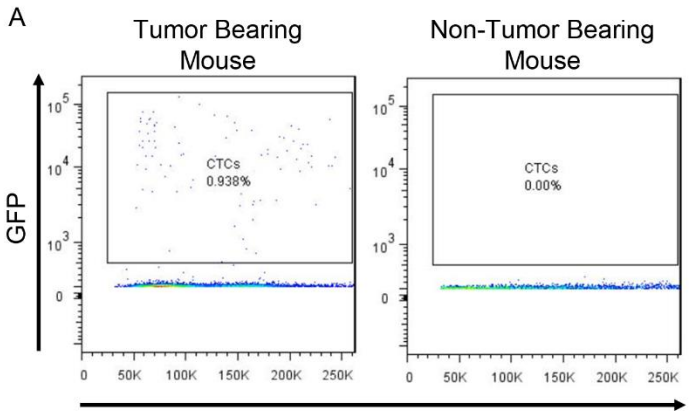

B

CTC Count per Mouse

Sample	%CTCs in sample	#CTCs/mL
Tumor bearing 1	0.066%	52
Tumor bearing 2	0.026%	16
Tumor bearing 3	47.7%	42412
Tumor bearing 4	0.938%	360
Tumor bearing 5	3.42%	3080
Tumor bearing 6	0.110%	28
Non-Tumor bearing 1	0	0
Non-Tumor bearing 2	0	0
Non-Tumor bearing 3	0	0
Non-Tumor bearing 4	0	0

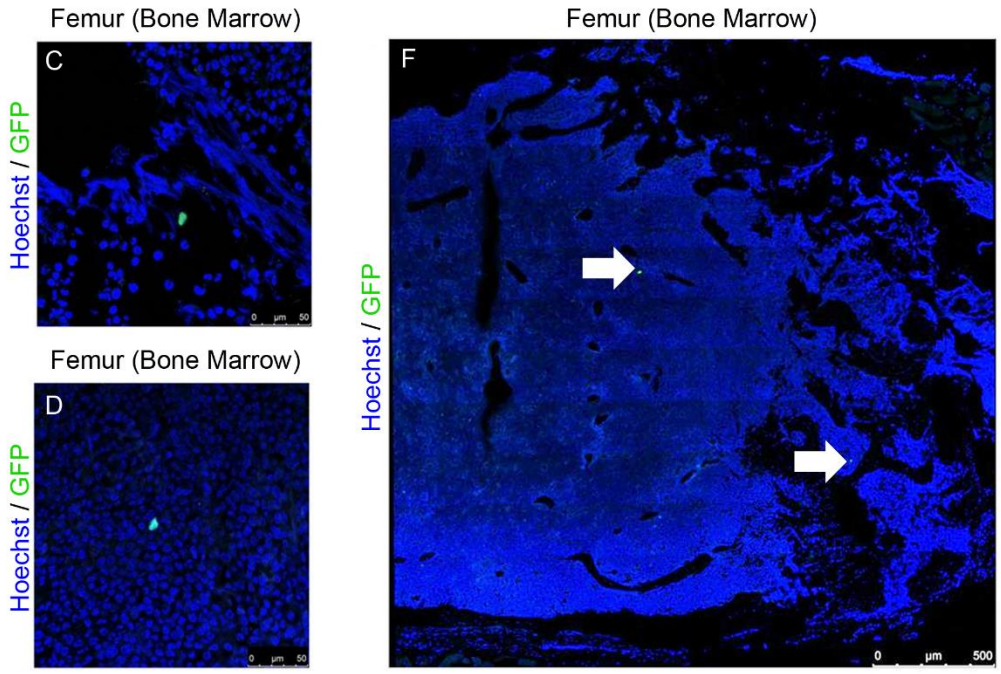

G

Tumor Stage:	Small Primary	Large Primary	4 week post-DI	6 week post-DI	8 week post-DI	Recurrent
Average # CTCs/ml	0.4	1.7	0.275	0.5	1.5	1.2
Average #DTCs/ml	1.4	4.625	0.5	1.6	2.8	3

(A) Flow cytometry of unstained peripheral blood from non-tumor bearing *nu/nu* mouse (left) and H2B-eGFP-labeled *HER2/neu-Prim1* tumor bearing *nu/nu* mouse (right) for GFP vs FSC-A. (B) Quantification of the number of GFP+ CTCs recovered from intracardiac puncture of tumor

bearing or non-tumor bearing mice. (C-F) Fluorescence microscopy imaging of Hoechst and GFP fluorescence in tissue sections showing GFP+ DTCs in mouse femurs femur (DTCs are at arrows in panel F). (G) Quantification of the average number of ostensible CTCs recovered per ml of blood across mice bearing H2B-eGFP-labeled *HER2/neu-Prim1* primary tumors, residual disease, or recurrent tumors.

Figure 3.7. Residual Tumor Cells are Quiescent

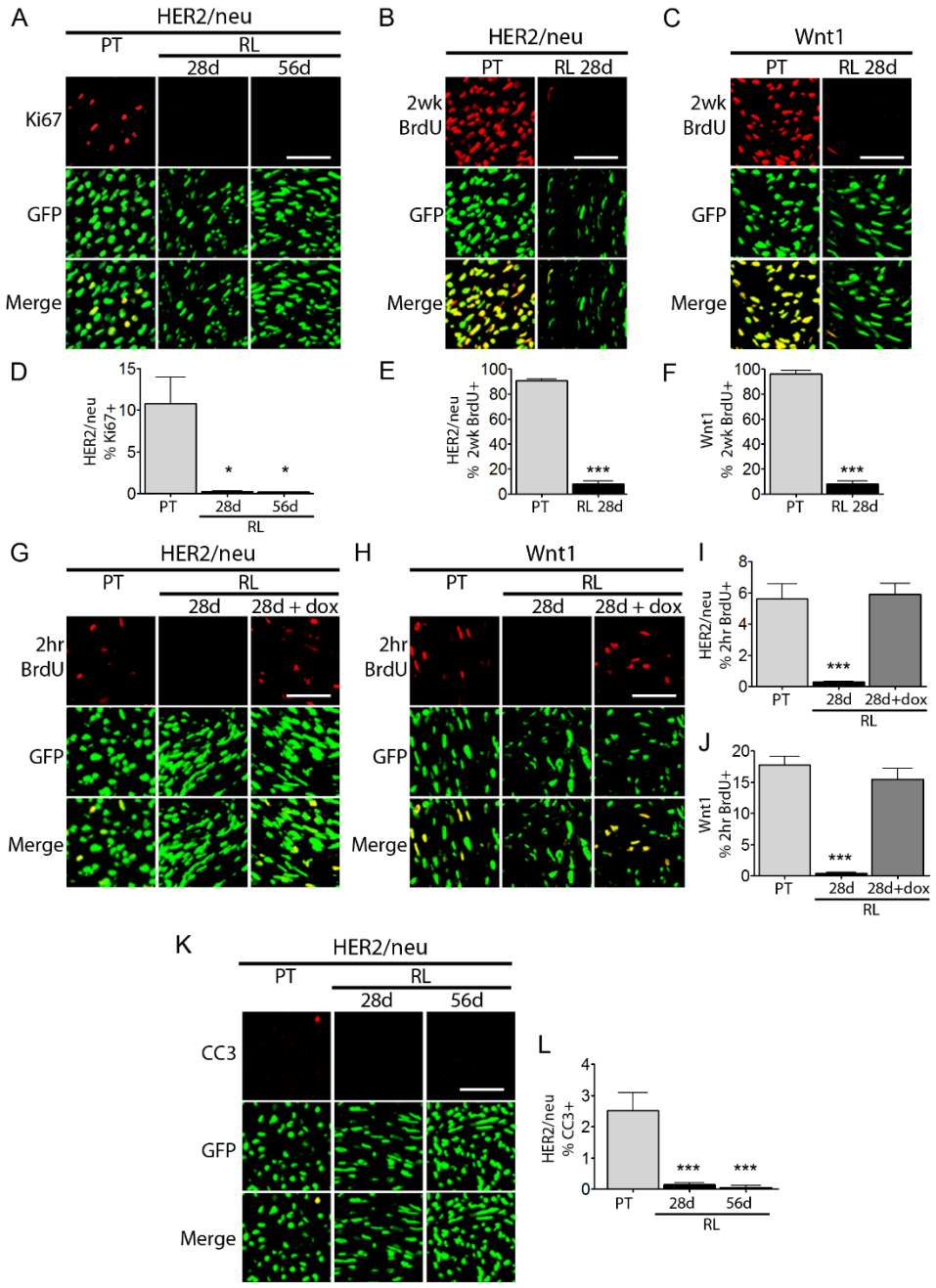

(A) Immunofluorescence (IF) staining for Ki67 on sections from H2B-eGFP-labeled orthotopic *HER2/neu-Prim1* primary tumors (PT, left) and residual lesions (RL) 28 d (middle) or 56 d (right) after HER2/neu de-induction. (B, C) IF staining for BrdU on sections from H2B-eGFP-labeled *HER2/neu-Prim1* (B) or *Wnt1-Prim1* (C) orthotopic primary tumors (left) or MRLs 28 d after

oncogene deinduction (right) in mice labeled with BrdU for 2 wk prior to sacrifice. (D) Quantification of the percent of H2B-eGFP-labeled tumor cells staining positive for Ki67 in (A). (E, F) Quantification of the percent of H2B-eGFP-labeled tumor cells staining positive for BrdU in (B, C), respectively. (G, H) IF staining for BrdU on sections from H2B-eGFP-labeled orthotopic primary tumors (left), or MRLs 28 d after deinduction (middle) or 72 hr following reinduction (right). Mice were labeled with BrdU for 2 hr prior to sacrifice. (I, J) Quantification of the percent of H2B-eGFP-labeled tumor cells staining positive for BrdU in (G, H), respectively. (K) IF staining for cleaved caspase-3 (CC-3) on sections from H2B-eGFP-labeled *HER2neu-Prim1* orthotopic PT (left), RL 28d (middle) or RL 56d (right) after HER2/neu de-induction. (L) Quantification of the percent of H2B-eGFP-labeled tumor cells staining positive for CC-3 in (K). Scale bars (A-C, G, H, K): 50μm, (K): 100μm. ***p-value vs. primary tumor (PT) <0.001.

Figure 3.8. Minimal Residual Lesions are Well-Vascularized and Not Hypoxic

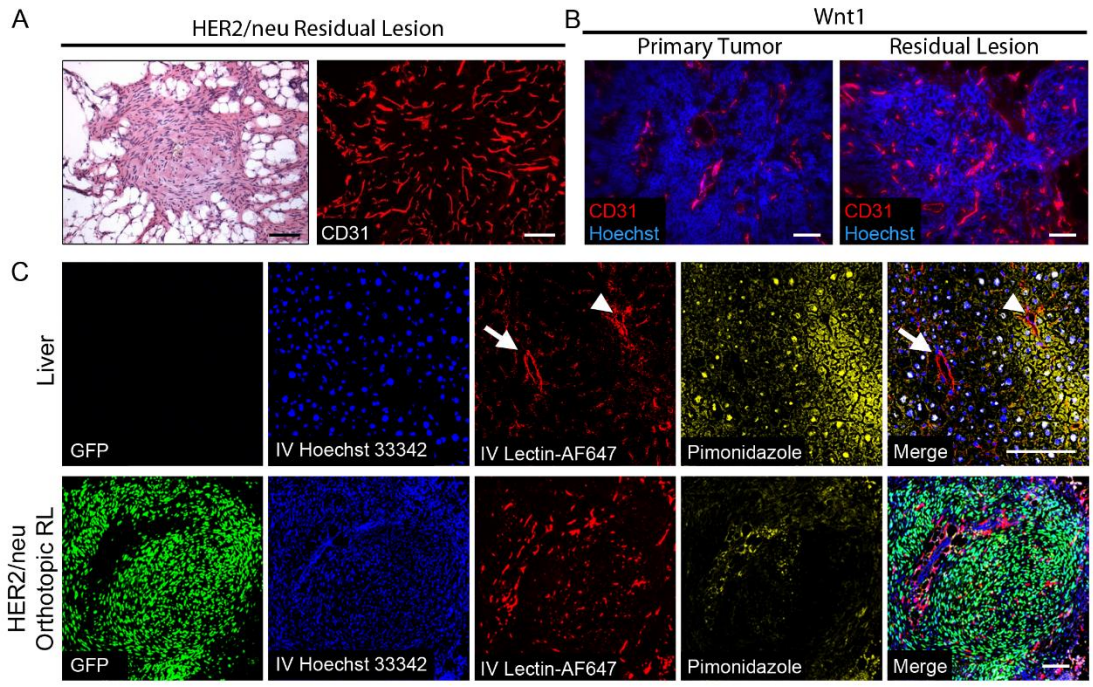

(A) H&E (left) and IF staining for CD31 (right) on sections of a representative *HER2/neu-Prim1* orthotopic MRL. (B) IF staining for CD31 on sections of an intact *MTB;TetO-Wnt1* primary tumor (left) or MRL (right). (C) Fluorescence microscopy of liver (top) or orthotopic MRL (bottom) from same mouse for H2B-eGFP, intravenously injected Hoechst 33342 and Lectin-AF647, and immunofluorescence staining for pimonidazole. Arrowhead denotes area positive pimonidazole staining surrounding hepatic vein; arrow denotes absence of pimonidazole staining surrounding hepatic artery. Scale bars: 100μm for all images shown.

Figure 3.9. CD31 Co-localizes with Intravenously Injected Lectin-AF647

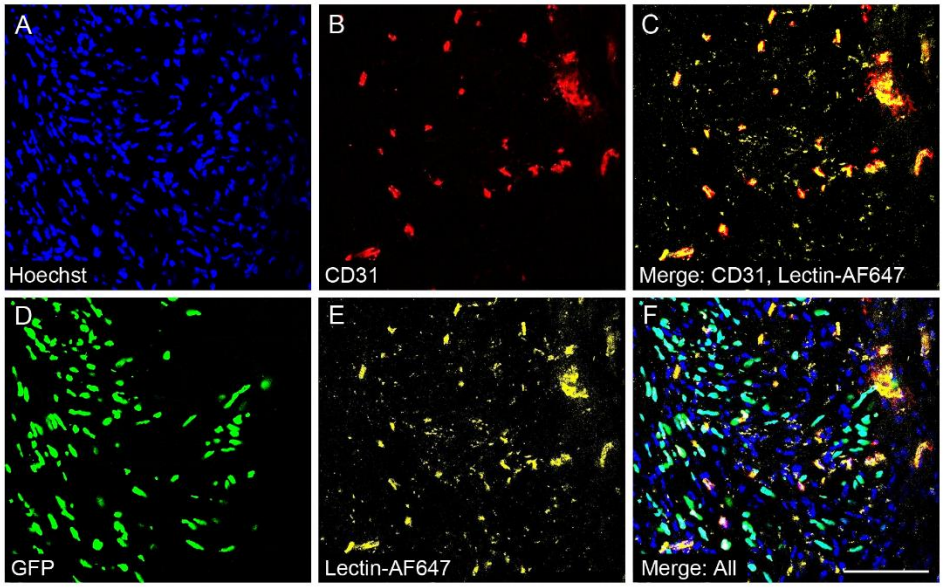

(A-F) Fluorescence microscopy for Hoechst (blue, A), IF for CD31 (red, B), H2B-eGFP (Green, D), lectin-AF647 (Yellow, E), merge of CD31 and Lectin-AF647 (C), or merge of all channels (F) on H2B-eGFP-labeled orthotopic *HER2/neu-Prim1* MRL. Scale bar 100μm for all images shown

Figure 3.10. Residual Metastases Exhibit Cellular Dormancy

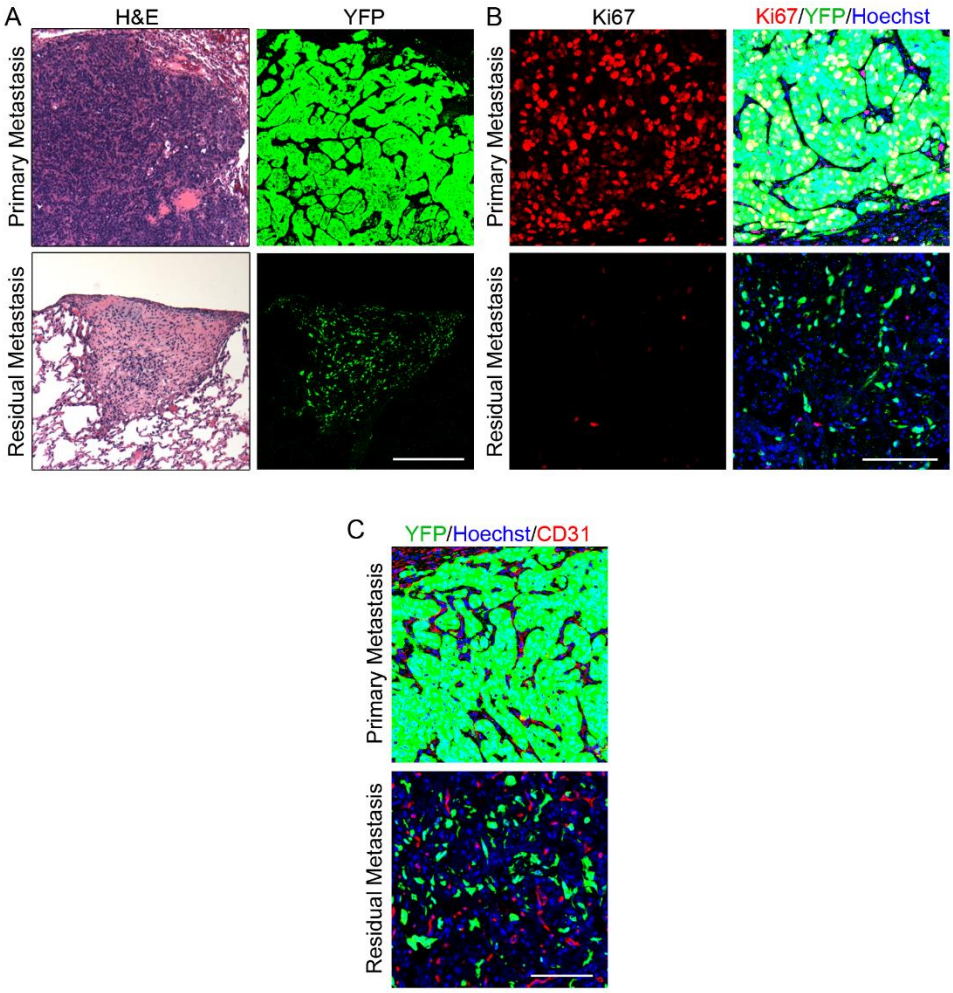

(A-D) Lung metastasis in *MTB;TetO-HER2/neu;TTC;rYFP* mouse on doxycycline (top) or residual lung metastasis following doxycycline withdrawal (bottom). (A) Hematoxylin and eosin-stained sections (left) or YFP fluorescence microscopy (right). (B) IF for Ki67 (left) or Ki67, YFP and Hoechst (right). (C) IF for YFP, Hoechst, and CD31. Scale bars (A): 250μm, (B-C): 100μm.

Figure 3.11. Human Breast Cancer Xenografts Develop Micrometastases in Lung

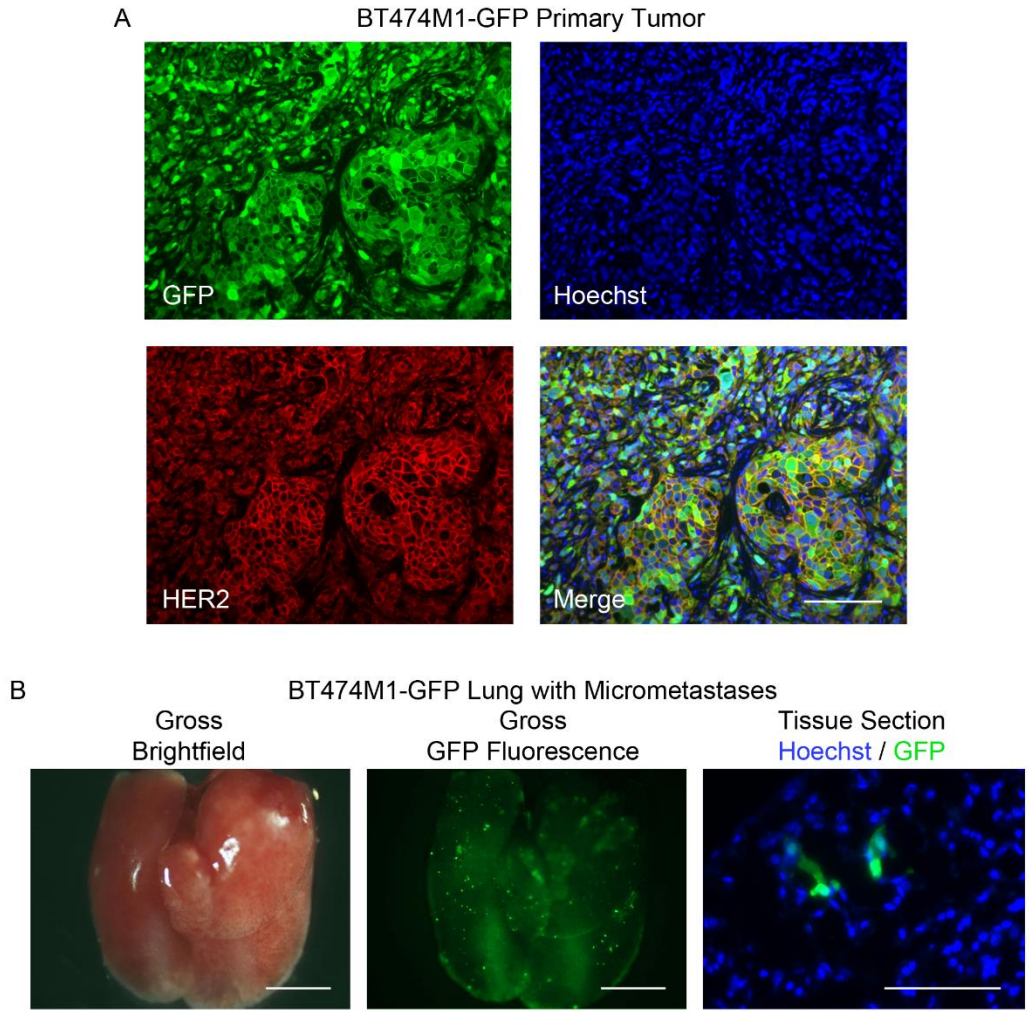

(A) IF staining for GFP, Hoechst, HER2, or a merge of these three channels, on BT474M1-GFP orthotopic primary tumors. (B) Brightfield, (left) or fluorescence (middle) gross images of lung, or fluorescence microscopy of lungs from mice with BT474M1-GFP tumors bearing micrometastases. Scale bars (A): 100μm, (B left, middle): 750μm, (B right): 50μm.

Figure 3.12. Human Breast Cancer Xenografts Exhibit Quiescence Following Targeted Therapy

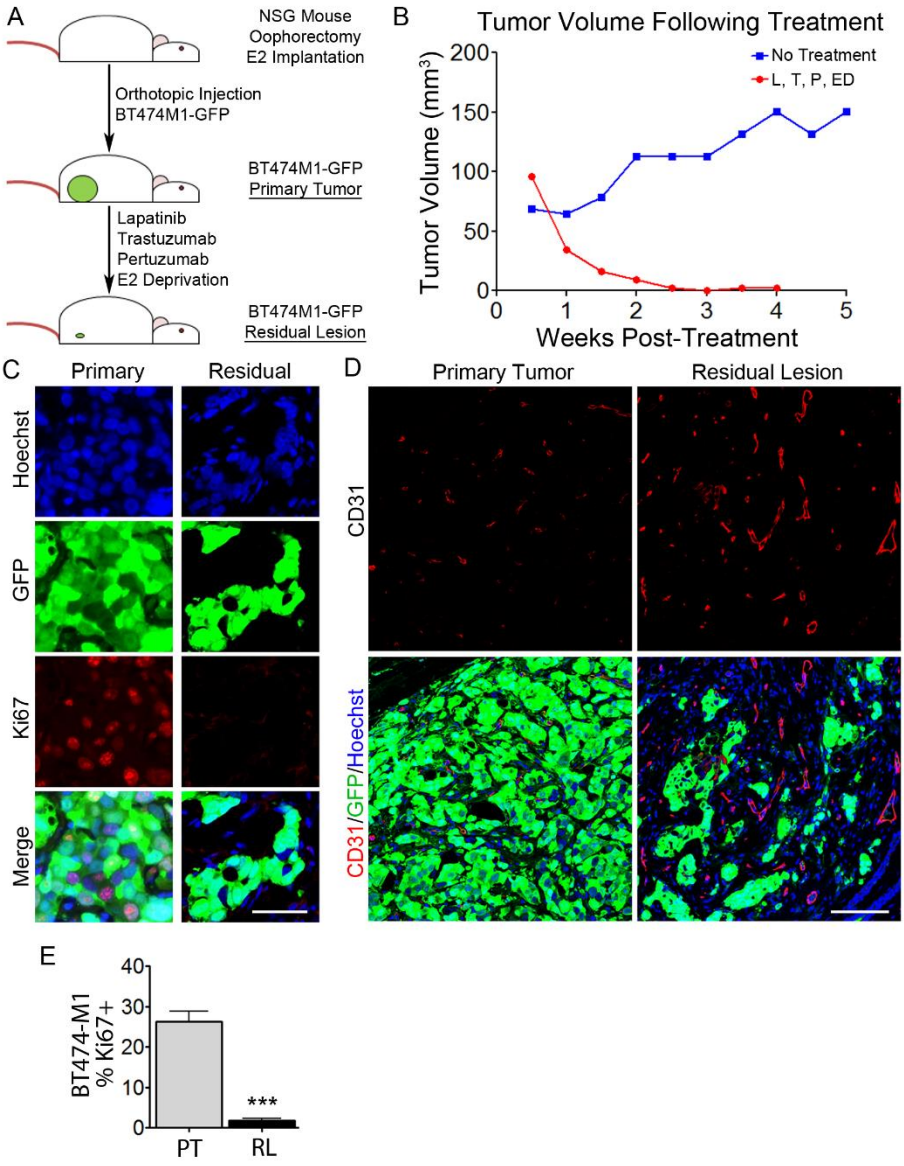

(A) Schematic of generation of xenograft primary tumors and MRLs following targeted therapy. (B) Tumor volume for mice treated with vehicle control or with combination Lapatinib (L), Trastuzumab (T), Pertuzumab (P), and estrogen deprivation (ED). (C) IF staining for Ki67, GFP and Hoechst on sections of BT474M1-GFP primary tumor (left), or residual disease (right). (D) IF staining for CD31, GFP, and Hoechst, on sections of BT474M1-GFP primary tumor (left) or residual lesion (right), showing either CD31 alone (top), or CD31 in combination with GFP and

Hoechst (bottom). (E) Quantification of the percent of GFP-labeled BT474M1 tumor cells staining positive for Ki67 from (C), on sections from primary tumors (PT) or residual lesions (RL). ***p-value vs. primary tumor cells < 0.001. Scale bars (C): 50μm, (D): 100μm

Figure 3.13. Proliferative Residual Tumor Cells are Juxtaposed with Normal Mouse Mammary Duct in *HER2/neu-Prim1* model)

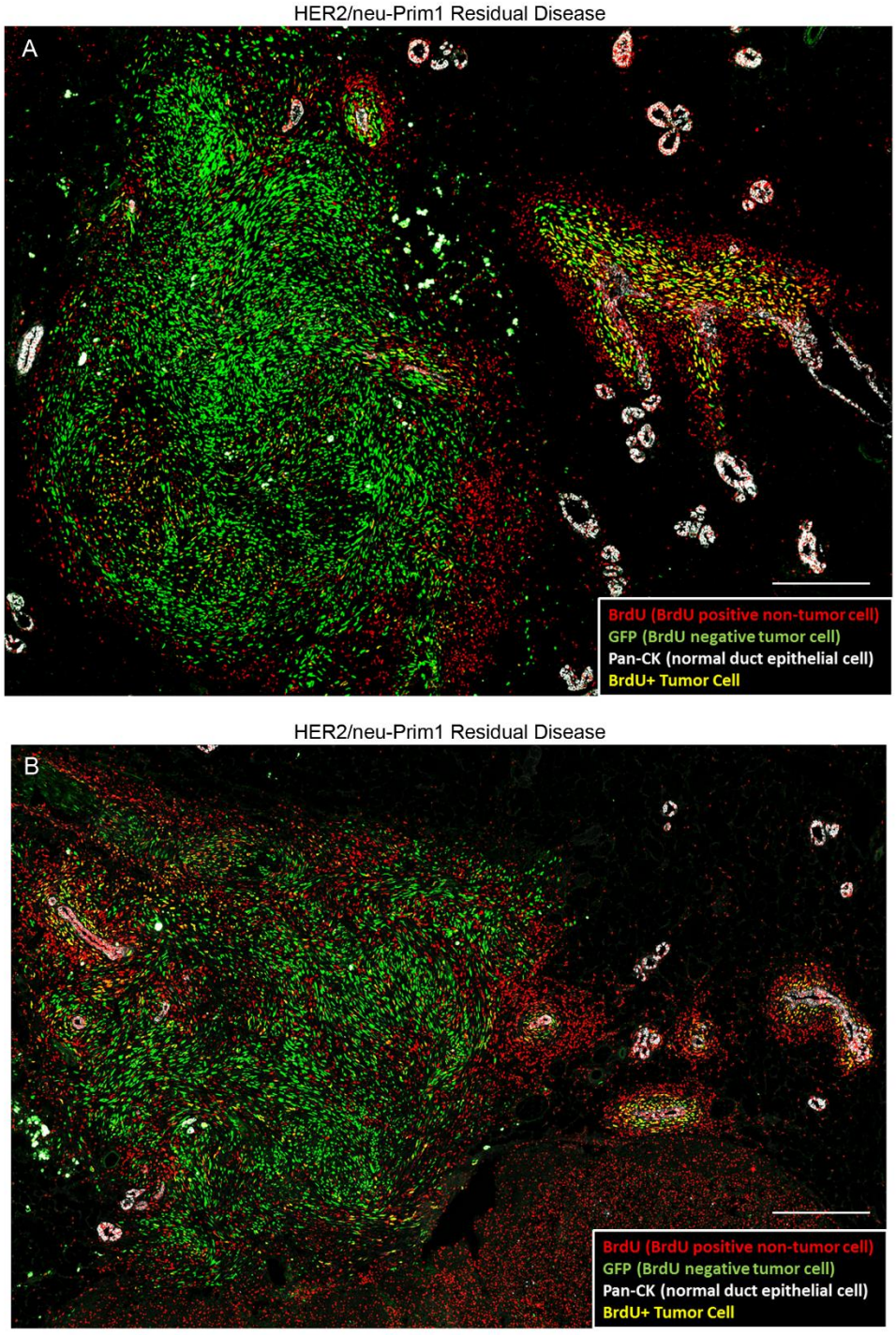

(A, B) IF staining for GFP (green), Pan-Cytokeratin (Pan-CK, white), or BrdU (red), following 2 wk

BrdU exposure prior to sacrifice, 56d after doxycycline withdrawal, in tissue sections of H2B-eGFP-labeled *HER2/neu-Prim1* residual lesions in *nu/nu* mice. Yellow and orange colors show overlap of BrdU with GFP. Scale bars: 250μm

Figure 3.14. Proliferative Residual Tumor Cells are Juxtaposed with Normal Mouse Mammary Duct in *HER2/neu-Prim1* Model

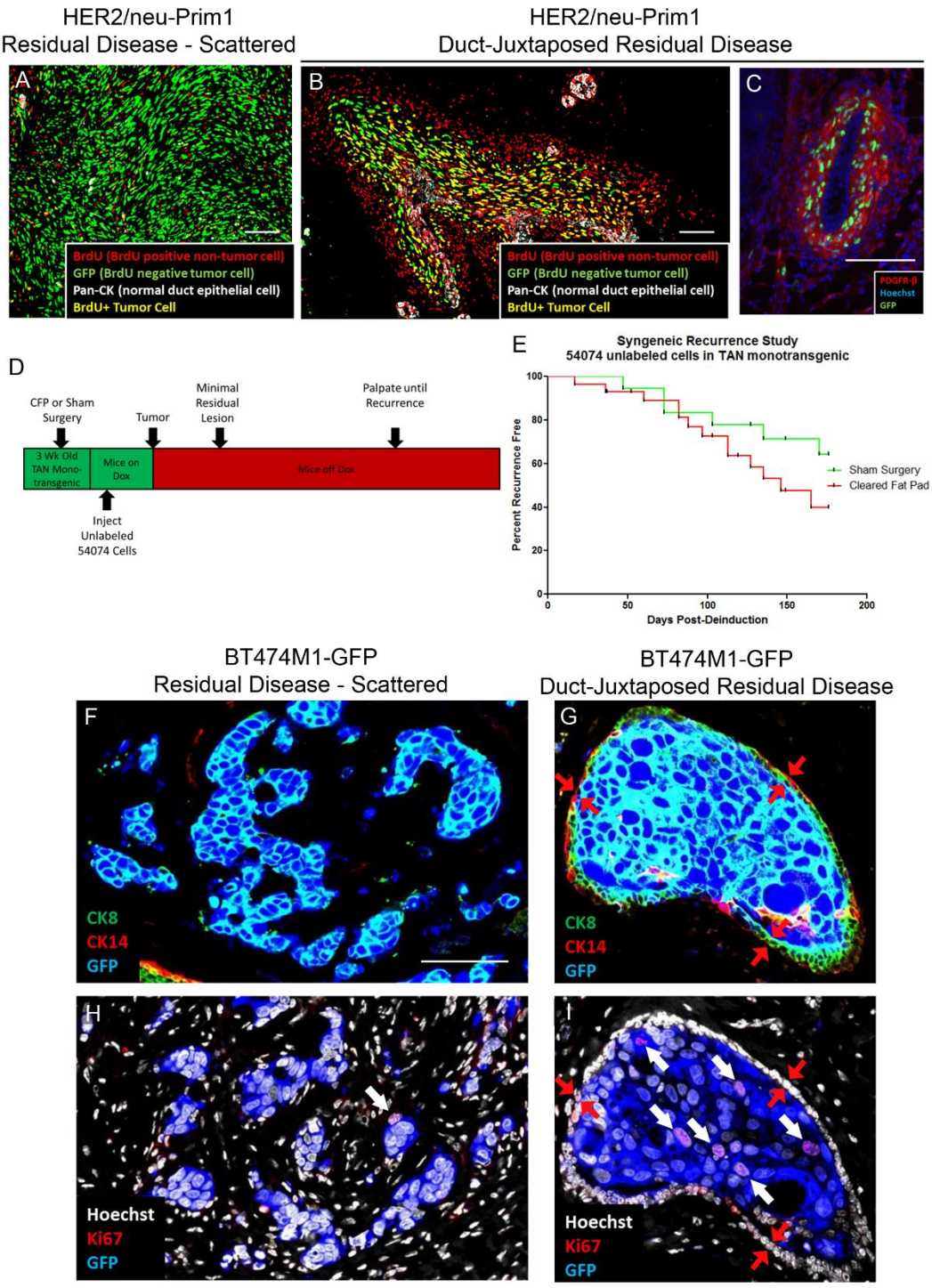

(A-B) IF staining for GFP (green), Pan-Cytokeratin (Pan-CK, white), or BrdU (red), following 2 wk

BrdU exposure prior to sacrifice in center of residual lesion (A) or tumor cells near BrdU+ normal mammary ducts near residual lesion (B). IF staining for GFP (green), Hoechst (blue) and PDGFR-β (red) of normal mammary duct near residual lesion (C). Experimental schematic (D) and recurrence-free-survival results (E) for TAN monotransgenic mice bearing HER2/neu-Prim1 tumors following sham surgery or fat pad clearing surgery. (F-I) BT474M1-GFP residual disease either scattered (F, H) or juxtaposed to normal mouse mammary gland cells encapsulated inside ducts (G, I), stained for GFP (blue) and either CK8 (green) and CK14 (red, F, G), or Hoechst (white) and Ki67 (Red, H, I). Scale bars: 100μm

Figure 3.15. Analysis of RNA Isolated from *MTB/TAN/TTC/rYFP* No Culture Orthotopic Residual Lesions

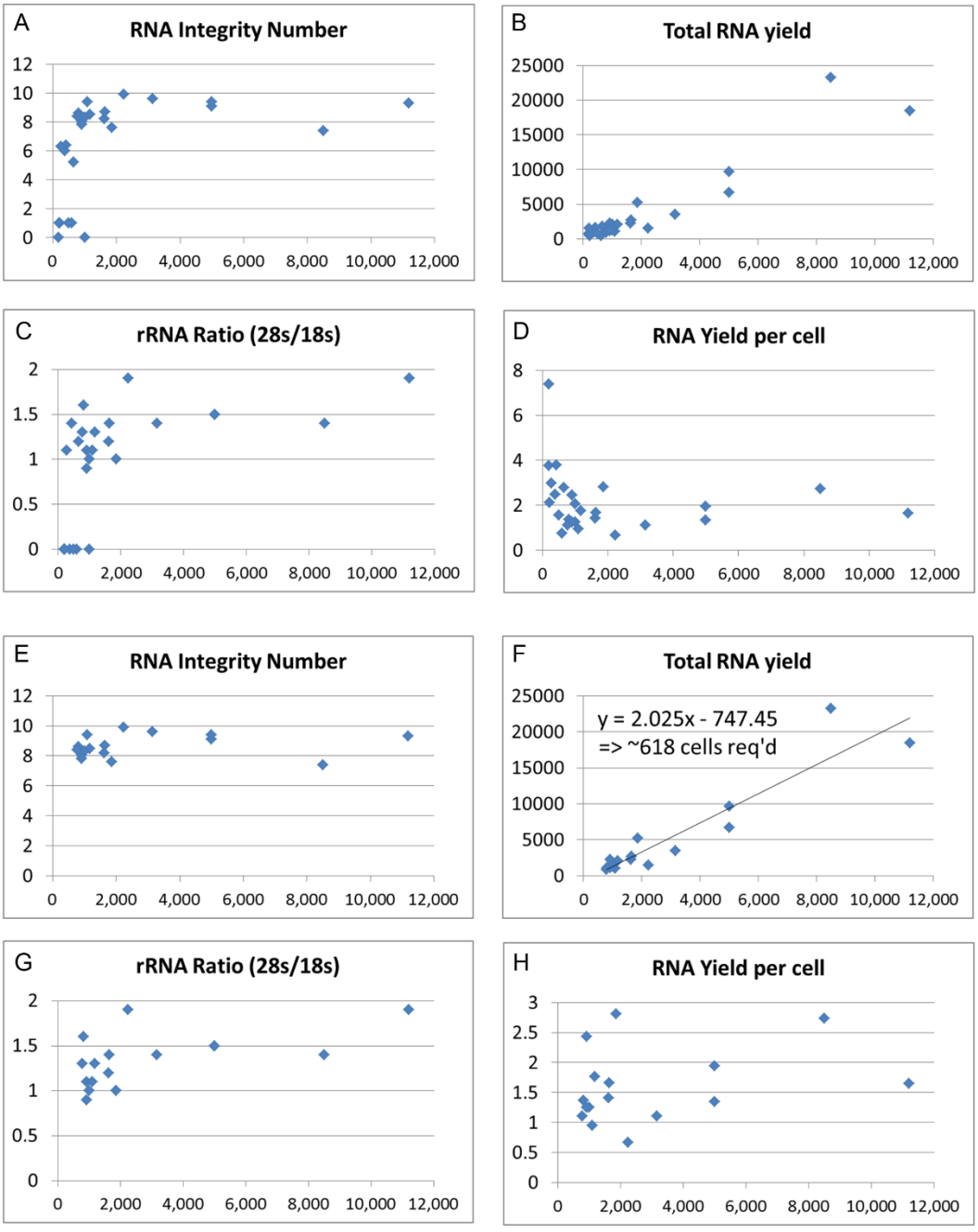

Agilent Bioanalyzer 2100 analysis of 2µl of RNA (of 12µl total isolated RNA) isolated from minimal residual lesion tumor cells in *MTB/TAN/TTC/rYFP* no culture orthotopic residual lesions, showing number of tumor cells isolated per residual lesion (x-axis) compared to RNA integrity number

(RIN) (A, E), total RNA yield from 12µl (B, F), ribosomal RNA (rRNA) ratio (C, G), or RNA yield per cell (D, H). Data shown either for all samples (A-D), or samples with RNA quality eligible for WTA with rRNA ratio>0 and RIN>7 (E-H). Linear fit for total RNA yield vs number of tumor cells (F).

Figure 3.16. Residual Tumor Cells Express Genes Associated with Dormancy

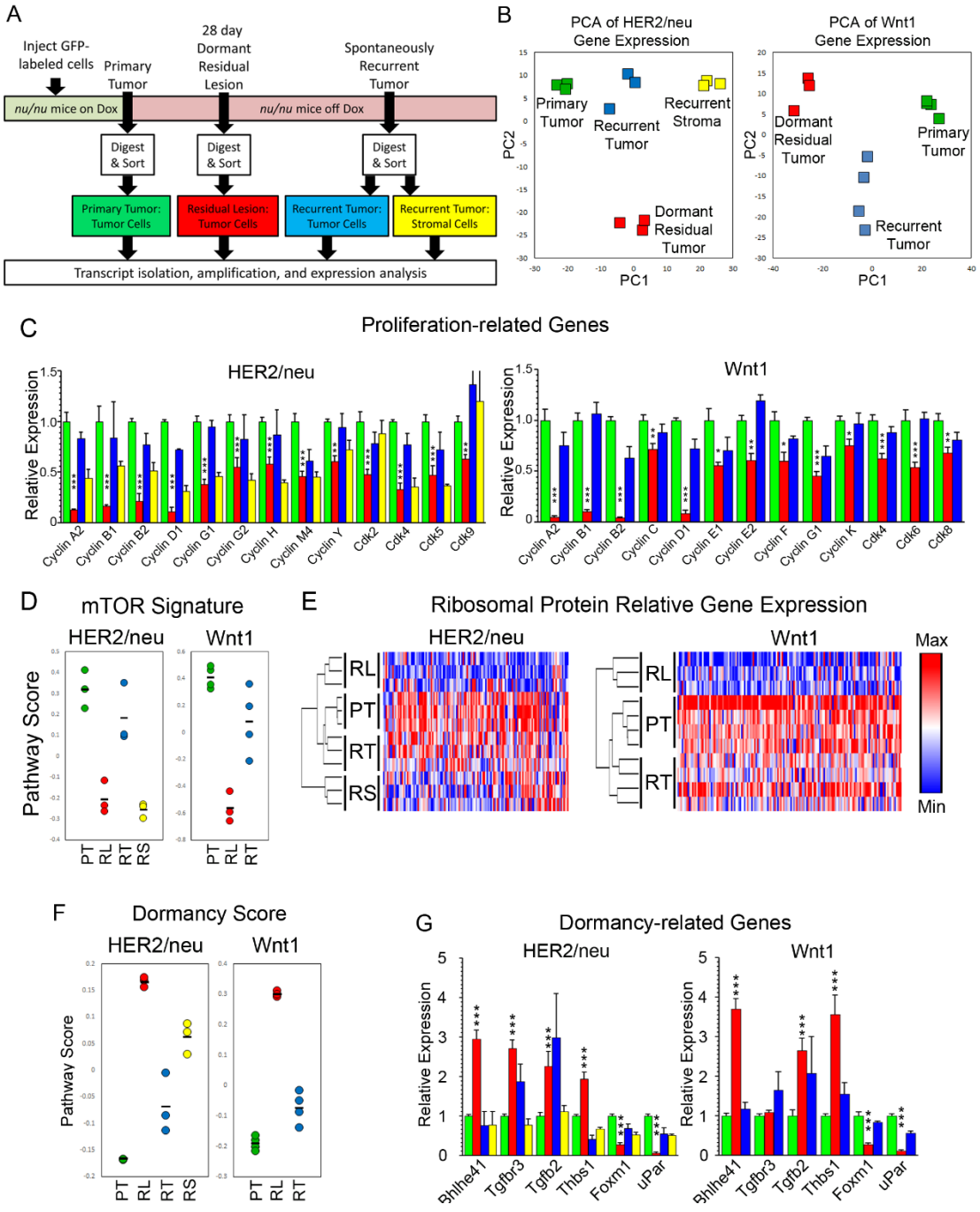

(A) Schematic for isolation and analysis of primary tumor cells (green), dormant residual tumor cells (red), recurrent tumor cells (blue), and stromal cells from recurrent tumors (yellow). (B) Dot plot showing first (PC1) and second (PC2) principal components from principal component

analysis of gene expressed in FACS-isolated primary tumor cells, dormant residual tumor cells, and recurrent tumor cells from *HER2/neu-Prim1* (left) and *Wnt1-Prim1* (right) models. (C, F) Bar graphs showing mean expression level and standard error of the mean (SEM) for genes associated with cell cycle (C), or dormancy (F). (E, G) Dormancy score (E) and mTOR signature score (G) for HER2/neu (left) and Wnt1 (right) models, with primary tumors (PT), residual lesions (RL), recurrent tumors (RT), and recurrent tumor stroma (RS) absolute values (colored circles) or mean values (black lines). (H) Heat map showing hierarchical clustering based upon expression of ribosomal protein genes for primary tumor cells (PT), dormant residual tumor cells (RL), recurrent tumor cells (RT), and recurrent tumor stromal cells (RS).

Figure 3.17. Dormant Residual Disease Resides in Desmoplastic Stroma

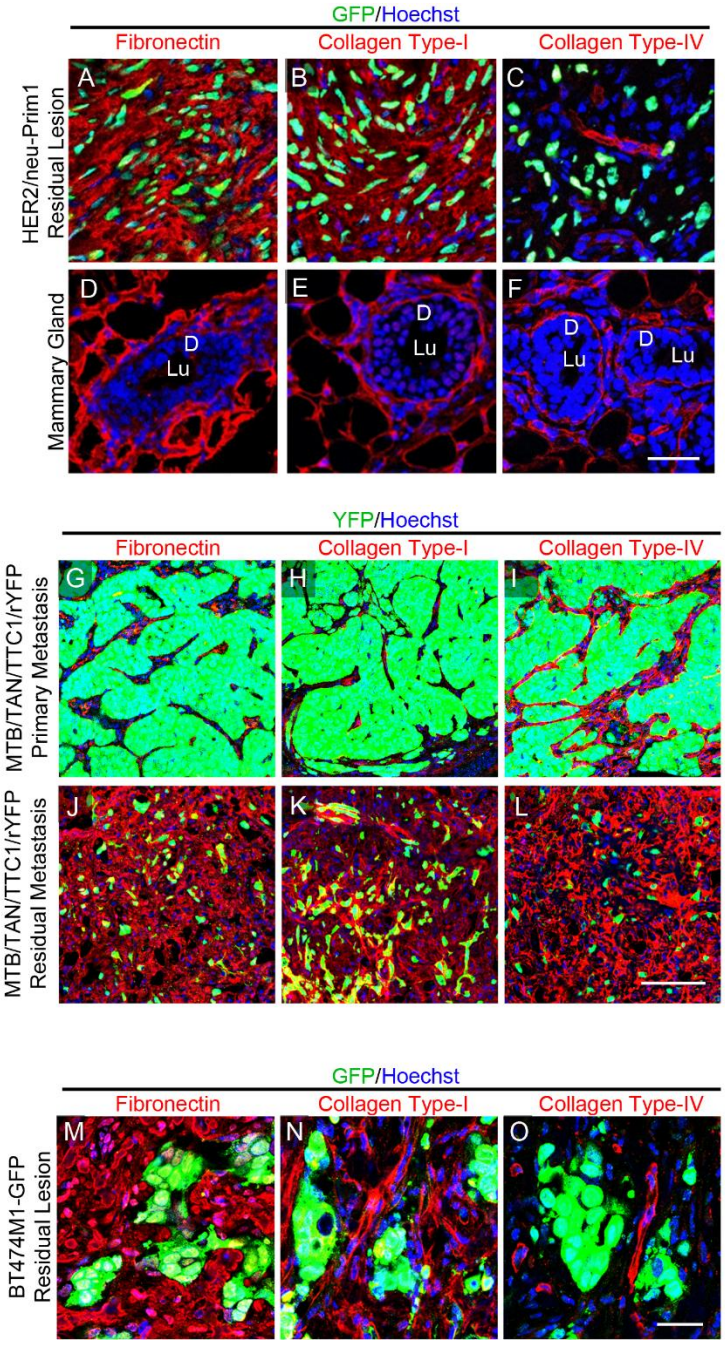

IF staining for Fibronectin (A, D, G, J, M), collagen type-I (B, E, H, K, N), or collagen type-IB (C, F, I, L, O), on tissue sections from *HER2/neu-Prim1* residual lesions (A-C), normal mammary gland (D-F), *MTB/TAN/TTC/rYFP* primary metastasis (G-I), *MTB/TAN/TTC/rYFP* residual metastasis (J-L), or BT474M1-GFP residual lesion (M-O). Mammary gland (D-F) is labeled for duct (D) and

lumen (Lu).

Figure 3.18. Comparison of Intact Donors to No Culture Orthotopic Tumors with Array Comparative Genomic Hybridization (aCGH) and Whole Exome Sequencing (WES) on Bulk Tumor Tissue and RNA-Seq on FACS-isolated Tumor Cells

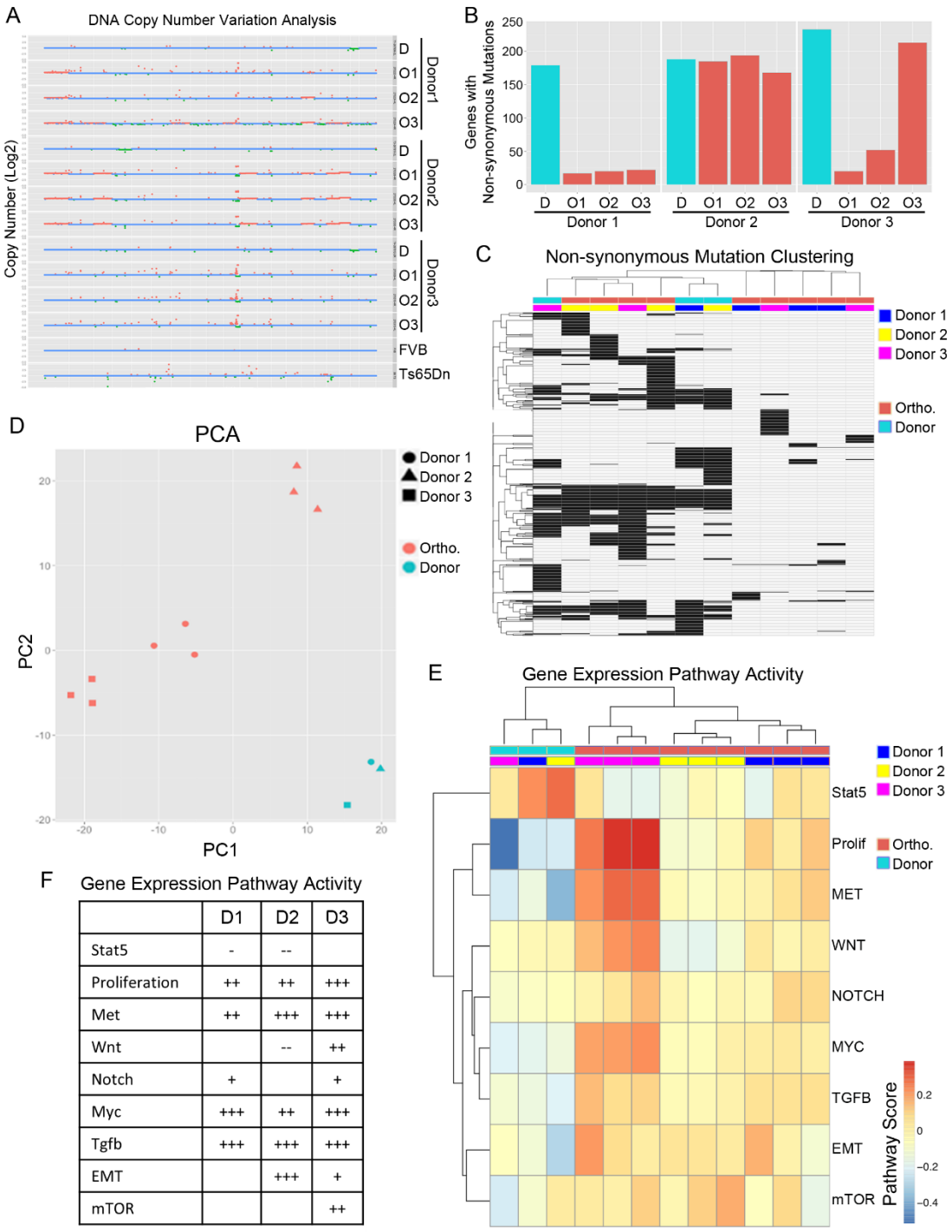

F Gene Expression Pathway Activity

	D1	D2	D3
Stat5	-	--	
Proliferation	++	++	+++
Met	++	+++	+++
Wnt		--	++
Notch	+		+
Myc	+++	++	+++
Tgfb	+++	+++	+++
EMT		+++	+
mTOR			++

(A) Copy Number Variation analysis of aCGH data showing copy number gains (orange) or copy number losses (green) at loci in genomic DNA isolated from donor (D) or orthotopic (O1-O3) tumors from the same donor tumor (Donor1-Donor3), or germline DNA from an FVB or Ts65Dn control. (B) Quantification of number of genes with non-synonymous mutations in donor (blue, D) or orthotopic (orange, O1-O3) tumors from the same donor (Donor1-Donor3). (C) Unsupervised hierarchical clustering based on mutations from (B), showing either orthotopic or intact donor tumors resulting from the same donor (see legend). (D) Principal component analysis (PCA) of genome-wide expression data for FACS-isolated tumor cells from donor or orthotopic tumors from the same donor (see legend). (E) Gene expression pathway activity measured for Stat5 (Stat5), proliferation (Prolif), cMET (MET), Wnt, Notch, Myc, TGF-β1 and TGF-β3 (TGFB), EMT or mTOR. (F) Statistical analysis of (E) comparing expression in orthotopic tumors to donor tumors for donors 1-3 (D1-D3), showing down-regulation of pathways (-) or up-regulation of pathways (+) in orthotopic tumors compared to intact donors. One symbol p-value <0.05, two symbols p-value <0.01, three symbols p-value <0.001.

Figure 3.19. Expression of HER2/neu and Epithelial Markers in Some No Culture Orthotopic Recurrent Tumors

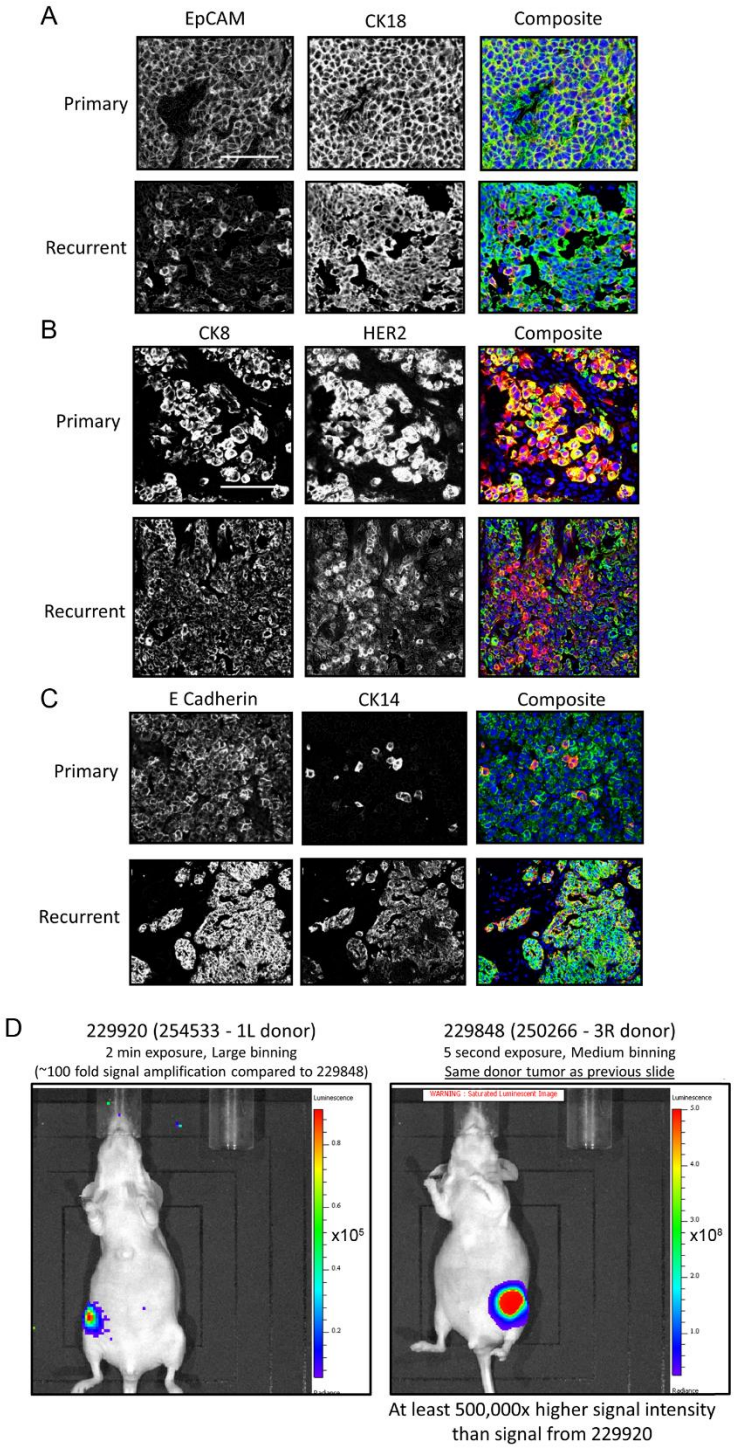

(A-C) IF staining on tissue sections of *MTB/TAN/TTC/rYFP* no culture orthotopic primary (top) or

recurrent tumors (bottom) in *nu/nu* mice, showing Hoechst (blue) and (A) EpCAM, CK18, and merge of EpCAM (red) and CK18 (green); (B) CK8, HER2, and merge of CK8 (green) and HER2 (red); or (C) E Cadherin, CK14, and marge of E Cadherin (green) and CK14 (red). (D) Bioluminescence imaging of a 4x4 recurrent tumor that did not appear to reactivate HER2/neu expression (left) or a 4x4 recurrent tumor that appeared to reactivate HER2/neu expression. Scale bars 100μm for (A-C).

Figure 3.20. Pathway Scores for No Culture Orthotopic *MTB/TAN/TTC/rYFP* Donor and Orthotopic Primary Tumor, Residual Lesion, and Recurrent Tumor

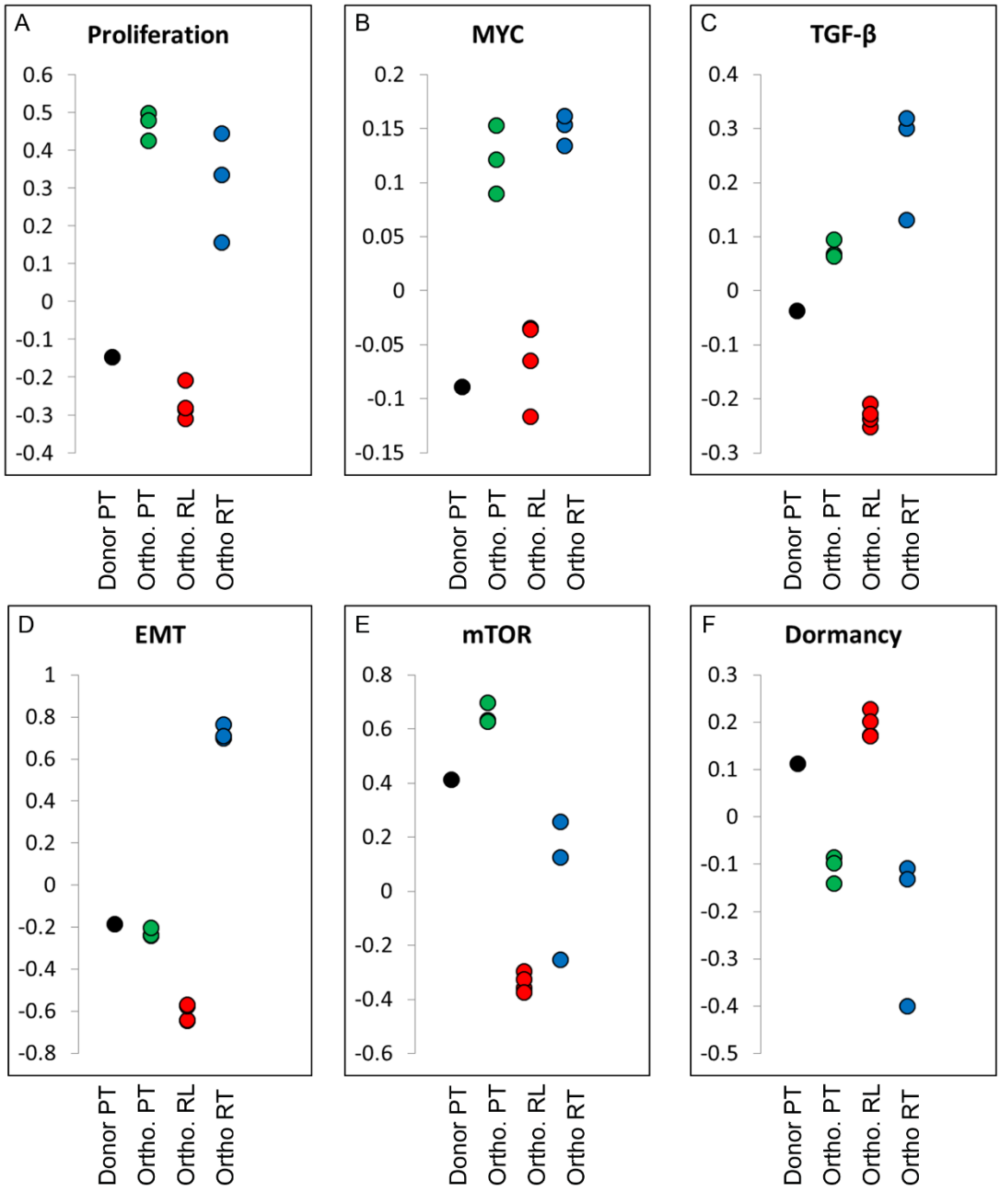

G

p-value for T-test RL vs:	MYC	TGF-β	EMT	Prolif	MET	mTOR	Dormancy
PT	1.10E-03	2.94E-06	2.68E-05	2.70E-06	7.63E-06	3.02E-07	3.14E-05
RT	2.89E-04	2.30E-04	1.04E-07	5.52E-04	6.02E-03	3.26E-02	3.87E-03

(A-F) Pathway scores for intact *MTB/TAN/TTC/rYFP* donor primary tumor (black), orthotopic

primary tumors (green), orthotopic residual lesions (red), or orthotopic recurrent tumors (blue) for gene expression signatures associated with proliferation (A), c-Myc activity (B), TGF-β1 and TGF-β3 signaling (C), EMT (D), mTOR activity (E), or dormancy (F). (G) p-values for student's t-test comparing pathway scores of primary tumor (PT) or recurrent tumor (RT) to residual lesion (RL).

Figure 3.21. Residual Tumor Cells from HER2/neu but not Wnt1 Models Express Genes Associated with EMT

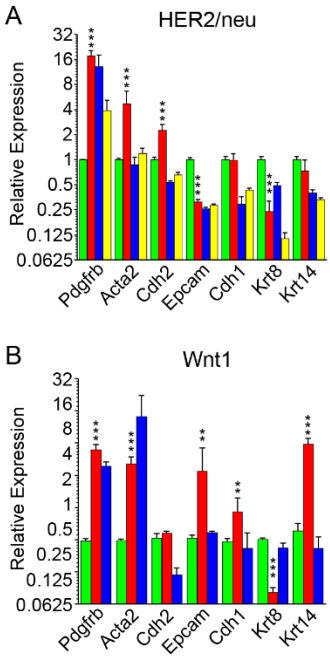

(A, B) Bar graphs showing mean expression level and standard error of the mean (SEM) for genes associated with EMT in HER2/neu (A) or Wnt1 (B) models.

Figure 3.22. *HER2/neu-Prim1* but not Wnt1-Prim1 Residual Disease is Enriched for Mesenchymal Tumor Cells

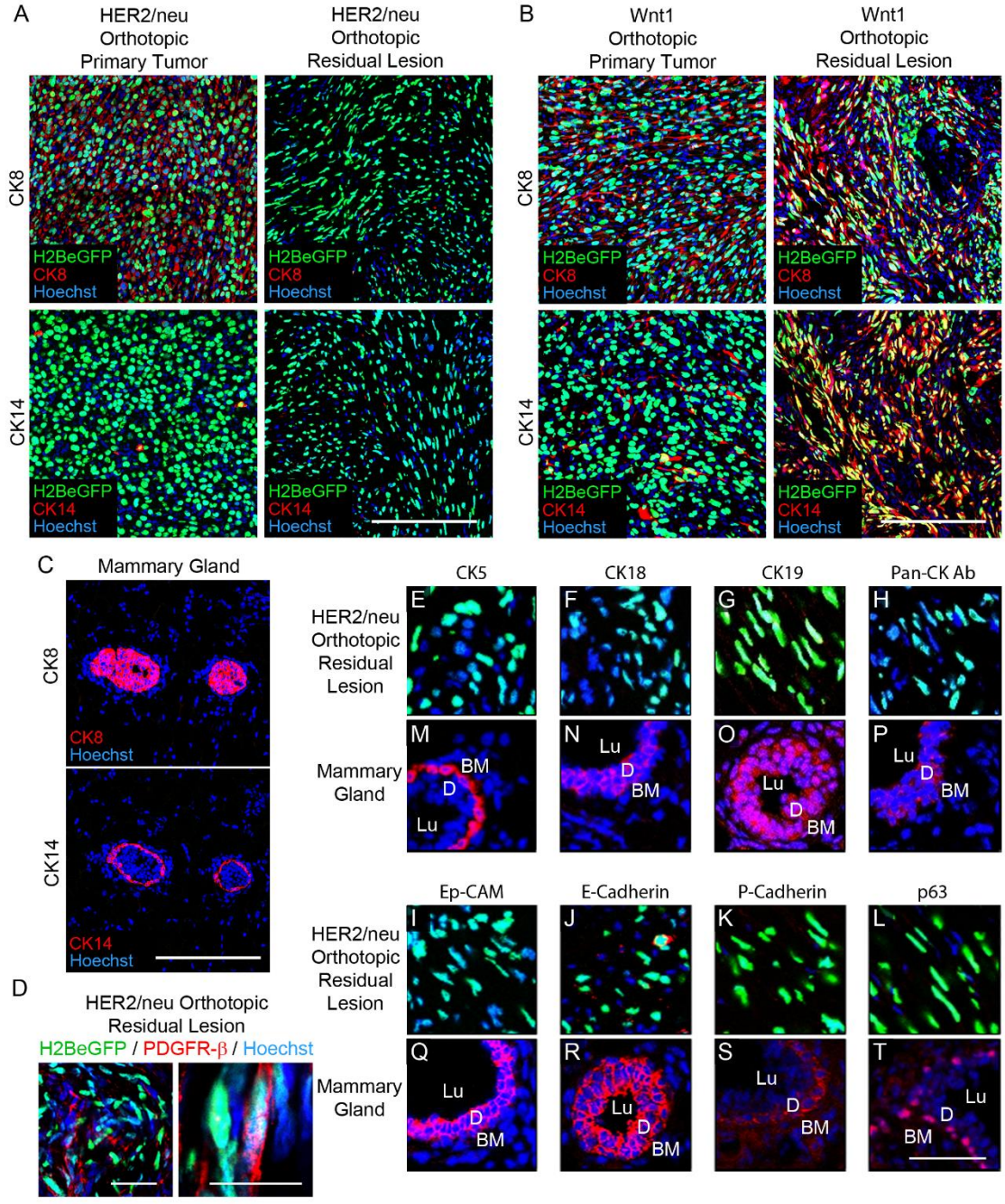

(A-C) IF staining for Hoechst (blue) and H2B-eGFP (green) along with luminal epithelial marker CK8 (red, top) or myoepithelial marker CK14 (red, bottom), on sections of H2B-eGFP-labeled orthotopic *HER2/neu-Prim1* (A) or *Wnt1-Prim1* (B) primary tumor (left), residual lesion 28 d after

doxycycline withdrawal (right), or normal mammary gland (C). (D-G) IF staining for PDGFRβ (red), Hoechst (blue) and GFP (green) on residual lesion 28d after doxycycline withdrawal. (E-T) IF staining for Hoechst (blue) and H2B-eGFP (green) along with epithelial markers (red) CK5 (E, M), CK18 (F, N), CK19 (G, O), Ep-CAM (I, Q), E-Cadherin (J, R), P-Cadherin (K, S), and p63 (L, T), or with a Pan-CK antibody (H, P), on sections of MRLs from H2B-eGFP-labeled orthotopic *HER2/neu-Prim1* tumors (E-L)) or normal mammary ducts (M-T). Scale bars 200μm for (A-C), 50μm for D (left) and (E-T, scale bar shown in T), 20μm for D (right).

Figure 3.23. Distribution of Mesenchymal Tumor Cells in *HER2/neu-Prim1* Residual Lesion

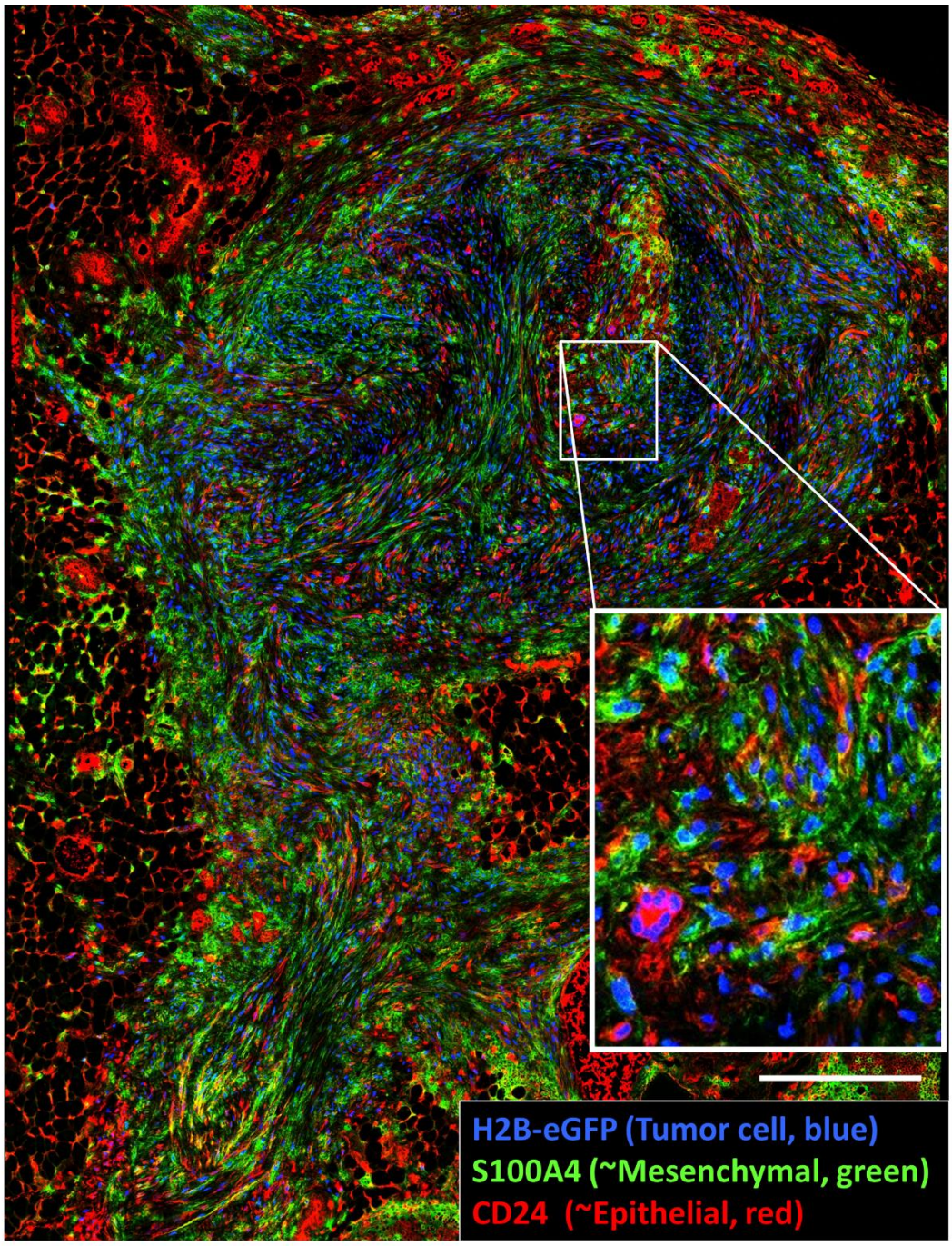

IF staining for H2B-eGFP (blue), mesenchymal marker S100A4 (Fibroblast-specific Protein 1, green), and CD24 (red). Scale bars 250μm

Figure 3.24. Flow Cytometry Analysis of EMT in *HER2/neu-Prim1* cells in vitro and in vivo

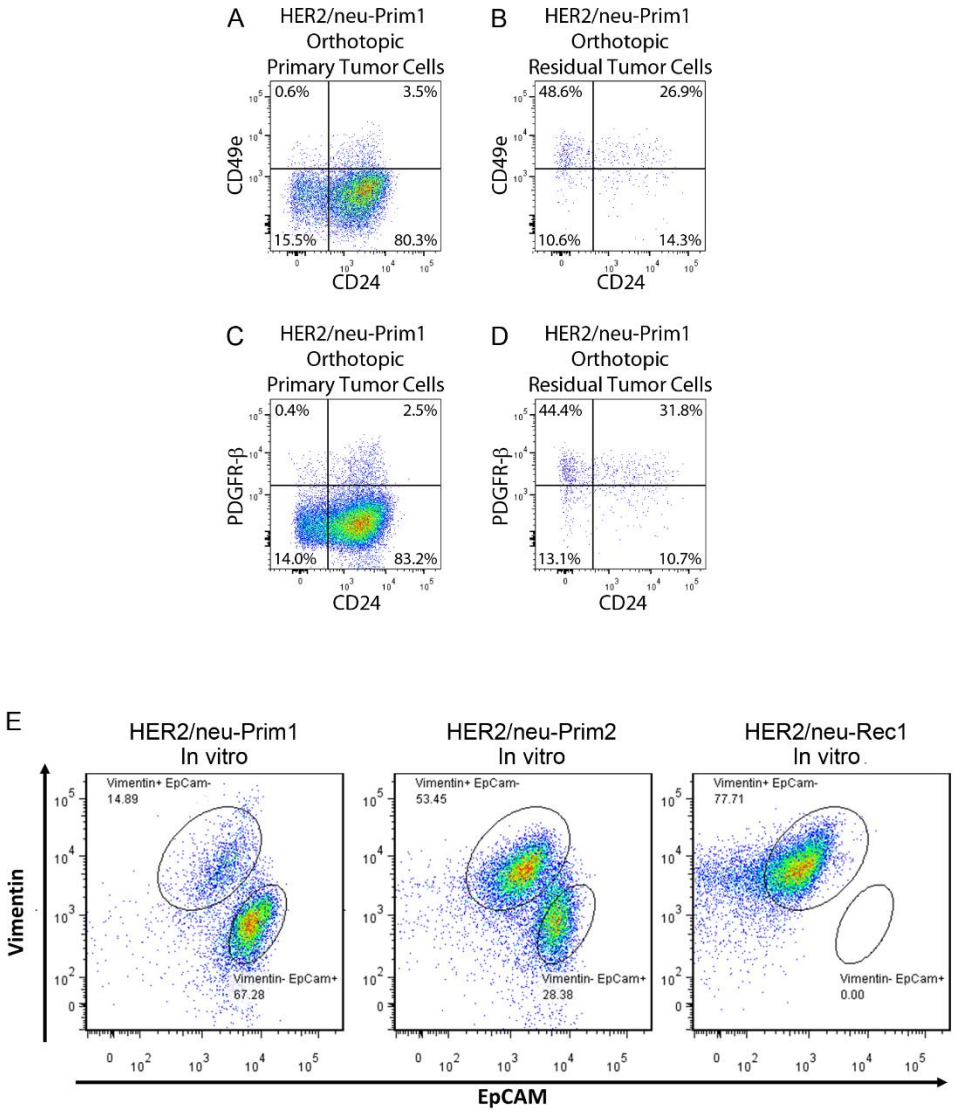

(A-D) Flow cytometry analysis of GFP+DAPI- tumor cells from H2B-eGFP-labeled *HER2/neu-Prim1* primary tumors (A, C) or residual lesions (B, D), staining for either CD49e vs CD24 (A, B) or PDGFR-β vs CD24. (E) Flow cytometry staining of *HER2/neu-Prim1* (54074), *HER2neu-Prim2* (99142), or *HER2/neu-Rec1* tumor cells in vitro for intracellular vimentin vs. extracellular EpCAM.

Figure 3.25. Identification of Residual Tumor Cells Lacking Epithelial Markers in Intact Mice

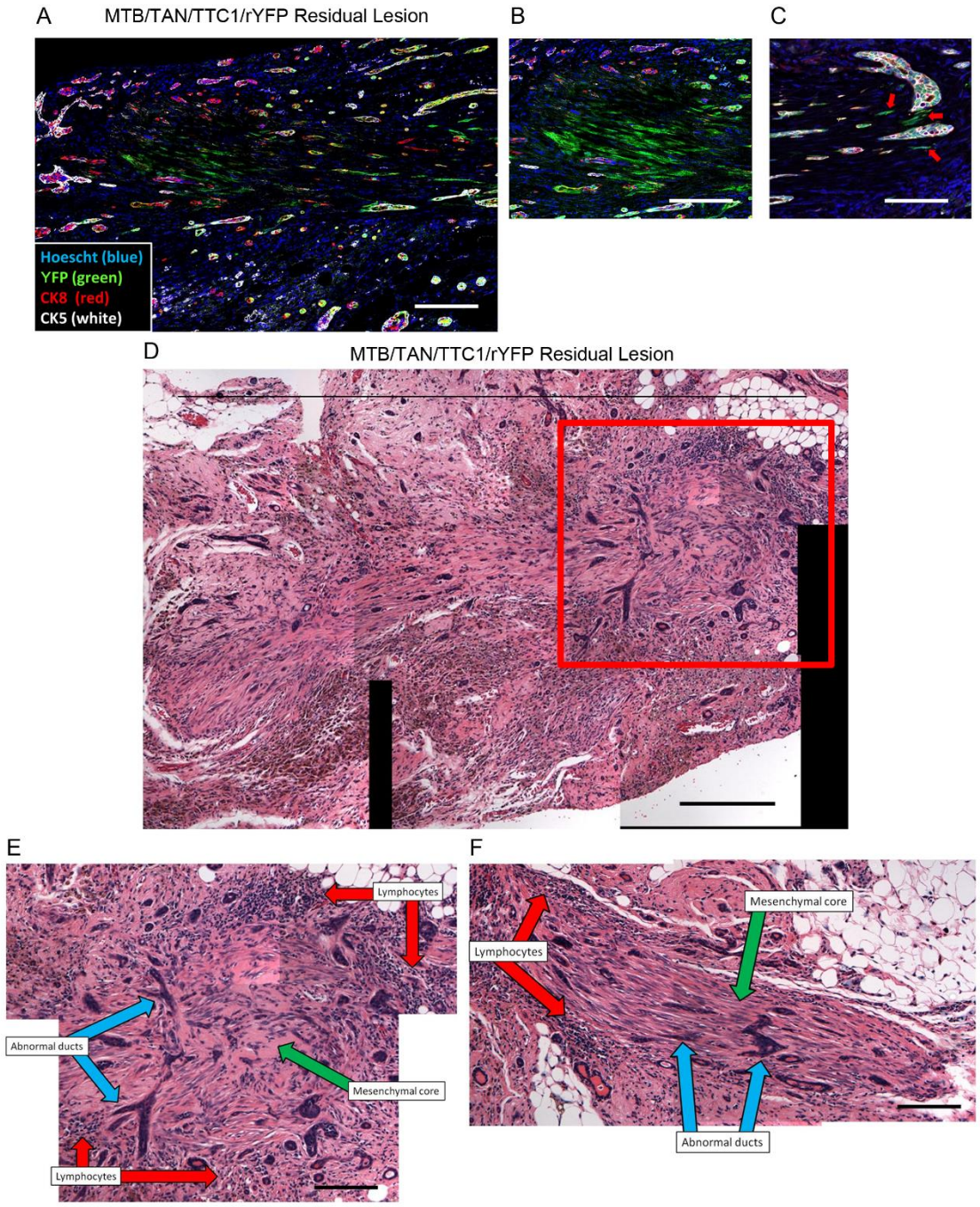

(A-C) IF staining on tissue sections of *MTB/TAN/TTC/rYFP* intact residual lesions for Hoechst (blue), YFP (green), CK8 (red) or CK5 (white), showing spindle-shaped YFP+ tumor cells that

lack expression of epithelial markers CK5 and CK8 (red arrows in panel C). (D-F) Images of H&E staining of intact residual lesions show reproducible features, including a mesenchymal core (green arrow), abnormal ductal morphology (blue arrows), and a corona of lymphocytes (red arrows). Scale bars 100μm for (A-C, E, F), 300μm for (D).

Figure 3.26. Residual Disease is Enriched for Rare Tumor Cell Subpopulations Present in Primary Tumors

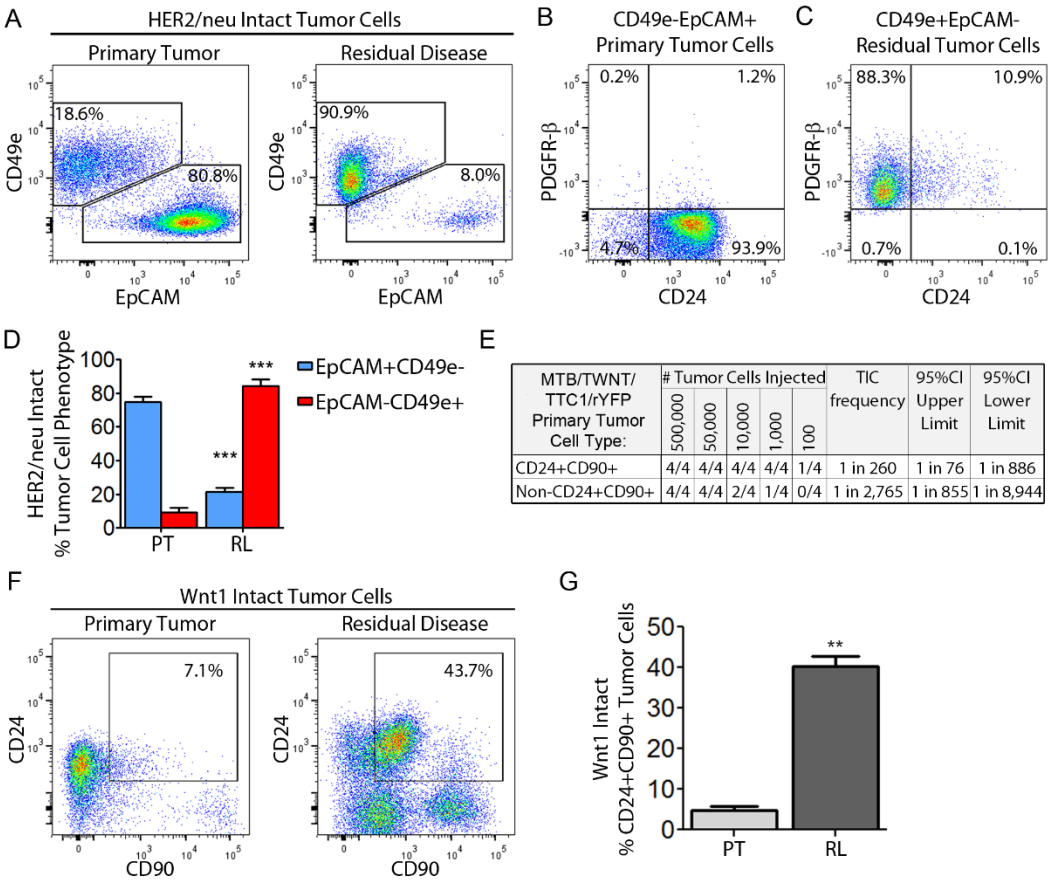

MTB/TWNT/ TTC1/rYFP Primary Tumor Cell Type:	# Tumor Cells Injected 500,000	50,000	10,000	1,000	100	TIC frequency	95%CI Upper Limit	95%CI Lower Limit
CD24+CD90+	4/4	4/4	4/4	4/4	1/4	1 in 260	1 in 76	1 in 886
Non-CD24+CD90+	4/4	4/4	2/4	1/4	0/4	1 in 2,765	1 in 855	1 in 8,944

(A) Flow cytometry for EpCAM and CD49e on YFP+ CD45-DAPI- singlet tumor cells in *MTB/TAN/TTC/rYFP* primary tumor cells (left) or dormant residual tumor cells (right). (B, C) Flow cytometry on populations in (A) for CD24 and PDGFR-β expression on CD49e-EpCAM+ primary tumor cells (B) or CD49e+EpCAM- residual tumor cells (C). (D) Quantification of percent CD49e-EpCAM+ or CD49e+EpCAM- tumor cells in primary tumors or residual lesions, using gates from (A), in *MTB/TAN/TTC/rYFP* mice. (E) Limiting dilution assay of CD24+Thy1+ tumor cells, or non-CD24+Thy1+ tumor cells, from *MTB/TWNT/TTC/rYFP* primary tumors. (F) Flow cytometry for CD24 and Thy1 expression on YFP+CD45-DAPI- singlet tumor cells in *MTB/TWNT/TTC/rYFP* primary tumor cells (left) or residual tumor cells (right). (G) Quantification of percent CD24+Thy1+ or non-CD24+Thy1+ tumor cells in primary tumors or residual lesions, using gates

from (G), in *MTB/TWNT/TTC/rYFP* mice. **p value vs. primary tumor (PT) <0.01, ***p value vs. PT <0.001.

Figure 3.27. Mesenchymal Markers Identified in HER2/neu Residual Disease are Prognostic for Poor Recurrence-Free Survival in HER2+ Breast Cancer

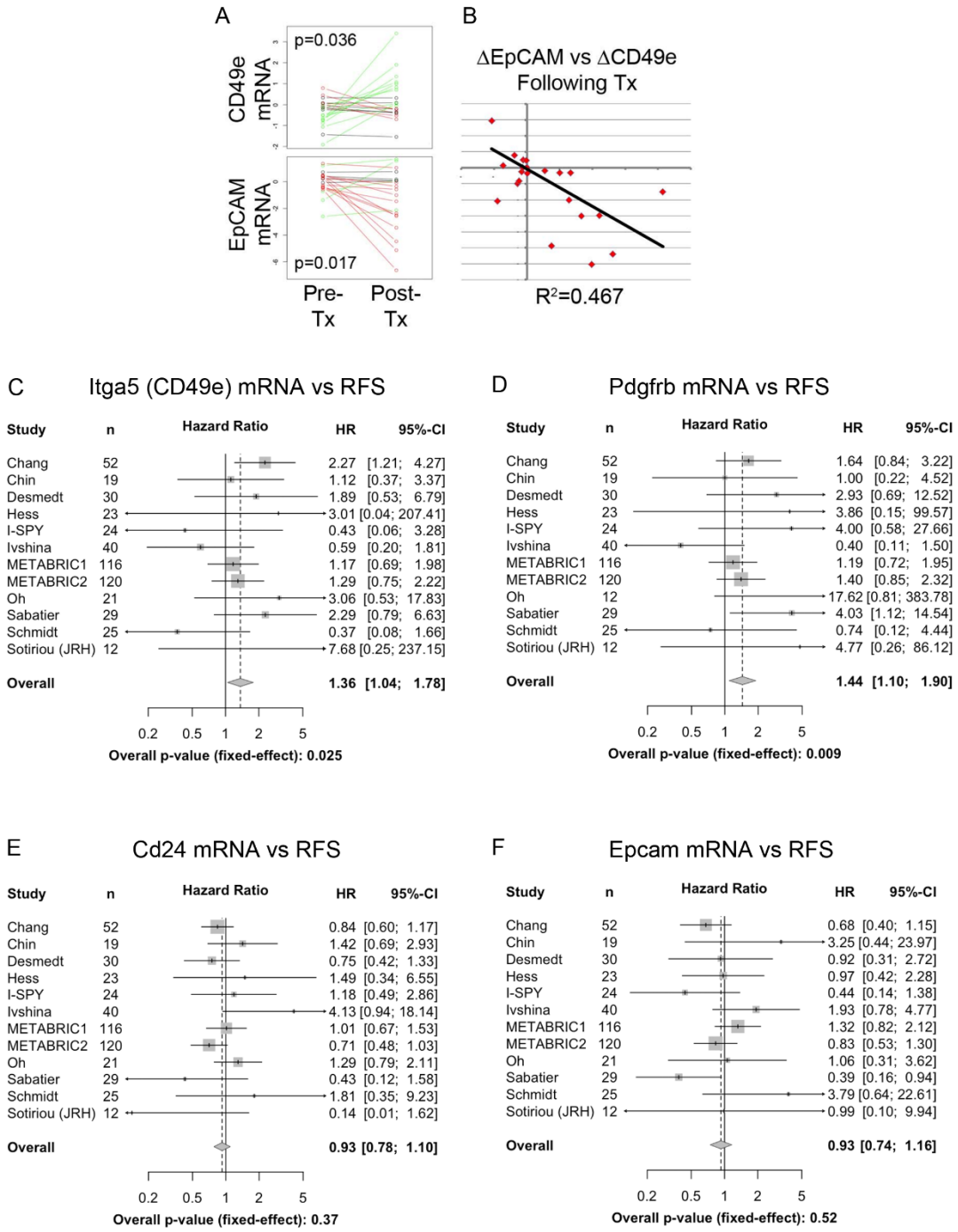

(A) Gene expression data for CD49e (Itga5) or EpCAM prior to (Pre-tx) and following (Post-tx) neoadjuvant therapy. (B) Change in expression of EpCAM (y-axis) and CD49e (x-axis) between

Pre-Tx and Post-Tx time points in breast cancer patients. (C-F) 10 year recurrence-free survival (RFS) meta-analysis of 12 data sets of HER2+ breast cancer, adjusted for tumor grade and size, based on expression levels of Itga4 (CD49e, C), Pdgfrb (PDGFR-β, D), Cd24 (E), or Epcam (F).

Figure 3.28. Genes Associated with Stem-like Cells are Up-regulated in Residual Lesion Tumor Cells in HER2/neu and Wnt1 Models

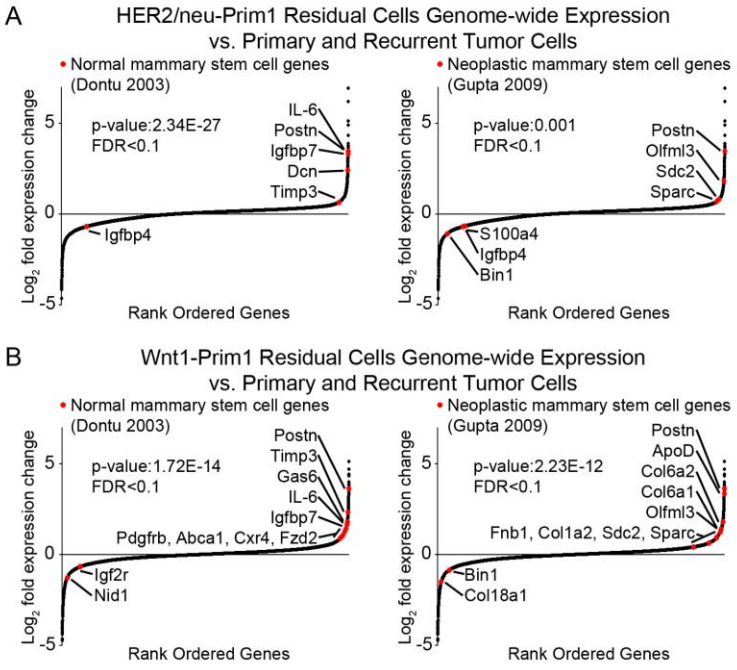

(A-B) Gene expression in residual lesion tumor cells relative to primary and recurrent tumor cells showing genes previously identified as up-regulated in normal mammary stem cells (left) or neoplastic mammary stem-like cells (right) and differentially expressed in residual tumor cells (FDR<0.1) for HER2/neu (A) or Wnt1 (B) models.

Figure 3.29. Residual Tumor Cells from MTB/TWNT/TTC/rYFP No Culture Orthotopic Tumors Give Rise to Mammary Epithelial Trees

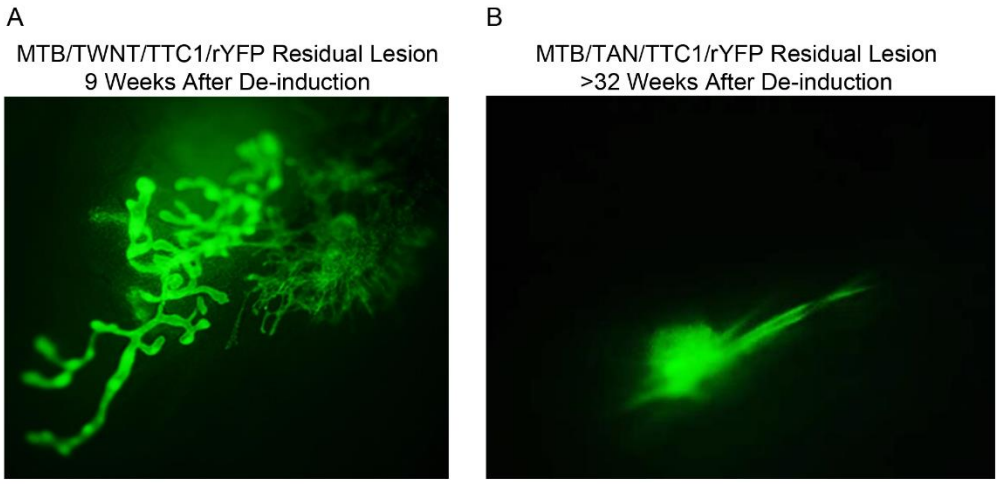

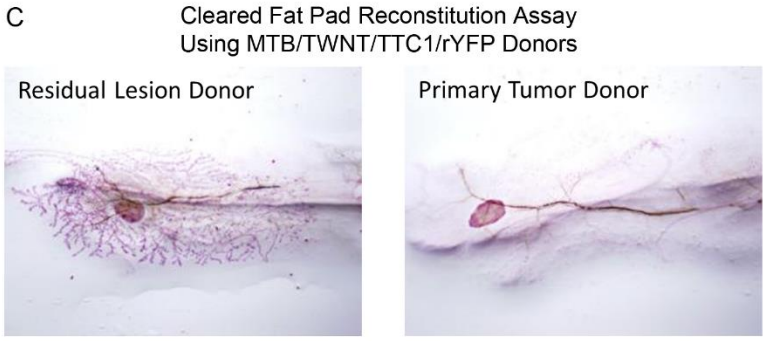

D

Donor Cells Injected into Hosts not on Doxycycline	# Sites forming Mammary Epithelial Tree
M/TWNT/TTC1/rYFP Residual Lesion Tumor Cells	7/12
M/TWNT/TTC1/rYFP Primary Tumor Cells	2/12

(A-B) YFP+ residual disease showing branching mammary epithelial tree from *MTB/TWNT/TTC/rYFP* residual disease 9 weeks after de-induction (A) but not in *MTB/TAN/TTC/rYFP* residual disease more than 32 weeks after deinduction. (C) Carmine stained mammary fat pad shows mammary duct arising in cleared fat pad injected with 1000 residual lesion tumor cells (left) but not in cleared fat pads injected with 1000 primary tumor donor

cells (right). (D) Quantification of the number of cleared fat pads injected with residual lesion or primary tumor cells that give rise to mammary epithelial trees.

Figure 3.30. Immunohistochemistry (IHC) for Proteins Identified by Up-regulation of Genes in Analysis of Residual Disease

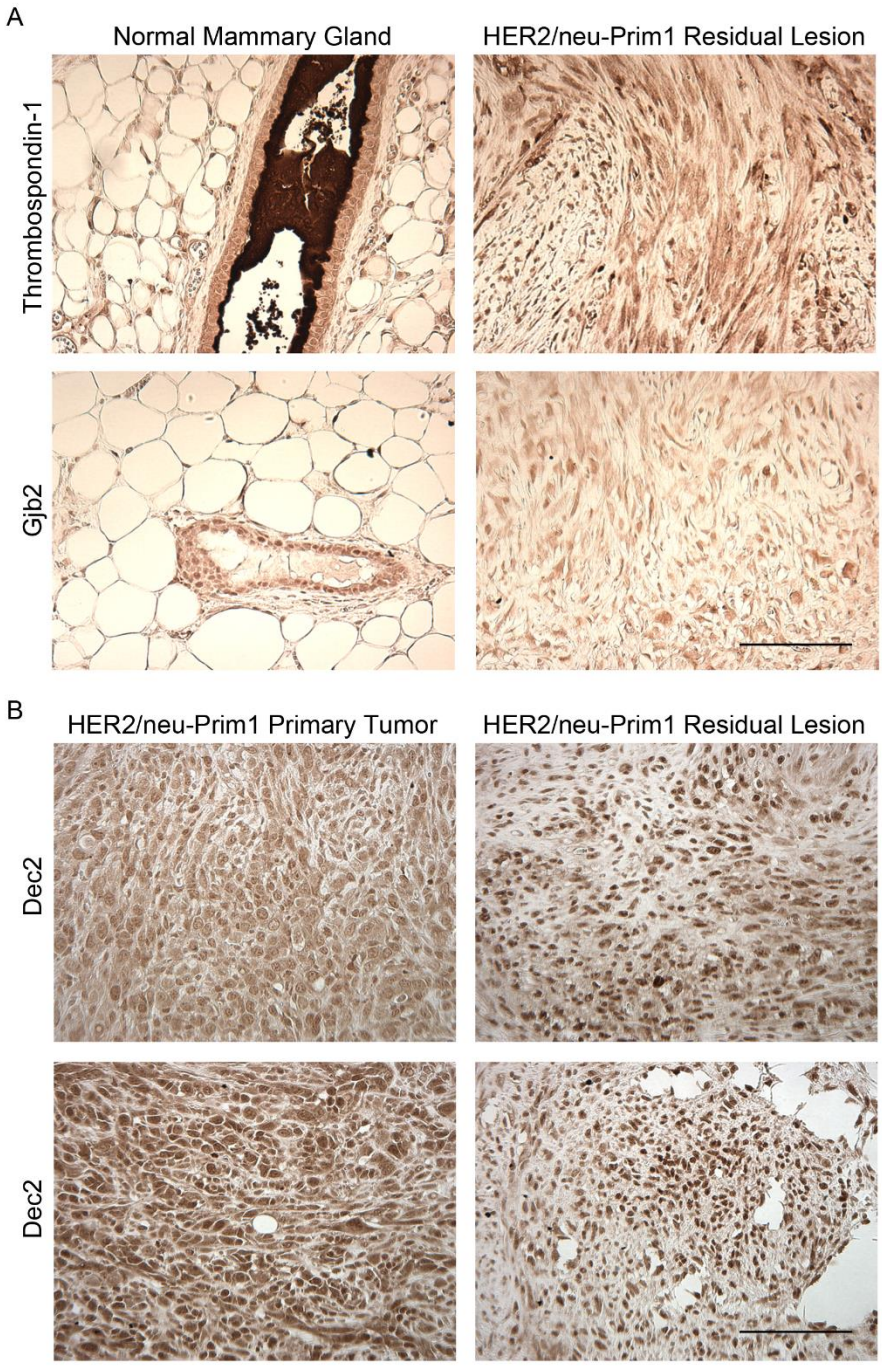

(A) IHC for thrombospondin-1 (top) or Gjb2 (bottom), two proteins whose transcripts were up-regulated in residual disease for which a commercially available antibody was also available,

reveals expression of these proteins both in normal mammary gland epithelial cells (left) and in *HER2/neu-Prim1* residual lesions (right). (B) IHC for Dec2 in primary tumors (left) or residual lesions (right) shows heterogeneous nuclear staining in primary tumors and residual lesions. Scale bars 100μm for (A, B).

Table 3.1. Agilent Bioanalyzer Analysis Results of RNA from FACS-isolated Tumor Cells from Residual Lesions in vivo

Cell Line	Cells sorted	# Cells	RNA Integrity Number	RNA Concentration (pg/uL)	Total RNA yield	rRNA Ratio (28s/18s)	RNA Yield per cell
H2BeGFP-labeled HER2/neu-Prim1 Orthotopic	GFP+ DAPI-	1,006	0	172	2064	0	2.052
		652	5.2	151	1812	1.2	2.779
		427	6.4	135	1620	1.4	3.794
		189	0	59	708	0	3.746
		912	8	185	2220	1.1	2.434
		1,621	8.2	190	2280	1.2	1.407
		1,178	8.5	173	2076	1.3	1.762
M/TAN/ TTC1/rYFP No Culture Orthotopic	YFP+CD45- DAPI-	1859	7.6	436	5232	1	2.814
		11200	9.3	1536	18432	1.9	1.646
		3148	9.6	291	3492	1.4	1.109
		1638	8.7	226	2712	1.4	1.656
		814	8.6	93	1116	1.6	1.371
		1096	9.4	87	1044	1.1	0.953
		221	1	39	468	0	2.118
		386	6	80	960	0	2.487
		271	6.3	67	804	1.1	2.967
		1005	8.3	105	1260	1	1.254
		606	1	38	456	0	0.752
		2239	9.9	125	1500	1.9	0.670
		780	8.4	72	864	1.3	1.108
		493	1	64	768	0	1.558
		203	1	125	1500	0	7.389
H2BeGFP-labeled Wnt1-Prim1 Orthotopic	GFP+ DAPI-	8,500	7.4	1,936	23232	1.4	2.733
		5,000	9.1	808	9696	1.5	1.939
		912	7.8	95	1140	0.9	1.250
		5000	9.4	560	6720	1.5	1.344

Results for running Agilent Bioanalyzer 2100 with 'Pico' chips using RNA from FACS-isolated tumor cells sorted out of fluorescently labeled residual lesions in vivo.

Table 3.2. Gene Sets Down-regulated in Dormant Residual Tumor Cells in *HER2/neu-Prim1* and *Wnt1-Prim1* Models

Gene Sets Down-regulated in Wnt1 Dormant Residual Tumor Cells

	SP_PIR_KEYWORDS	# Down-regulated Genes in Cluster	p-value	FDR (Benjamini)
Cluster 1	Enrichment Score: 38.87			
	cell cycle	132	1.80E-49	4.30E-47
	mitosis	74	1.10E-38	1.40E-36
	cell division	88	1.50E-38	1.50E-36
Cluster 2	Enrichment Score: 24.81			
	kinetochore	36	1.60E-25	1.10E-23
	chromosomal protein	42	1.00E-16	4.10E-15
Cluster 3	Enrichment Score: 17.26			
	ribonucleoprotein	71	1.00E-23	6.10E-22
	ribosomal protein	52	1.70E-19	9.20E-18
Cluster 4	Enrichment Score: 16.28			
	dna replication	34	2.00E-17	8.90E-16
Cluster 6	Enrichment Score: 11.13			
	DNA damage	38	8.40E-09	2.30E-07
	dna repair	34	5.30E-08	1.40E-06
Cluster 7	Enrichment Score: 11			
	atp-binding	152	9.10E-12	2.90E-10
	nucleotide-binding	176	3.00E-10	9.10E-09
Cluster 8	Enrichment Score: 7.67			
	ubl conjugation	83	7.20E-13	2.50E-11
	isopeptide bond	42	1.90E-06	3.80E-05
Cluster 9	Enrichment Score: 6.33			
	ribosome biogenesis	15	9.10E-07	1.90E-05
	rrna processing	15	3.00E-05	5.00E-04
Cluster 10	Enrichment Score: 6.03			
	cytoskeleton	71	2.00E-06	4.00E-05
	microtubule	34	1.50E-05	2.80E-04
Cluster 12	Enrichment Score: 5.62			
	chromosomal protein	42	1.00E-16	4.10E-15
Cluster 15	Enrichment Score: 4.79			
	molecular chaperone	7	1.80E-04	2.50E-03
Cluster 20	Enrichment Score: 3.52			
	mitochondrion	78	7.80E-04	1.00E-02
	transit peptide	47	4.60E-03	4.40E-02

Gene Sets Down-regulated in HER2/neu Dormant Residual Tumor Cells

	SP_PIR_KEYWORDS	# Down-regulated Genes in Cluster	p-value	FDR (Benjamini)
Cluster 1	Enrichment Score: 25.71			
	ribonucleoprotein	85	3.90E-31	6.20E-29
	ribosomal protein	67	1.70E-29	2.10E-27
Cluster 2	Enrichment Score: 24.79			
	cell division	79	7.80E-28	7.40E-26
	cell cycle	107	3.10E-27	2.40E-25
	mitosis	62	6.50E-25	3.40E-23
Cluster 4	Enrichment Score: 12.94			
	mitochondrion	149	4.70E-26	2.80E-24
	transit peptide	85	1.50E-14	5.80E-13
Cluster 5	Enrichment Score: 11.29			
	chromosomal protein	33	5.30E-09	1.30E-07
Cluster 6	Enrichment Score: 9.67			
	kinetochore	26	4.40E-13	1.60E-11
Cluster 7	Enrichment Score: 9.26			
	ubl conjugation	88	1.90E-12	6.40E-11
	isopeptide bond	51	6.30E-09	1.40E-07
Cluster 8	Enrichment Score: 9.1			
	rrna processing	22	7.50E-10	2.10E-08
	ribosome biogenesis	16	5.40E-07	9.50E-06
Cluster 9	Enrichment Score: 7.04			
	dna replication	27	3.40E-10	1.00E-08
Cluster 10	Enrichment Score: 6.69			
	nucleotide-binding	189	1.20E-09	3.30E-08
	atp-binding	152	2.10E-08	4.10E-07
Cluster 11	Enrichment Score: 6.44			
	dna repair	33	1.90E-06	3.00E-05
	DNA damage	35	3.20E-06	4.60E-05
Cluster 14	Enrichment Score: 5.85			
	cytoskeleton	67	6.10E-04	6.30E-03
Cluster 19	Enrichment Score: 4.99			
	molecular chaperone	6	2.70E-03	2.30E-02
Cluster 25	Enrichment Score: 3.72			
	microtubule	28	9.00E-03	6.70E-02

Clusters of SP-PIR Keywords identified by DAVID functional ontology analysis of genes down-regulated in dormant residual tumor cells compared to all other cell types (false discovery rate (FDR)<0.1, fold-change (FC) >1.5-fold).

Table 3.3. Gene Sets Up-regulated in Dormant Residual Tumor Cells in *HER2/neu-Prim1* and *Wnt1-Prim1* Models

Gene Sets Up-regulated in Wnt1 Dormant Residual Tumor Cells

	SP_PIR_KEYWORDS	# Up-regulated Genes in Cluster	p-value	FDR (Benjamini)
	Enrichment Score: 26.84			
Cluster 1	signal	276	8.20E-36	3.20E-33
	glycoprotein	302	2.00E-31	4.00E-29
	Secreted	151	6.80E-24	9.00E-22
	disulfide bond	211	1.50E-21	1.20E-19
Cluster 2	Enrichment Score: 15.65			
	extracellular matrix	42	2.00E-15	1.30E-13
Cluster 3	Enrichment Score: 14.27			
	cell adhesion	67	1.20E-21	1.20E-19
Cluster 4	Enrichment Score: 6.43			
	membrane	331	2.40E-10	1.40E-08
	transmembrane	305	7.70E-08	3.40E-06
Cluster 5	Enrichment Score: 4.94			
	heparin-binding	11	1.10E-04	3.10E-03

Gene Sets Up-regulated in HER2/neu Dormant Residual Tumor Cells

	SP_PIR_KEYWORDS	# Up-regulated Genes in Cluster	p-value	FDR (Benjamini)
	Enrichment Score: 12.94			
Cluster 1	signal	163	2.60E-16	8.00E-14
	glycoprotein	186	2.80E-16	6.00E-14
	Secreted	92	9.90E-13	1.20E-10
	disulfide bond	124	1.50E-09	1.30E-07
Cluster 2	Enrichment Score: 5.93			
	extracellular matrix	21	5.30E-06	3.10E-04
Cluster 3	Enrichment Score: 5.75			
	cell adhesion	33	1.10E-07	7.60E-06
Cluster 6	Enrichment Score: 2.83			
	heparin-binding	7	4.50E-03	1.50E-01
Cluster 7	Enrichment Score: 2.31			
	membrane	196	1.20E-03	5.00E-02
	transmembrane	184	3.40E-03	1.30E-01

Clusters of SP-PIR Keywords identified by DAVID functional ontology analysis of genes up-regulated in dormant residual tumor cells compared to all other cell types (FDR<0.1, FC >1.5-fold).

Table 3.4. Copy Number Variation (CNV) Analysis of Gene Sets Up-regulated in Dormant Residual Tumor Cells

Copy Number Variation Analysis of MTB/TAN/TTC1/rYFP Tumors and No Culture Orthotopic 'Syngeneic' Tumors

Group	Sample	Copy Number Gain		Copy Number Loss		
		CN > 2.3	CN > 3.5	CN < 1.7	CN < 1.5	CN < 0.5
Donor 1	Intact Donor	1	0	540	0	0
	Orthotopic 1	1478	35	3	1	0
	Orthotopic 2	1677	35	3	0	0
	Orthotopic 3	5760	35	681	1	0
Donor 2	Intact Donor	15	0	730	1	0
	Orthotopic 1	5074	47	72	71	0
	Orthotopic 2	5075	47	77	71	0
	Orthotopic 3	5072	48	77	71	0
Donor 3	Intact Donor	24	22	537	1	0
	Orthotopic 1	121	69	134	134	0
	Orthotopic 2	256	76	135	134	0
	Orthotopic 3	159	60	134	134	0
Controls	FVB	0	0	0	0	0
	B6 TS	157	13	16	11	0

CNV analysis of aCGH data showing copy number gains or copy number losses in genomic DNA isolated from donor or orthotopic tumors from the same donor tumor, or germline DNA from an FVB or Ts65Dn control.

Table 3.5. Gene Sets Differentially Regulated in Dormant Residual Tumor Cells

Gene Sets Up-Regulated in M/TAN/TTC/YFP No Culture Orthotopic Dormant Residual Tumor Cells

	SP_PIR_KEYWORDS	# Down-regulated Genes in Cluster	p-value	FDR (Benjamini)
Cluster 1	Enrichment Score: 8.37			
	transducer	183	5.90E-09	1.50E-06
	g-protein coupled recept	175	2.10E-08	3.50E-06
	receptor	276	2.50E-08	3.20E-06
Cluster 2	Enrichment Score: 7.83			
	transmembrane	535	7.50E-10	3.80E-07
	membrane	534	1.70E-06	1.70E-04
Cluster 3	Enrichment Score: 3.28			
	lipid transport	13	7.10E-04	4.30E-02
Cluster 4	Enrichment Score: 2.43			
	glycoprotein	353	1.10E-04	7.70E-03
	disulfide bond	230	2.40E-02	4.30E-01
	Secreted	138	2.60E-02	4.40E-01
	signal	272	2.90E-02	4.40E-01

Gene Sets Down-Regulated in M/TAN/TTC/YFP No Culture Orthotopic Dormant Residual Tumor Cells

	SP_PIR_KEYWORDS	# Down-regulated Genes in Cluster	p-value	FDR (Benjamini)
Cluster 1	Enrichment Score: 25.07			
	cell cycle	129	5.10E-29	9.30E-27
	cell division	87	4.90E-25	6.80E-23
	mitosis	68	9.20E-23	1.00E-20
Cluster 2	Enrichment Score: 15.35			
	cytoskeleton	125	3.30E-16	3.10E-14
Cluster 3	Enrichment Score: 11			
	nucleotide-binding	265	6.40E-16	5.20E-14
	atp-binding	216	2.00E-14	1.20E-12
	kinase	116	1.50E-07	4.70E-06
Cluster 4	Enrichment Score: 10.16			
	kinetochore	30	9.20E-14	5.10E-12
Cluster 5	Enrichment Score: 9.11			
	actin-binding	58	4.50E-11	1.70E-09
Cluster 6	Enrichment Score: 8.93			
	chromosomal protein	33	3.90E-06	9.00E-05
Cluster 8	Enrichment Score: 8.61			
	dna replication	34	2.20E-12	1.00E-10

Clusters of SP-PIR Keywords identified by DAVID functional ontology analysis of genes up-regulated (left) or down-regulated (right) in dormant residual tumor cells compared to all other cell types, in *MTB/TAN/TTC/rYFP* no culture orthotopic model (FDR<0.1, FC >1.5-fold).

Table 3.6. TIC Frequency Calculation for All Tumor Cells in Intact *MTB/TAN/TTC/rYFP* Primary Tumors or Residual Lesions

HER2/neu Donor Tumor Type	# Tumor Cells Injected					TIC frequency	95%CI Upper Limit	95%CI Lower Limit
	50,000	5,000	1,000	250	50			
Primary Tumor A	4/4	4/8	1/8	0/8	0/8	1 in 7,702	1 in 18,156	1 in 3,267
Primary Tumor B	3/3	8/8	5/8	5/8	1/8	1 in 593	1 in 1,155	1 in 305
Primary Tumor C	8/8	3/8	3/8	1/8	0/8	1 in 5,727	1 in 12,613	1 in 2,600
Residual Lesion D	4/4	8/8	7/8	3/8	1/8	1 in 486	1 in 936	1 in 252
Residual Lesion E	0/4	0/8	0/8	0/8	0/8	<1 in 224,473	NA	NA
Residual Lesion F	0/4	0/8	0/8	0/8	0/8	<1 in 224,473	NA	NA

Calculation of TIC frequencies for all YFP+ CD45-DAPI- singlet tumor cells from either *MTB/TAN/TTC/rYFP* primary tumors or residual lesions, injected into *nu/nu* mice on doxycycline.

Table 3.7. TIC Frequency Calculation for All Tumor Cells in Syngeneic Orthotopic *MTB/TAN/TTC/rYFP* Primary Tumors or Residual Lesions

HER2/neu Donor Tumor Type	HER2/neu Orthotopic Tumor Type	# Tumor Cells Injected				TIC frequency	95%CI Upper Limit	95%CI Lower Limit
		500	50	5	1			
Donor Tumor A	Primary Tumor A	1/8	0/8	0/8	0/8	1 in 4,193	1 in 593	1 in 29,638
	Residual Lesion A	1/8	0/8	0/8	0/8	1 in 4,193	1 in 593	1 in 29,638
Donor Tumor B	Primary Tumor B	8/8	8/8	6/8	1/8	1 in 4	1 in 2	1 in 9
	Residual Lesion B	1/8	0/8	0/8	0/8	1 in 4,193	1 in 593	1 in 29,638
Donor Tumor C	Primary Tumor C	8/8	8/8	0/8	0/8	1 in 22	1 in 11	1 in 48
	Residual Lesion C	NA	2/16	0/8	0/8	1 in 398	1 in 100	1 in 1,591

Calculation of TIC frequencies for all YFP+ CD45-DAPI- singlet tumor cells from syngeneic orthotopic primary tumors or residual lesions in *nu/nu* mice generated from the same *MTB/TAN/TTC/rYFP* donor tumors, injected into *nu/nu* mice on doxycycline.

Table 3.8. TIC Frequency Calculation for EpCAM+CD49e- Tumor Cells in Intact *MTB/TAN/TTC/rYFP* Primary Tumors or Residual Lesions

HER2/neu Donor Tumor Type (EpCAM+ Tumor Cells Only)	# Tumor Cells Injected					TIC frequency	95%CI Upper Limit	95%CI Lower Limit
	50,000	5,000	1,000	250	50			
Primary Tumor A	8/8	8/8	4/8	1/8	0/8	1 in 1,384	1 in 705	1 in 2,718
Residual Lesion B	0/4	0/8	0/8	0/8	0/8	< 1 in 224,473		

Calculation of TIC frequencies for epithelial singlet tumor cells (EpCAM+CD49e-YFP+CD45-DAPI- singlets) from either *MTB/TAN/TTC/rYFP* primary tumors or residual lesions, injected into *nu/nu* mice on doxycycline.

Table 3.9. TIC Frequency Calculation for All Tumor Cells in Intact *MTB/TWNT/TTC/rYFP* Primary Tumors or Residual Lesions

Wnt1 Donor Tumor Type	# Tumor Cells Injected					TIC frequency	95%CI Upper Limit	95%CI Lower Limit
	50,000	5,000	1,000	250	50			
Primary Tumor A	5/6	5/8	3/8	2/8	0/8	1 in 8,406	1 in 3,562	1 in 19,837
Residual Lesion B	4/4	0/8	0/8	0/8	0/8	1 in 31,190	1 in 11,850	1 in 82,092

Calculation of TIC frequencies for all YFP+ CD45-DAPI- singlet tumor cells from either *MTB/TWNT/TTC/rYFP* primary tumors or residual lesions, injected into *nu/nu* mice on doxycycline.

Table 3.10. TIC Frequency Calculation for All Tumor Cells in Syngeneic Orthotopic *MTB/TWNT/TTC/rYFP* Primary Tumors or Residual Lesions

Wnt1 Donor Tumor Type	Wnt1 Orthotopic Tumor Type	# Tumor Cells Injected					TIC frequency	95%CI Upper Limit	95%CI Lower Limit
		50,000	10,000	1,000	100	10			
Donor Tumor A	Primary Tumor A	7/8	4/8	0/8	0/8	0/8	1 in 20,717	1 in 10,363	1 in 41,420
	Residual Lesion A	2/8	0/8	0/8	0/8	0/8	1 in 218,487	1 in 55,163	1 in 865,380
Donor Tumor B	Primary Tumor B	6/8	2/10	0/10	0/10	0/12	1 in 40,033	1 in 19,563	1 in 81,923
	Residual Lesion B	1/4	0/10	0/10	0/10	0/12	1 in 285,390	1 in 41,155	1 in1,979,066

Calculation of TIC frequencies for all YFP+ CD45-DAPI- singlet tumor cells from syngeneic orthotopic primary tumors or residual lesions in *nu/nu* mice, generated from the same *MTB/TWNT/TTC/rYFP* donor tumors, injected into *nu/nu* mice on doxycycline.

Table 3.11. TIC Frequency Calculation for All Tumor Cells from H2B-eGFP-labeled Orthotopic *HER2/neu-Prim1* Primary Tumors or Residual Lesions

HER2/neu-Prim1 H2BeGFP Donor Tumor Type	*nu/nu* recipient on Doxycycline?	# Tumor Cells			TIC frequency	95%CI Upper Limit	95%CI Lower Limit
		500	50	5			
Primary Tumor	Yes	6/6	6/6	5/6	1 in 3	1 in 1	1 in 8
Residual Lesion	Yes	6/6	6/6	3/5	1 in 5	1 in 2	1 in 17
Primary Tumor	No	0/6	0/6	0/6	< 1 in 3,073		
Residual Lesion	No	4/6	0/6	1/6	1 in 427	1 in 168	1 in 1,085

Calculation of TIC frequencies for all GFP+CD45-DAPI- singlet tumor cells from H2B-eGFP-labeled *HER2/neu-Prim1* primary tumors or residual lesions, injected into *nu/nu* mice either on doxycycline or not on doxycycline.

Methods

Statistics

Unless otherwise noted, all statistical analyses providing a p-value were conducted using student's two-sided T-test assuming homoscedastic variance, performed in Excel (Microsoft).

Mice

Animal care and experiments were performed with the approval of, and in accordance with, guidelines of the University of Pennsylvania IACUC. Bitransgenic and nude mice were generated and tumors were induced, deinduced, monitored for tumor recurrence, and sacrificed as described [108, 121, 126]. NSG mice were acquired from Jackson Laboratory (stock #005557). For HER2 blockade, NSG mice were administered 100mg/kg Lapatinib by oral gavage 5 days/week and 20mg/kg Trastuzumab and 20mg/kg Pertuzumab three times per week.

Tissue Culture and Reagents

Primary tumor cells were cultured, and stable H2B-eGFP expression was achieved as described [108, 126].

BT474-M1 tumor cells were a generous gift from Dr. Mien-Chie Hung. Cells were grown as above, in media consisting of 10% fetal bovine serum (FBS, Gibco), 1% Penicillin/Streptomycin in Dulbecco's modified eagle's medium (DMEM)/F12 (GIBCO 11330-032). Stable GFP expression was achieved by transduction with GFP Bsd Lentiviral particles (Gentarget, LVP001) followed by culture in media containing 10μg/ml blasticidin.

Orthotopic Recurrence Assay

Recurrence assays were performed as described [108]. Recurrence-free survival curves were displayed as Kaplan-Meier survival curves using Prism 5.03 (Graph Pad Software, Inc).

Intravital Labeling

Intravital labeling was performed as a series of intravenous (i.v.) injections prior to sacrifice. Pimonidazole HCl (Hypoxyprobe™-1, NPI Inc.) was resuspended in phosphate buffered saline (PBS) at 20μg/μl, and injected i.v. at 60mg/kg 90 min prior to sacrifice. Hoechst 33342 (230001000, Thermo Fisher Scientific Inc.) was resuspended in PBS at 5μg/μl and injected i.v. at 20mg/kg 15 min prior to sacrifice. Lectin-AF647 was prepared by resuspending 1mg

Lycopersicon Esculentum Lectin (B-1175, Vector Labs, Inc) in 425µl of PBS and mixing with 75µl of Streptavidin, AlexaFluor® 647 Conjugate (S-32357, Life Technologies Corporation). Lectin-AF647 was centrifuged briefly to remove protein aggregates and was injected i.v. 10 min prior to sacrifice. Mammary glands bearing MRLs 28d following oncogene deinduction, as well as livers from same mice, were harvested at sacrifice and placed directly into Optimal Cutting Temperature (OCT, Tissue-Tek, VWR).

Immunofluorescence and Direct Fluorescence

Normal mammary glands or mammary glands bearing MRLs were harvested, embedded in OCT compound, and frozen. 8µm tissue sections were either fixed and permeabilized in dehydrated acetone at -20°C for 10 min, or fixed in 4% paraformaldehyde for 10 min at room temperature (RT) and permeabilized in 0.1% Triton-X-100 in PBS for 20 min. Following fixation and permeabilization, sections were washed 2x5 min in PBS, blocked for 1 hr with 10% normal goat serum with 3% BSA in PBS and incubated overnight (O/N) at 4°C with primary antibody diluted in blocking buffer. Primary antibodies used to stain tissues fixed in paraformaldehyde were: CD31 (1:200, AB28364, AbCam), CK5 (1:1000, PRB-160P, Covance), CK14 (1:10,000, PRB-155P, Covance), CK19 (1:50, AB15463, AbCam), Pan-CK Ab (1:100, SC-15367, Santa Cruz), E-Cadherin (1:100, 13-1900, Zymed), P-Cadherin (1:50, 13-200, Zymed), p63 (1:500, AB53039, AbCam), Collagen Type-I (1:250, AB34710, AbCam), Ki67 (1:50, M7249, Dako), and BrdU (1:200, OBT0030, AbD Serotec). Primary antibodies used to stain tissues fixed in acetone were: Ep-CAM (1:100, 14-5791, eBioscience) and CK18 (1:100, NB110-56910, Novus Biologicals). For BrdU staining, following fixation and permeabilization, sections were incubated with 2N HCl for 10 min at 25°C and then 20 min at 37°C, followed by incubation in 0.1M sodium tetraborate for 15 min, and then blocked (as above) and stained with primary antibody. For staining of tissues with primary antibodies raised in mice, specifically those against Fibronectin (1:200, 610077, BD Transduction), the M.O.M.™ Immunodetection Kit (Vector Laboratories) was used with Avidin/Biotin Blocking Kit (Vector Laboratories). Following O/N incubation with primary antibody, tissues were washed 2x10 min in PBS, and incubated for 1 hr at RT with AlexaFluor-conjugated secondary antibody (1:1000 dilution, Life Technologies Corporation). Sections were then washed

10 min in PBS, 10 min in PBS with a 1:10,000 dilution of Hoechst 33258 (Sigma-Aldrich Co.), and 5 min in PBS. Sections were mounted in ProLong® Gold Antifade Reagent (Molecular Probes®, Life Technologies Corporation), sealed with clear nail polish, and allowed to dry.

Slides were imaged with a Leica TCS SP5 (Leica Microsystems) confocal microscope using Leica Application Suite Advanced Fluorescence (LAS AF, Leica Microsystems) software. Images showing Ki67 or BrdU staining of H2B-eGFP-labeled HER2/neu-Prim1 tumor cells in Figure 3.7 is presented as a masked image, wherein a binary mask is generated from the GFP channel and applied to the Ki67 or BrdU channel, so that only Ki67 or BrdU co-staining with tumor cells is shown. For all images used for quantification, either the entire MRL, or 1mm x 1mm of the primary tumor, was imaged as a mosaic image.

Image Quantification

Images were quantified using CellProfiler (Broad Institute) software. Briefly, to quantify Ki67 or BrdU, a mask was generated (as above) using H2B-eGFP nuclei from a mosaic image. The number of nuclei that stained positive for Ki67 or BrdU was determined using this mask. The fraction of tumor cells expressing BrdU or Ki67 was calculated as the total number of nuclei that stained positive for Ki67 or BrdU divided by the total number of nuclei.

Flow Cytometry and Fluorescence-activated Cell Sorting (FACS)

Immediately following harvest, tissues from mice were digested enzymatically using collagenase/hyaluronidase (Stemcell Technologies) for 90 min at 37ºC, followed by pipetting vigorously in DNAse (Worthington Biochemical Corporation) and Dispase (Stemcell Technologies) for 5 min at 37C. Tissue digests were strained through a 40μm filter (BD Falcon). Single-cell suspensions were stained with fluorophore-conjugated antibodies for 30 min at 4ºC in 1%BSA and 5mM Ethylenediaminetetraacetic acid disodium salt (EDTA) in PBS. Antibodies used were: CD45;AF700 (1:50, 560510, BD Biosciences), CD49e;PE (1:50, 557447, BD Pharmingen), CD24;Pe-Cy7 (1:200, 560536, BD Biosciences), EpCAM;APC-Cy7 (1:50, 118218, BioLegend), and PDGFR-β;APC (1:50, 17-1402, eBiosciences). Cells were washed twice in FACS diluent (PBS with 1% bovine serum albumin (BSA, Sigma) and 5mM EDTA (Sigma)), and resuspended in FACS diluent with 1μg/ml DAPI (Sigma-Aldrich Co.) for identifying viable cells. Compensation

was performed using AbC™ anti-mouse bead kit (A10344, Life Technologies Corporation) and anti-rat/hamster bead kit (A10389, Life Technologies Corporation), according to manufacturer's instructions. Flow cytometry was performed on a BD FACSCanto™ system using BD FACSDiva™ software (BD Biosciences).

Data were analyzed using FlowJo. Dead cells, debris, and doublets were removed by sequentially analyzing gates for DAPI, SSC-A vs. FSC-A, SSC-W vs. SSC-H and FSC-W vs. FSC-H staining, respectively.

With the exception of enzymatic digest at 37ºC, all steps for flow cytometry, FACS, and limiting dilution experiments were performed at 4ºC. For tumors harvested from mice bearing a YFP-reporter, tumor cells were defined as YFP+CD45-DAPI- cells, excluding all dead cells, debris, and doublets as above.

Expression Analysis of Purified Tumor and Stromal/Immune Cells

Tissue digestion was performed as above for flow cytometry, with the exceptions that digestion in collagenase/hyaluronidase was limited to 20 min. Tissue/cells were maintained on ice or at 4ºC for all other steps prior to resuspension in Trizol after sorting, in order to minimize transcriptional changes. To further minimize transcriptional changes, antibody staining was omitted and sorting was based on GFP expression and DAPI staining.

Removal of dead cells, debris, and doublets, was performed as above for flow cytometry. Cell sorting was performed on a BD FACSVantage cell sorter. Cells were sorted into complete media (including doxycycline for primary tumor cells), chilled to 4ºC, and maintained on ice. Immediately following sorting, cells were pelleted and resuspended in TRIZOL.

Phenol/chloroform extraction was used in conjunction with the QIAGEN RNeasy kit to isolate mRNA. Isolated RNA was analyzed on an Agilent Bioanalyzer, and only samples with an RNA integrity number of at least 7.0 were selected for subsequent amplification and expression analysis. 500pg of RNA was used as the input for whole transcriptome amplification (WTA) with NuGEN Ovation Pico WTA V2.0 kits.

An expression heat map of ribosomal protein gene expression was generated using GENE-E (www.broadinstitute.org/cancer/software/GENE-E/).

CHAPTER 4

Modeling the Impact of Immune Modulation on Breast Cancer Recurrence

The immune system is a critical player in the development and progression of cancer. Whereas the immune system may promote tumor growth through inflammatory signaling in some cancers, it may alternatively serve a critical role in the elimination of cancer in other settings [13]. Recent clinical trials with checkpoint blockade inhibitors have revealed a central role for therapies that activate the immune system, however the impact of directly activating antigen presenting cells with anti-CD40 stimulatory antibodies on breast cancer recurrence remains unknown. Alternately, results from the Nurses' Health Study indicate that daily intake of aspirin (acetylsalicylic acid) is associated with a dramatic decrease in tumor recurrence, though the biological basis for this observation is unclear. Anti-cancer therapies may also elicit different immune responses, which can have a significant impact on subsequent treatment with immune-based therapies. Given the increasing importance of immune-oncology and the dramatic rise in the use of targeted therapy in the clinic, we investigated the role of the immune system and inflammation in residual disease following oncogenic pathway inhibition.

Characterization of leukocytes in residual disease

Prior observation of mesenchymal residual tumor cells revealed a complex inflammatory infiltrate surrounding residual tumor cells (Figure 3.25). To identify the phenotype of these residual tumor cells we performed IF for macrophage marker F4/80 and T-cell marker CD3 on tissue sections of residual lesions in intact quadtransgenic *MTB/TAN/TTC/rYFP* mice. In regions previously identified to harbor mesenchymal tumor cells (Figure 3.25), we identified large numbers of macrophages juxtaposed with dormant residual tumor cells, as well as a corona of T cells (Figure 4.1A). This pattern was seen repeatedly in areas with mesenchymal residual tumor cells, and could be discretized into sections with mesenchymal residual tumor cells and macrophages (Figure 4.1B, region a), sections with abnormal ductal morphology and T-cell infiltration

surrounding the macrophages (Figure 4.1B, region b), and areas with no apparent residual tumor cells or recurrent pattern of inflammatory infiltrate (Figure 4.1B, region c).

Previous reports have indicated that macrophage invasion in primary tumors is associated with poor prognosis [151-153]. These reports look at expression of either CD68 or CD163 in breast cancer patients but did not explore alternate transcripts specific to macrophages, and did not stratify patients to determine the prognostic impact of these markers on breast cancer subtypes. Combining survival data from several publicly available datasets as before (Figure 3.27), we asked whether expression of macrophage related markers was prognostic for poor RFS and stratified our results by breast cancer subtype, as well as grade and lymph node status. Consistent with prior reports, we identified increased expression of CD68 and CD163 as correlated with poor 5- and 10-year RFS (Figure 4.2A, E). Interestingly, for both CD68 and CD163, these markers were prognostic for poor RFS only in breast cancer patients with estrogen receptor positive (ER+) breast cancer who had received treatment, whereas they associated with improved outcome in patients with ER- breast cancer who had been treated with systemic therapy, and did not hold the same prognostic value in patients who had not been treated with systemic therapy (Figure 4.2A, E). Increased expression of alternate markers specific to macrophages, including CSF1R and CD14, were not associated with poor RFS, and both were instead associated with improved RFS in patients with ER- breast cancer (Figure 4.2 C, D). Similarly, the myeloid marker CD11b and the M1 macrophage-associated marker CD11c – which is also a marker for dendritic cells – were associated with improved RFS in patients with ER- breast cancer (Figure 4.2 B, F). These findings indicate that, while increased expression of the macrophage markers CD68 and CD163 are prognostic for poor RFS in ER+ breast cancer, macrophage-associated markers are associated with improved RFS in ER- breast cancer. Interestingly, increased expression of CSF1R was associated with improved RFS even in patients with ER+ breast cancer, a finding that is consonant with recent preclinical results suggesting CSF1R inhibition may promote metastases in some models of breast cancer [154]. Differences in survival when looking at alternate markers that should be specific to macrophages, such as CD68, CSF1R, and CD14, suggest that while the proteins associated with these transcripts are

used as markers specific to all macrophages, different transcripts may be associated with heterogeneous macrophage subpopulations.

While these data suggested a complex role for macrophage biology in primary tumors, they did not inform whether macrophages present in residual disease are critical for tumor recurrence. To determine whether macrophages are involved in tumor recurrence, we looked at transcript levels of macrophage-related markers in recurrent tumors compared to primary tumors in mouse models. We identified 8 different macrophage markers as significantly up-regulated in recurrent tumors compared to primary tumors, in tumors driven by three different oncogenes: *HER2/neu*, *Wnt1*, and *c-Myc* (Figure 4.3A). These data suggested that macrophages were associated with tumor recurrence in breast cancer models driven by different oncogenes.

To better phenotype and study macrophages, we used an orthotopic model of *HER2/neu-Prim1* tumor cells labeled with H2B-eGFP, and this model facilitates both easier identification of residual disease, and studies in larger cohorts of mice in a shorter time frame than is possible with intact animals. IF staining revealed that residual lesions in *HER2/neu-Prim1* tumors in *nu/nu* mice harbored a large number of F4/80+ macrophages, similar to the intact system (Figure 4.3B). To determine the relative proportion of different myeloid populations in residual lesions, we used flow cytometry to phenotype CD45+CD11b+ leukocytes in residual lesions. The majority of myeloid cells were Ly6C-Ly6G-, and expressed F4/80 and CD115 (CSF1R), consistent with a macrophage phenotype (Figure 4.3C), suggesting that macrophages were the primary myeloid cell population in residual disease.

We previously observed that residual lesions exposed to BrdU for 2 weeks contained a large number of BrdU-positive non-tumor cells. If these cells were macrophages, it would raise the possibility that the residual lesion macrophages were either locally proliferative, or were newly generated myeloid cells recruited from a distant site. If either of these was the case, they would open the opportunity to inhibit macrophage proliferation in, or recruitment to, the residual lesion. Thus, we used flow cytometry to investigate the uptake of BrdU over 2 weeks by myeloid cells in the residual lesion. CD45+CD11b+Ly6C-Ly6G-F4/80+CD115+ macrophages and

CD45+CD11b+Ly6C-Ly6G-F4/80+CD115+ resident monocytes incorporated BrdU at a more than 3-fold higher rate than dormant residual tumor cells or than CD45+CD11b+Gr1+ myeloid-derived suppressor cells (MDSCs) (Figure 4.3D), supporting the idea that macrophages either proliferated in, or were recruited to, dormant residual lesions.

Finally, to further characterize macrophages in residual lesions, we performed IF for CD163, CD206, Ym1, and RELMα (Fizz1). These markers are generally associated with 'alternatively activated' macrophages, a phenotype that has been associated tumor associated macrophages (TAMs) in previous reports [155]. Macrophages inside the residual lesion expressed CD206, but only macrophages around the border of the residual lesion expressed CD163, and no macrophages near the residual lesion expressed Ym1 or RELMα (Figure 4.3 E-I). We also observed CD206 expression in red pulp macrophages, which are not alternatively activated macrophages, and thus it was unclear that expression of CD206 alone was sufficient to indicate that residual lesion macrophages were alternatively activated (Figure 4.3E).

Together, these results provide a picture of residual lesion macrophages as a dynamic population that do not express markers of alternatively activated macrophages sometimes associated with TAMs.

Activating macrophages with anti-CD40 antibodies does not inhibit tumor recurrence

Our results indicated that macrophages comprised the major leukocyte population in residual disease. Recent reports indicate that antibodies stimulating CD40 on macrophages can activate them in a manner that inhibits tumor progression in desmoplastic pancreatic tumors [156]. As residual lesions are highly desmoplastic (Figure 3.17), we hypothesized that activation of macrophages with the anti-CD40 antibody FGK45 might inhibit tumor recurrence in mice following oncogenic pathway inhibition.

Prior to administering FGK45, we wanted to know whether tumor cells expressed CD40, and thus whether FGK45 might bind directly to the tumor cells, as this would complicate our subsequent interpretation of results. Using both flow cytometry and IF, we found that while leukocytes in

primary tumors and residual lesion-juxtaposed lymph nodes expressed CD40, primary tumor cells and residual lesion tumor cells did not express CD40 (Figure 4.4). As leukocytes expressed CD40, we next asked whether macrophages would express an activated phenotype upon treatment with anti-CD40 antibodies. To test this, we administered FGK45 or isotype control to mice bearing regressing tumors 72 hours after doxycycline withdrawal, and harvested tumors from these mice 60 hours after FGK45 administration. Macrophages in regressing tumors showed increased expression of activation markers CD86 and CD40, but not MHC-II, after stimulation with FGK45 (Figure 4.5).

As FGK45 administration inhibits pancreatic tumor progression concurrent with a depletion of pancreatic tumor stroma, we examined tumor stroma in mice treated with FGK45, at the same time point where macrophages had also shown increased expression of activation markers CD40 and CD86. Collagen type-I and Masson's trichrome staining did not reveal any differences in ECM density between treated and untreated mice (Figure 4.6A, B). These results, as well as the lack of increased MHC-II activation on FGK45-stimulated macrophages, were inconsistent with results observed in the previous study in pancreatic cancer [156]. However, as FGK45-treated macrophages increased their expression of activation markers CD40 and CD86, this suggested that the macrophages may have been sufficiently activated to have an impact on tumor progression, and we thus asked whether FGK45 administration impacted tumor recurrence.

We administered a single dose of FGK45 or isotype control to either intact *MTB/TAN* mice, or orthotopic *HER2/neu-Prim1* tumors in syngeneic *TAN* mice, either 72 hours after doxycycline withdrawal, or 4 weeks after doxycycline withdrawal, and monitored mice for recurrence (Figure 4.6C). Intact *MTB/TAN* mice treated with FGK45 72 hours after doxycycline administration showed a decreased recurrence latency, while no other cohort demonstrated a change in time to recurrence (Figure 4.6D, E). These results were surprising, as we had originally hypothesized that administration of a stimulatory anti-CD40 antibody would inhibit tumor recurrence, consistent with its role for inhibiting pancreatic cancer in mice and humans.

To follow up on these results, we wanted to know whether the increased rate of recurrence was due to the presence of macrophages or T-cells. We repeated the previous experiment in *MTB/TAN* mice with administration of FGK45 72 hours after doxycycline withdrawal, and mice were either ablated for macrophages with clodrolip, or ablated for T-cells with a combination of anti-CD4 and anti-CD8 antibodies (Figure 4.6F). Strikingly, none of the mice recapitulated the decreased recurrence latency that was seen in the first study (Figure 4.6G).

Given the relatively small number of animals used in the intact *MTB/TAN* studies (n=10 per cohort), the most likely explanation for our observation in Figure 4.6D is that the result was a random event. In this cohort, all mice recurred by 130 days, which is approximately the mean recurrence latency for *MTB/TAN* mice as a population (Figure 3.1), thus it is not implausible that all mice would develop recurrent tumors by that time in a cohort of 10 mice. Additionally, including both *MTB/TAN* and syngeneic orthotopic models, we followed recurrence in four cohorts of mice, thereby increasing our chance of seeing a false positive result.

Impact of non-steroidal anti-inflammatory drugs (NSAIDs) on tumor recurrence

Recent analysis of data from the Nurses' Health Study indicates that daily NSAID intake may significantly delay the time to tumor recurrence in breast cancer patients [157]. Previous studies investigating a link between aspirin intake and primary breast cancer incidence identified decreased rates of ER+ breast cancer in women regularly using NSAIDs [158]. This connection was attributed to the impact of blocking COX activity with aspirin or other NSAIDs on estrogen production from aromatase [159], and no impact was seen on ER- breast cancer. The findings from the Nurse's Health Study were especially interesting because they suggested that daily aspirin intake inhibited breast cancer recurrence in both ER+ and ER- breast cancer, thus suggesting that NSAID intake inhibited breast cancer recurrence through an as-of-yet unidentified mechanism.

We considered the possibility that administration of NSAIDs might inhibit cancer recurrence in *HER2/neu-Prim1* orthotopic tumors, and that these models may be useful to identify the mechanism underlying aspirin's protective effect in women with breast cancer. As macrophages

can exhibit an inflammatory phenotype, and macrophages constitute the major leukocyte population of residual lesion in our model, it is possible that if macrophages impact recurrence, they could do so through promoting inflammation near residual tumor cells. In support of a role for COX inhibitors, such as NSAIDs, in abrogating tumor recurrence in our models, we observed that COX2 staining on blood vessels and leukocytes by IF in H2B-eGFP-labeled *HER2/neu-Prim1* residual lesions in *nu/nu* mice (Figure 4.7A). As NSAIDs inhibit prostaglandin synthesis, we also examined gene expression of prostaglandin synthesis-related genes in primary and recurrent tumors, in models driven by either *HER2/neu*, *Wnt1*, or *c-Myc* oncogenes. We found an increase in transcripts associated with prostaglandin synthesis, including COX1, COX2, and PTGES, as well as transcripts associated with prostaglandin signaling, PTGER2 and PTGER4 (Figure 4.7B), supporting the possibility that NSAIDs may impact tumor recurrence in these models through its effect on prostaglandin signaling.

To test whether NSAIDs might have an impact on tumor recurrence, we performed a recurrence assay on *nu/nu* mice bearing orthotopic H2B-eGFP-labeled *HER2/neu-Prim1* tumors, given drinking water that either did or did not contain high-dose aspirin (60mg/kg/day). There was not a significant difference between times to recurrence in the two cohorts (Figure 4.7C). We subsequently found prior reports indicating that mice metabolize aspirin at a significantly higher rate than rats or humans, raising the possibility that aspirin was not an effective NSAID in mice [160]. It was also possible that an intact immune system was required in order to see an impact of COX inhibition on tumor recurrence. To address both of these possibilities, we performed recurrence studies in both *nu/nu* mice bearing *HER2/neu-Prim1* orthotopic tumors, and also *MTB/TAN* mice, where mice in both studies were randomized to receive either indomethacin in drinking water, or drinking water alone. While both studies showed a trend towards an increase in RFS, only the study in *HER2/neu-Prim1* orthotopic tumors in *nu/nu* mice was statistically significant (Figure 4.7 D, E).

The magnitude of the delay in time to recurrence is significantly smaller than was seen in the results from the Nurses' Health Study, thus it was unclear that these models were ideally suited to identify a role for NSAIDs in breast cancer recurrence.

Dexamethasone inhibits cancer recurrence at doses that also ablate macrophages

As macrophages are the primary myeloid population in residual disease in our models, and macrophage-related transcripts were increased in recurrent tumors relative to primary tumors, we hypothesized that ablation of macrophages might inhibit tumor recurrence. A previous report used dexamethasone to eliminate macrophages [161], consistent with dexamethasone's role as a broadly immunosuppressive corticosteroid.

To determine whether macrophage ablation with dexamethasone inhibited tumor recurrence, we performed a recurrence assay in both intact *MTB/TAN* and *HER2/neu-Prim2* orthotopic tumors in *nu/nu* mice, treated either with 80mg/kg (mpk) dexamethasone or vehicle control. In both studies, we observed a dramatic decrease in recurrence in cohorts treated with dexamethasone (Figure 4.8A, B). Given the high dose used in these studies, we wanted to know whether lower doses of dexamethasone also inhibited recurrence, and whether doses that inhibited recurrence tracked with doses that also ablated macrophages. To answer these questions, we performed a recurrence assay using *HER2/neu-Prim1* orthotopic tumors in *nu/nu* mice enrolled into one of 5 cohorts, either a control cohort, or a cohort administered one of four doses of dexamethasone: 80mpk, 10mpk, 1mpk or 0.1mpk. Mice treated with 80mpk or 10mpk dexamethasone exhibited statistically significant delays in time to recurrence compared to control cohorts, but the same effect was not seen at lower doses of dexamethasone (Figure 4.8C). Consistent with our hypothesis that macrophages in the minimal residual lesion promote recurrence, we observed that only doses of dexamethasone that also led to a significant decrease in the number of macrophages, determined by quantification of IF staining on tissue sections of residual lesions, had an impact on tumor recurrence (Figure 4.8D). Orthotopic residual lesions that never recurred, in mice treated with 80mpk dexamethasone for more than 200d, displayed a significantly lower number of cells than residual lesions observed 28d after doxycycline

withdrawal in untreated mice (Figure 4.8E). Consistent with broad immunosuppression, lymph nodes in these mammary glands displayed significant signs of atrophy, lacking germinal centers (Figure 4.8F).

Our findings supported the possibility that ablating macrophages inhibits tumor recurrence, however as dexamethasone is a broadly immunosuppressive drug, it remained unclear whether the delay in recurrence we observed was due to the impact of dexamethasone on macrophages.

Macrophage-specific ablation and tumor recurrence

As a first step to determine whether macrophage-specific ablation delayed tumor recurrence, we sought methods that could ablate macrophages in residual lesions with greater specificity than dexamethasone. Towards this end, we considered the use of liposome-encapsulated clodronate (clodrolip), a well-established method to systemically ablate macrophages [162]. While this method robustly ablated splenic macrophages, it did not ablate macrophages within the residual lesion (Figure 4.9 A). Next, we considered the possibility that residual lesion macrophage precursors were GR1+ monocytes. Administration of RB6-8C5, an antibody against GR1, ablated over 99% of peripheral blood monocytes (Figure 4.9 C, D). We performed a recurrence study with *HER2/neu-Prim1* orthotopic tumors in *nu/nu* mice treated either with RB6-8C5 or an isotype control antibody. Ablation of GR1 expressing cells did not inhibit tumor recurrence (Figure 4.9E) and did not ablate F4/80 macrophages in the residual lesion (data not shown).

Interestingly, we observed that mice treated with chronic RB6-8C5 developed massive splenomegaly (Figure 4.10A). In general, the size of recurrent *HER2/neu-Prim1* orthotopic tumor in an untreated *nu/nu* mouse at time of sacrifice is directly proportional to the size of the mouse's spleen (Figure 4.10B). In spite of this correlation, we found that mice treated with chronic RB6-8C5 developed massive splenomegaly prior to the development of recurrent tumors (Figure 4.10C). In contrast, mice treated with 80mpk or 10mpk dexamethasone had small spleens at time of recurrence, however mice treated with 1mpk or 0.1mpk dexamethasone did not have significantly smaller spleens upon tumor recurrence (Figures 4.10C-E). These data suggest that, while RB6-8C5 may have depleted a population of peripheral blood cells that can act as

macrophage precursors, chronic administration of the antibody may also lead to splenomegaly, possibly due to increased production of leukocyte populations.

As a next step to specifically ablate macrophages, we identified methods that ablate macrophages in a *c-fms*-dependent manner. *c-fms* is the gene encoding CSF1R, an indispensable receptor for the maturation and development of macrophages, and strategies targeting c-fms through antibodies or genetic-based ablation methods can be used to selectively eliminate macrophages. Thus, we tested the efficacy of the anti-c-fms antibody M279 compared to an isotype control for ablating F4/80+ macrophages in *HER2/neu-Prim1* orthotopic residual lesions, and found that the vast majority of macrophages were ablated, with some residual lesions showing practically no macrophages following M279 treatment (Figure 4.11A). We also used a second approach for ablating macrophages in a c-fms-dependent manner in intact *MTB/TAN* mice, by crossing these mice to transgenic 'Macrophage ablation through fas-induced apoptosis,' or Mafia, mice. The *Mafia* transgene contains a fusion protein product and GFP reporter both downstream of a c-fms-dependent promoter [163]. Upon administration of a small molecule dimerizing agent, AP20187, the cell membrane-localized protein product from the *Mafia* transgene dimerizes and initiates apoptotic signaling through the cell's Fas-induced apoptosis pathway. The GFP reporter allows easy identification of c-fms+ macrophages. Upon administration of AP20187, more than 80% of CD45+CD11b+c-fms-GFP+ macrophages in residual disease-bearing mammary glands from *MTB/TAN/Mafia* mice were ablated (Figure 4.11B).

Using these two c-fms-dependent macrophage ablation methods, we performed a recurrence assay in *HER2/neu-Prim1* orthotopic tumors in *nu/nu* mice with the anti-c-fms antibody M279 (Figure 4.11C), and in *MTB/TAN/Mafia* mice with AP20187 (Figure 4.11D). Both studies showed a trend towards a delay in recurrence in mice treated with macrophage ablating methods compared to controls, however only the result from the anti-c-fms antibody ablation study was statistically significant (Figure 4.11E-F).

The delay in recurrence with c-fms-dependent macrophage ablation was modest compared to the impact of dexamethasone-induced macrophage ablation. To better understand this discrepancy we investigated the phenotype of residual lesion macrophages in residual lesions 28 days after doxycycline withdrawal from these two models. As the anti-c-fms antibody has been reported to be ineffective against inflammatory macrophages [164], we stained for the inflammatory macrophage marker CD11c in parallel with F4/80. Residual lesions from control residual lesions 28d after doxycycline withdrawal showed a dense infiltrate of macrophages, many of which were CD11c+ (Figure 4.11G, left). In dexamethasone-treated residual lesions, almost no F4/80+ macrophages were present, and none of these macrophages expressed CD11c (Figure 4.11G, middle). In contrast, while few macrophages were also present in residual lesions from M279-treated mice, these macrophages uniformly displayed a CD11c+ phenotype (Figure 4.11G, right). Taken together, these findings suggest that the presence of CD11c+F4/80+ inflammatory macrophages in M279-treated mice may account for the relatively modest results seen with anti-c-fms therapy relative to dexamethasone, and thereby suggest that elimination of pro-inflammatory CD11c+F4/80+ macrophages may allow for more complete inhibition of tumor recurrence.

Inflammation and tumor recurrence

Our aforementioned results begin to suggest that CD11c+F4/80+ macrophages may promote recurrence. To test whether inflammation may generally promote recurrence, we performed a recurrence assay with *HER2/neu-Prim1* orthotopic tumors in *nu/nu* mice, in which mice were randomly assigned to a cohort that would have local inflammation induced within the residual lesion, or a cohort that would simply remain under observation with no other intervention. To induce inflammation, we injected 50ul of sterile saline using a fresh sterile syringe directly into the residual lesion of the *nu/nu* mouse every third day. To ensure that the needle tip was inside the residual lesion, the needle was inserted and removed from the mammary gland several times in order to identify a region that resisted insertion of the needle. Presumably, the relatively high levels of ECM in the residual lesion make it more difficult to insert a needle into the residual lesion

than into other parts of the mammary gland, therefore this method allowed accurate localization of residual disease inside of a mammary gland without surgical intervention.

Using *HER2/neu-Prim1* orthotopic tumors in *nu/nu* mice, we began saline injection 3 days after doxycycline withdrawal, and repeated every three days (q3d). Residual lesions harvested 28d after doxycycline withdrawal from mice chronically injected with saline produced higher levels of the pro-inflammatory cytokine IL6 than residual lesions from uninjected mice (Figure 4.12A). We then performed a recurrence assay using orthotopic *HER2/neu-Prim1* tumors in *nu/nu* mice, and upon doxycycline withdrawal, randomly enrolled mice into cohorts to either be injected chronically with saline q3d, or to remain uninjected (Figure 4.12B). Mice chronically injected with saline demonstrated a faster rate of recurrence than mice that were uninjected (Figure 4.12C), suggesting that inflammation promotes recurrence in this model.

Discussion

Together, our results portray a complex phenotype of leukocytes present in residual disease following oncogenic pathway inhibition. Across multiple studies, treatments that promote inflammation or activate macrophages promote recurrence, whereas studies that inhibit inflammation or deplete macrophages protect mice against recurrence. These results are generally consistent with clinical observations that anti-inflammatory drugs inhibit tumor recurrence in breast cancer patients, although they do not address the specific pharmacological mechanism by which NSAIDs might inhibit tumor recurrence in breast cancer patients.

Our observation that macrophages are recruited to residual lesions is consistent with reports that demonstrate recruitment of macrophages in a c-fms-dependent manner to breast cancer following treatment with cytotoxic chemotherapy [151]. In this study, c-fms-dependent ablation improved overall survival when given in combination with cytotoxic chemotherapy, paclitaxel. Alternately, a study showing that anti-CD40 macrophage activation following cytotoxic chemotherapy with gemcitabine can dramatically inhibit tumor growth [156]. We did not observe a dramatic decrease in time to recurrence using either c-fms-dependent macrophage ablation or macrophage stimulation with an anti-CD40 antibody. One possible explanation for the

differences between our findings and previous reports is that doxycycline withdrawal in our models most closely represents oncogenic pathway inhibition with targeted therapy, but may not have the immunological impact as chemotherapy. As various chemotherapies may have either immune stimulatory or immunosuppressive effects [165], this may account for a proportion of the differences we see between our results and results in systems using chemotherapy.

Indeed, the use of macrophage-ablating therapies in combination with antibody-based targeted therapies may inhibit the efficacy of these targeted therapies, given that macrophage-stimulatory agents can promote the activity of drugs such as trastuzumab and rituximab [166].

Nonetheless, our observations with dexamethasone-based macrophage ablation provide the exciting possibility that appropriately ablating inflammatory macrophages may dramatically inhibit tumor recurrence in some settings.

Figure 4.1. Distribution of Leukocyte Populations Relative to Mesenchymal Residual Tumor Cells

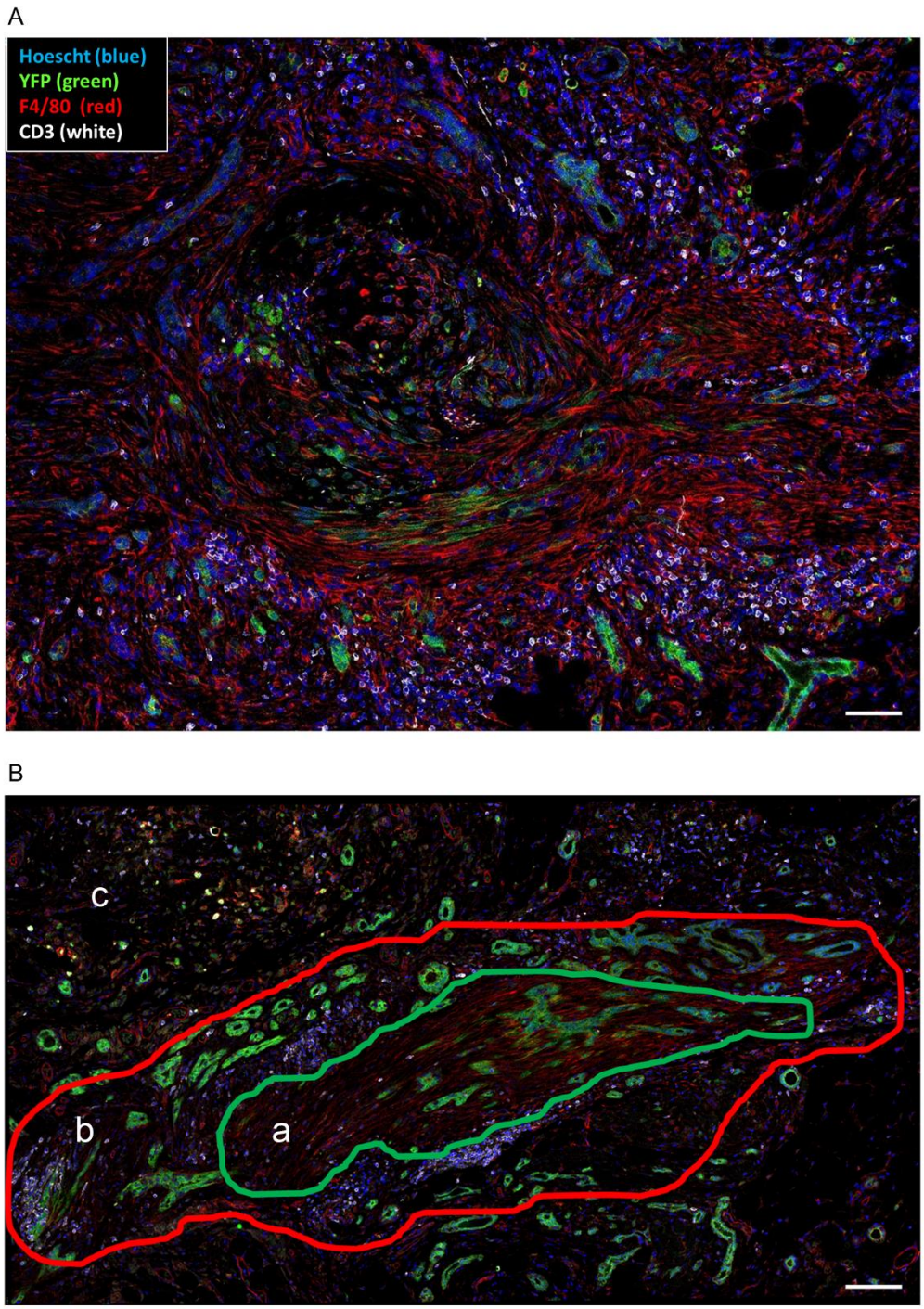

(A, B) IF imaging for Hoechst, tumor cell marker YFP, macrophage marker F4/80, or T-cell marker CD3, in a tissue section of a residual lesion from an intact *MTB/TAN/TTC/rYFP* mouse. (B)

Labels for different regions repeatedly identified across multiple residual lesions, including a region with mesenchymal tumor cells and macrophages (a), a region with abnormal ducts and T-cells (b), and a region with disorganized mammary fat pad morphology showing extensive autofluorescence and inflammatory infiltrate (c). Scale bars 100μm for all images.

Figure 4.2. Association Between Macrophage-related Transcripts and Recurrence-free Survival (RFS) for Breast Cancer Patients

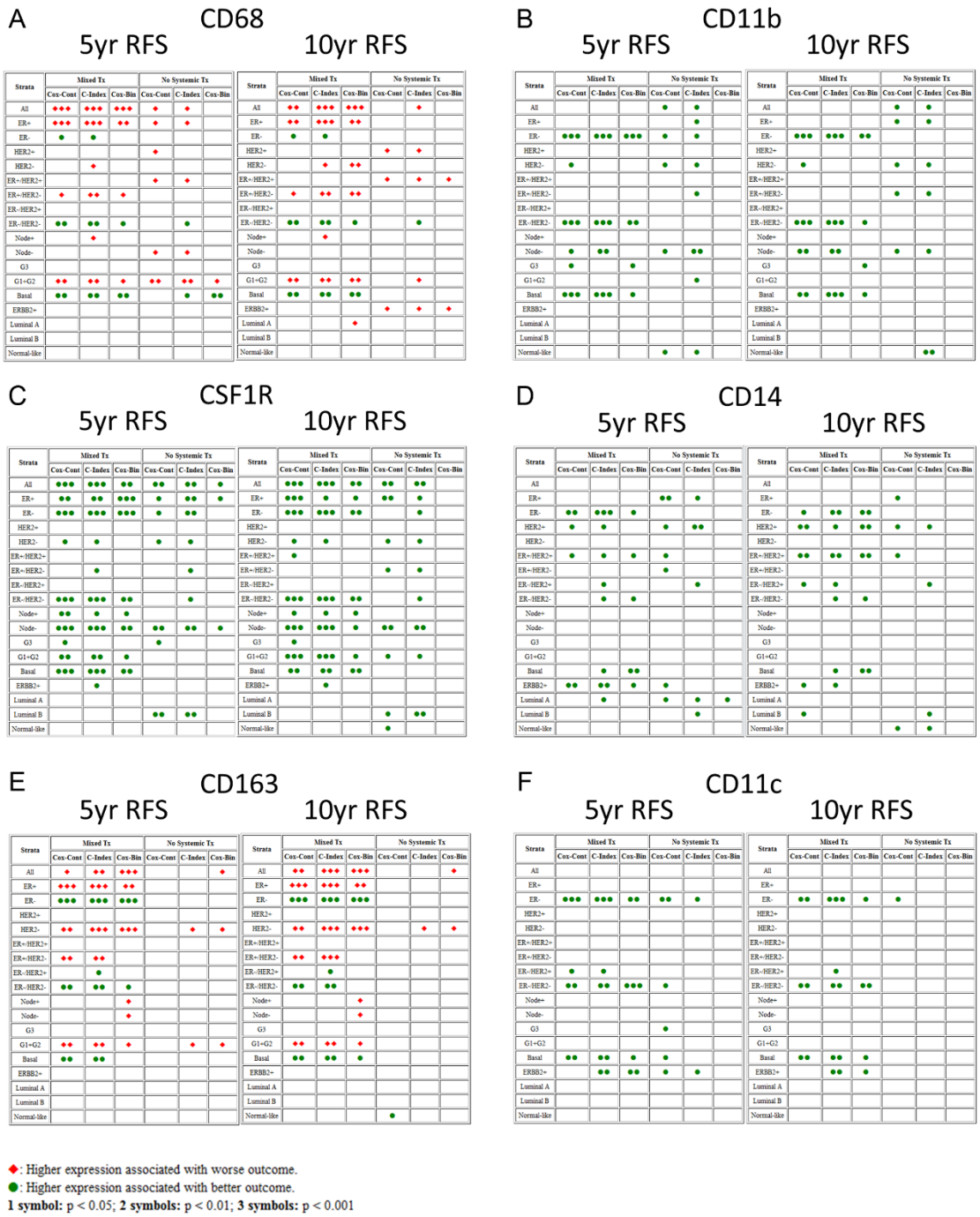

Association between increased expression of macrophage-related transcripts and 5 year (left) or 10 year (right) recurrence-free survival, showing prognostic impact for overexpression of either

CD68 (A), CD11b (B), CSF1R (C), CD14 (D), CD163 (E), or CD11c (F) on either all patients (All); patients stratified by high estrogen receptor (ER) expression (ER+) or low ER expression (ER-); high HER2 expression (HER2+) or low HER2 expression (HER2-); a combination of ER and HER2 expression status; presence (Node+) or absence (Node-) of disseminated tumor cells in lymph nodes; grade 3 (G3), or grades 1-2 (G1+G2) disease; or molecular subtype.

Figure 4.3. Evidence Supporting a Role for Macrophages in Tumor Progression in Transgenic Mouse Models of Breast Cancer

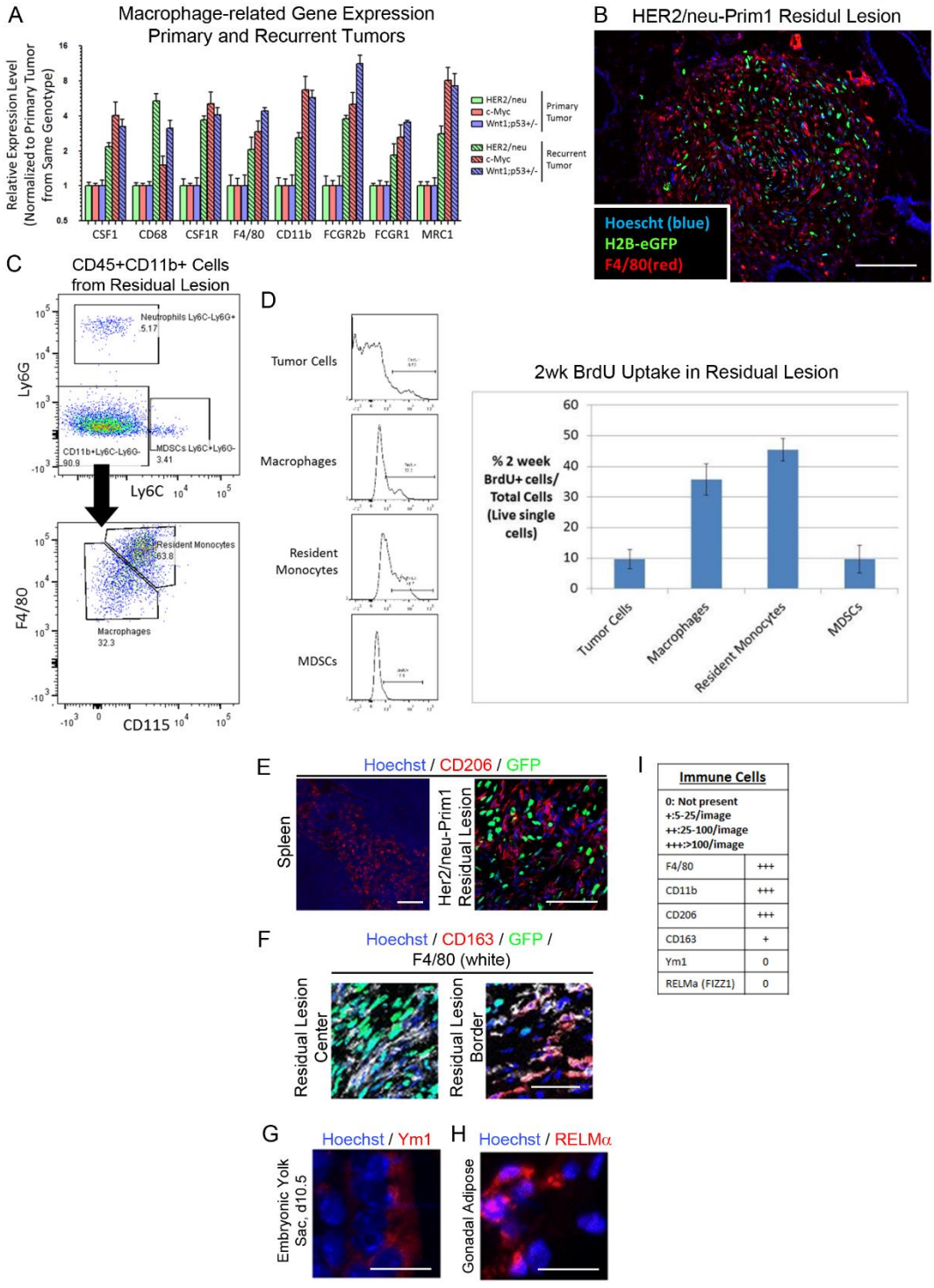

(A) Expression of macrophage-related transcripts in primary or recurrent tumors in HER2/neu, c-

Myc, and Wnt1;p53+/- models of breast cancer. (B) IF on tissue section of an H2B-eGFP-labeled *HER2/neu-Prim1* orthotopic residual lesion in a *nu/nu* mouse for Hoechst (blue), H2B-eGFP (green), or macrophage marker F4/80 (red). (C) Flow cytometry to identify different myeloid cell (CD45+CD11b+) populations in a *HER2/neu-Prim1* orthotopic residual lesion in a *nu/nu* mouse. (D) Flow cytometry on different myeloid populations or tumor cells to quantify 2 week uptake of BrdU. (E-H) IF to phenotype residual lesion macrophage populations. (I) Quantification of different macrophage populations. Scale bars 100μm for (B), 50μm for (E), 25μm for (F), 10μm for (G, H).

Figure 4.4. Residual Lesion Leukocytes but not Tumor Cells Express CD40

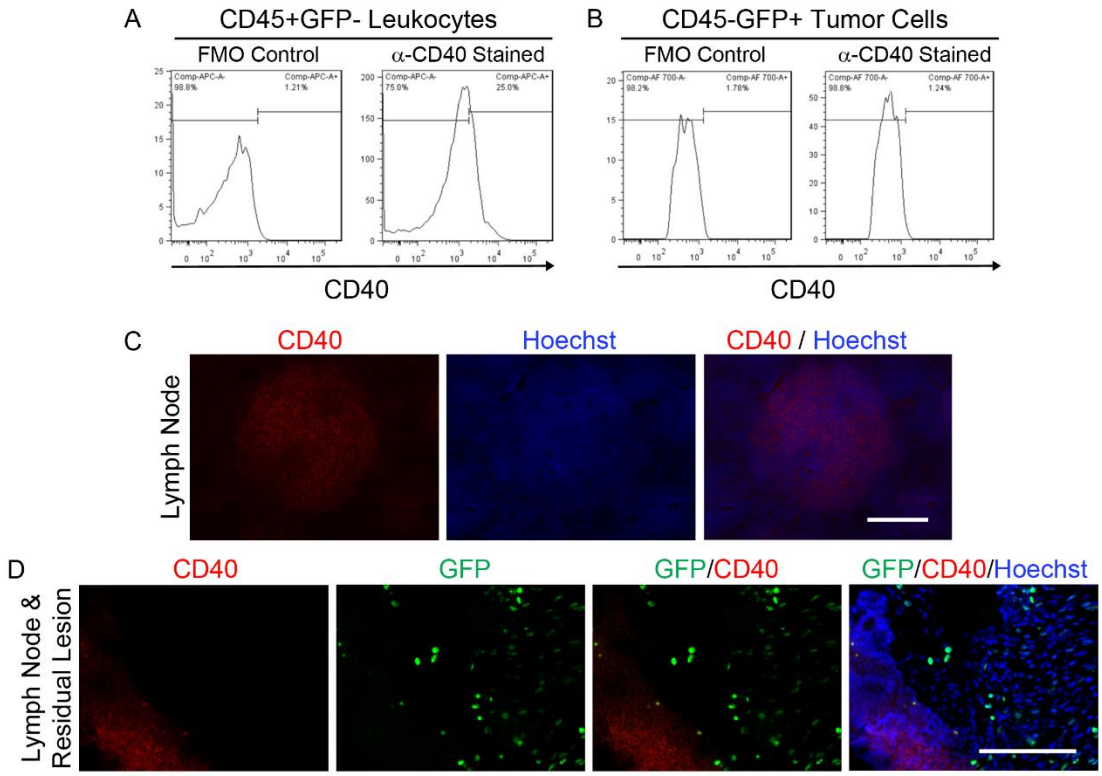

(A, B) Flow cytometry for either fluorescence-minus one (FMO) control staining or CD40 expression on CD45+GFP- leukocytes (A) or CD45-GFP+ tumor cells (B) in *MTB/TAN* recurrent tumors. (C) IF showing CD40 staining in non-germinal center regions of lymph nodes. (D) IF showing CD40 staining in lymph node, but not in adjacent residual lesion tumor cells. Scale bars 300μm for (C), 100μm for (D).

Figure 4.5. Macrophages are Activated by anti-CD40 Antibody FGK45

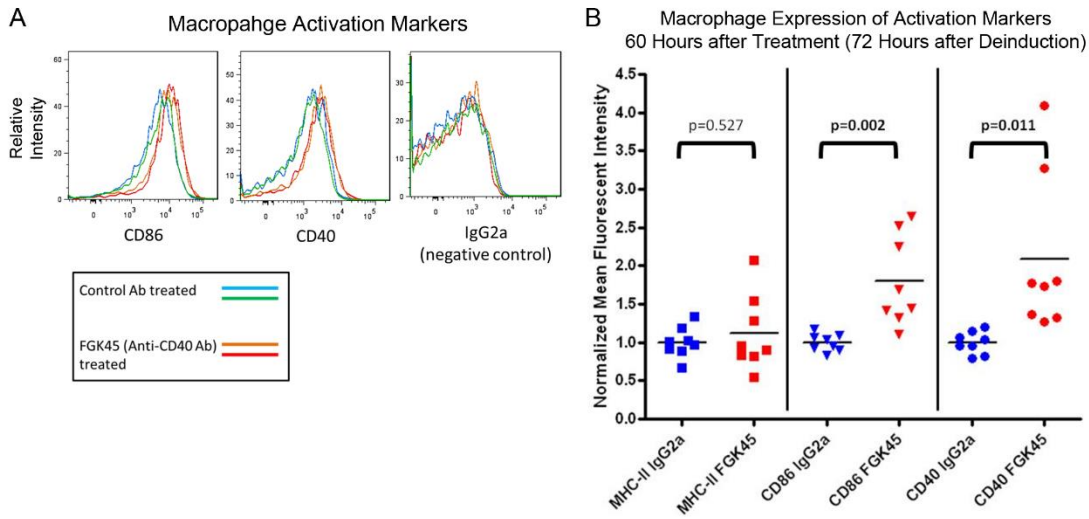

(A) Flow cytometry for macrophage activation markers CD86 or CD40, or IgG2a isotype control, on DAPI-CD45+CD11b+Ly6c-Ly6g- macrophages in tumors from *MTB/TAN* mice 72 hours after deinduction, either treated with an anti-CD40 antibody FGK45 (orange and red lines) or treated with an isotype control antibody (blue and green). (B) Quantification of expression of macrophage activation markers on IgG2a control antibody treated or FGK45-treated mice, from (A).

Figure 4.6. Impact of Treatment with FGK45 on ECM Protein Expression and Recurrence Latency

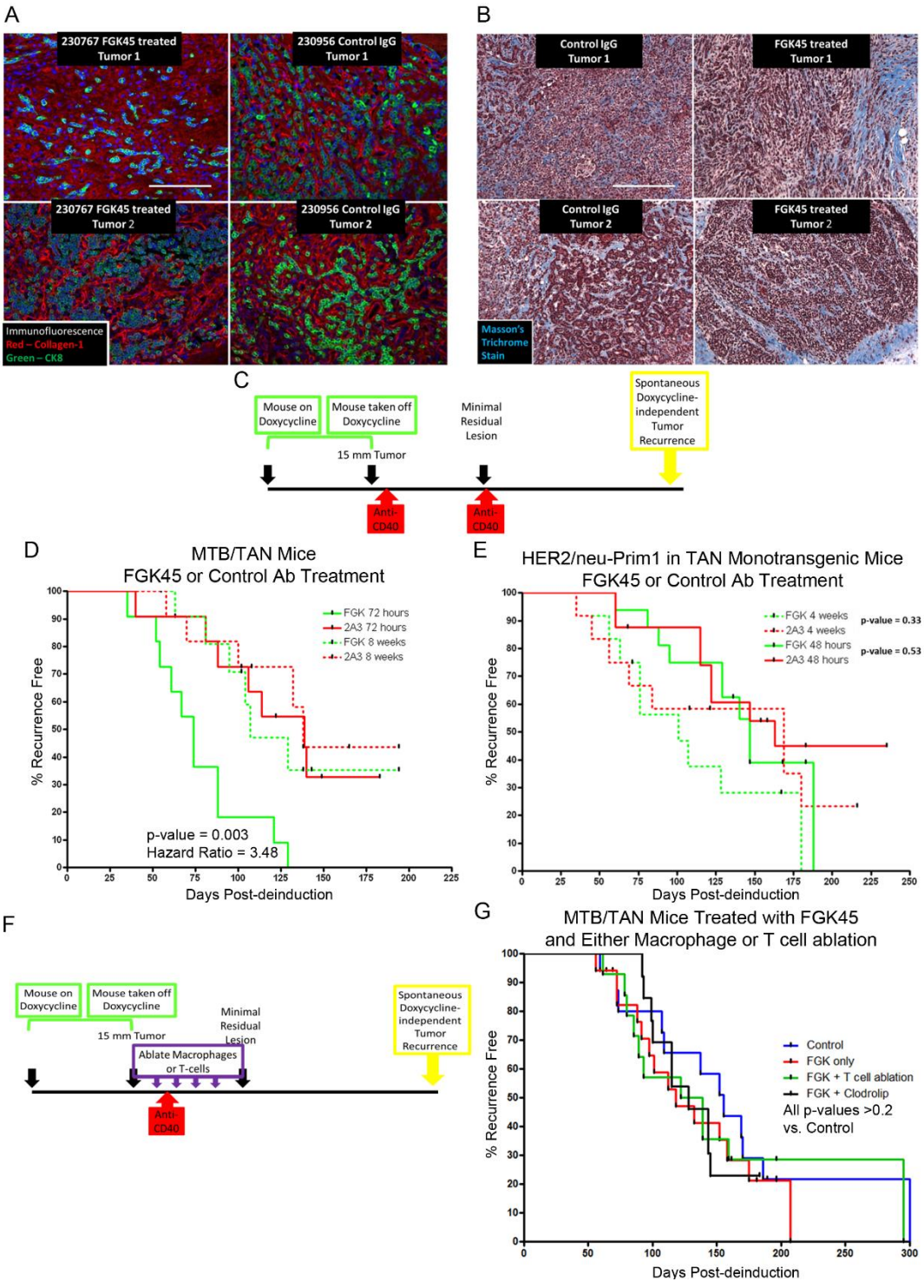

(A, B) IF for CK8 (green) and collagen-type I (red) (A) or brightfield images of Masson's

Trichrome (B) images tumors 60 hours after treatment with FGK45 or isotype control, administered 72 hours after doxycycline withdrawal in *MTB/TAN* mice. (C) Experimental schematic showing timing of administration of either FGK45 or isotype control antibody; 72 hours or 4 weeks after doxycycline withdrawal. (D, E) Kaplan-Meier curves displaying RFS in either *MTB/TAN* mice (D) or *HER2/neu-Prim1* syngeneic tumors in TAN monotransgenic mice (E), according to experimental schematic in (C). (F) Schematic for follow-up experiment including systemic ablation of either macrophages or T-cells, prior to and following administration of FGK45 antibody. (G) Kaplan-Meier curves displaying RFS of *MTB/TAN* mice treated according to (F). Scale bars 100μm for (A, B).

Figure 4.7. Evidence Supporting a Role for COX Signaling in Tumor Progression in Transgenic Mouse Models of Breast Cancer

A

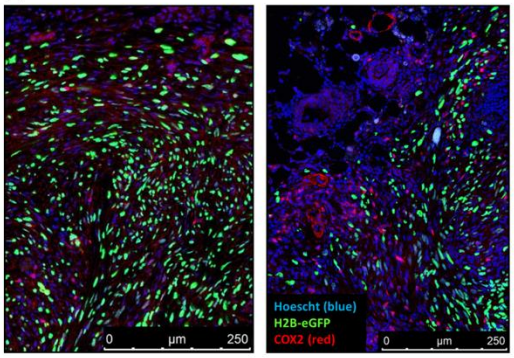

B

mRNA	Associated function	MTB/TAN Fold change (p-value)	MTB/TOM Fold change (p-value)	MTB/TWNT p53 Fold change (p-value)
COX1		8.26 (0.0000)	8.75 (0.0004)	7.89 (0.0007)
COX2		13.49 (0.0000)	4.90 (0.0414)	15.59 (0.0000)
PTGES	PGE2 synthase	10.51 (0.0000)	2.90 (0.0000)	1.29 (0.3134)
PTGER2	PGE2 receptor	2.74 (0.0119)	3.46 (0.0014)	1.92 (0.0443)
PTGER4	PGE2 receptor	1.36 (0.1625)	5.16 (0.0001)	1.57 (non-significant)

C

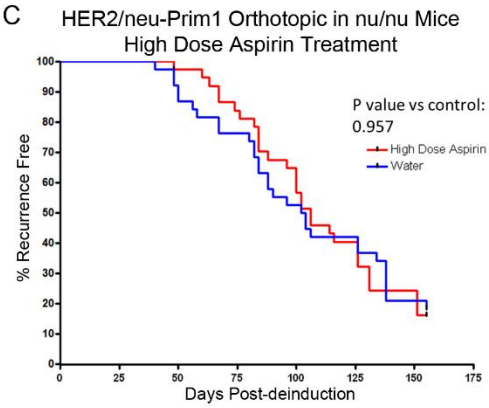

D

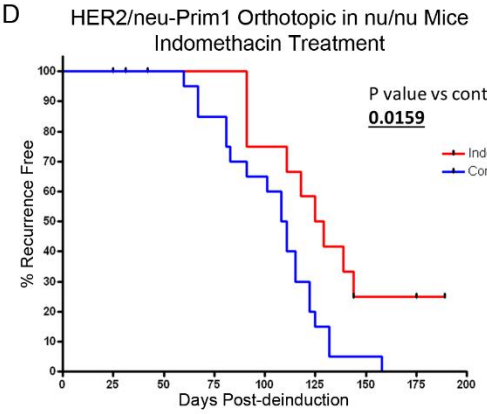

E

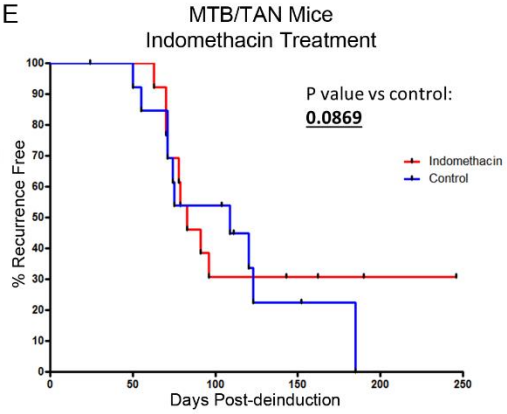

(A) IF on tissue section of an H2B-eGFP-labeled *HER2/neu-Prim1* orthotopic residual lesion in a *nu/nu* mouse for Hoechst (blue), H2B-eGFP (green), or COX2 (red). (B) Expression of macrophage-related transcripts in recurrent tumors relative to primary tumors (p-values in parenthesis), in HER2/neu, c-Myc (*MTB/TOM*), and Wnt1;p53+/- models of breast cancer. (C) Kaplan-Meier curves displaying RFS for *nu/nu* mice bearing *HER2/neu-Prim1* orthotopic tumors

treated with chronic high dose aspirin starting at time of doxycycline withdrawal. (D, E) Kaplan-Meier curves displaying RFS in either *HER2/neu-Prim1* tumors in *nu/nu* mice (D) or *MTB/TAN* mice (E) treated with chronic indomethacin starting at time of doxycycline withdrawal.

Figure 4.8. Dexamethasone Inhibits Tumor Recurrence at Doses that Ablate Macrophages within Residual Lesions

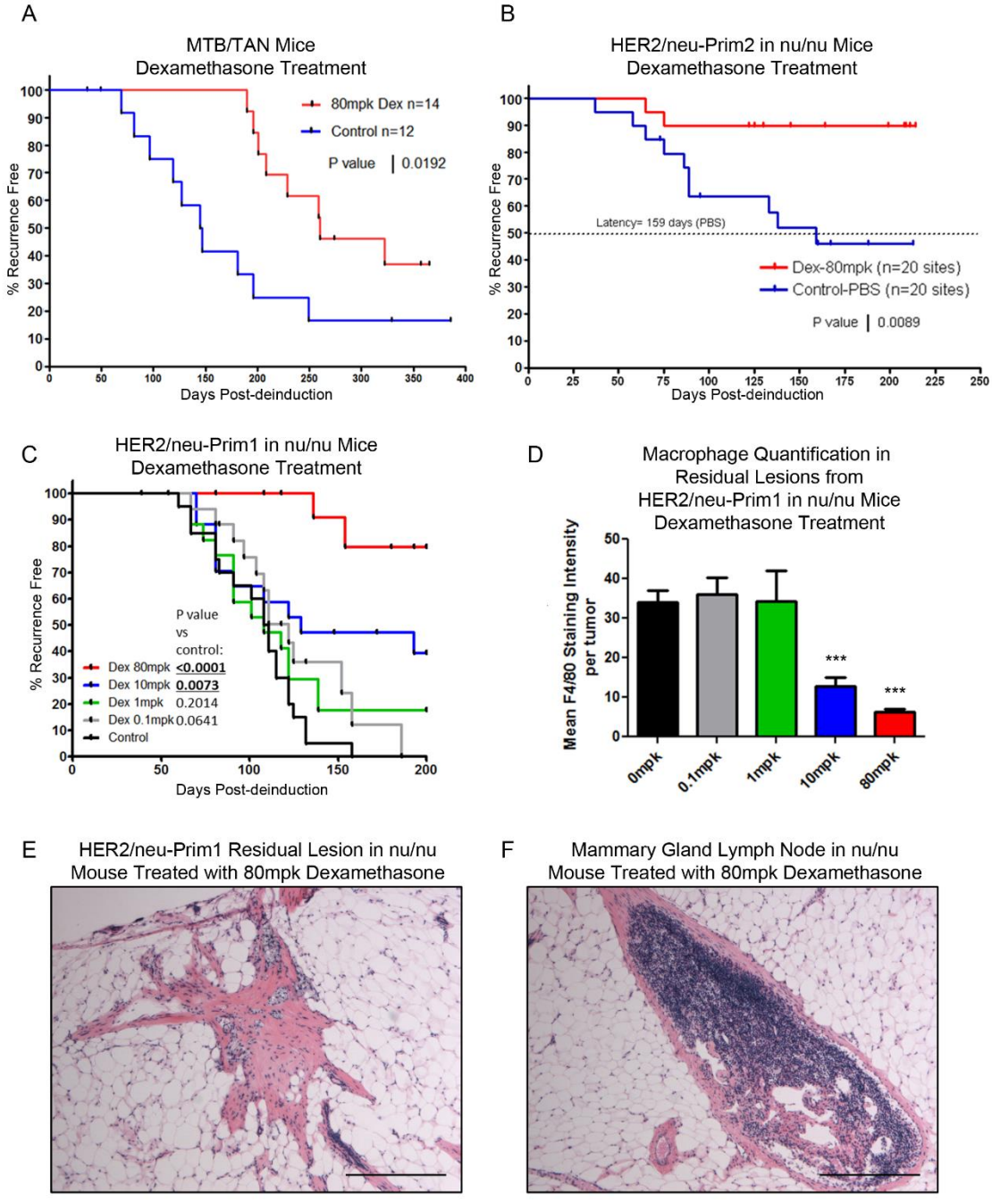

(A, B) Kaplan-Meier curves displaying RFS in either *MTB/TAN* mice (A) or *HER2/neu-Prim2* tumors in *nu/nu* mice (B) treated with chronic 80 mg/kg dexamethasone starting at time of doxycycline withdrawal. (C) Kaplan-Meier curves displaying RFS in *HER2/neu-Prim1* tumors in

nu/nu mice treated with different doses of dexamethasone or vehicle control. (D) Quantification of the number of macrophages present in residual lesions from mice treated with different doses of dexamethasone, as measured by intensity of F4/80 staining on tissue sections. (E, F) H&E staining of residual lesion (E) or lymph node (F) displaying atrophic morphology in mice treated with 80mg/kg dexamethasone. Scale bars 500μm for (E, F).

Figure 4.9. Impact of Clodronate Liposomes or anti-GR1 antibody on RFS

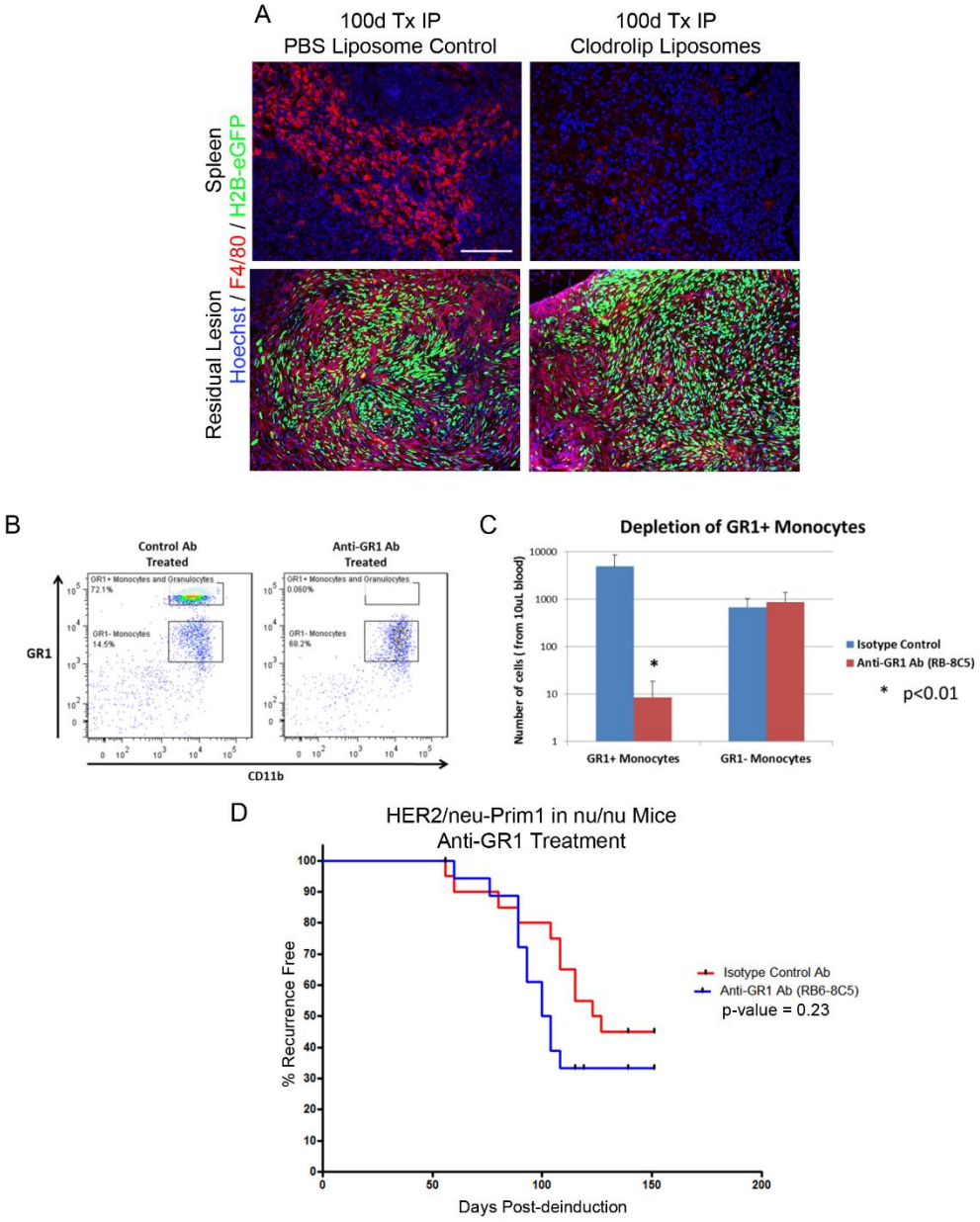

(A) IF on tissue section of an H2B-eGFP-labeled *HER2/neu-Prim1* orthotopic residual lesion in a *nu/nu* mouse for Hoechst (blue), H2B-eGFP (green), or F4/80 (red). (B) Flow cytometry of GR1 and CD11b on CD45+DAPI- leukocytes peripheral blood from *nu/nu* mice following retreatment with anti-GR1 antibody after a previous treatment one month earlier. (C) Quantification of depletion of GR1+ monocytes from (B). (D) Kaplan-Meier curves displaying RFS in *HER2/neu-Prim1* tumors in *nu/nu* mice treated with chronic anti-GR1 antibody or isotype control, starting at

deinduction. Scale bars 100μm for (A).

Figure 4.10. Spleen Size is Increased by anti-GR1 Treatment and Decreased by Dexamethasone

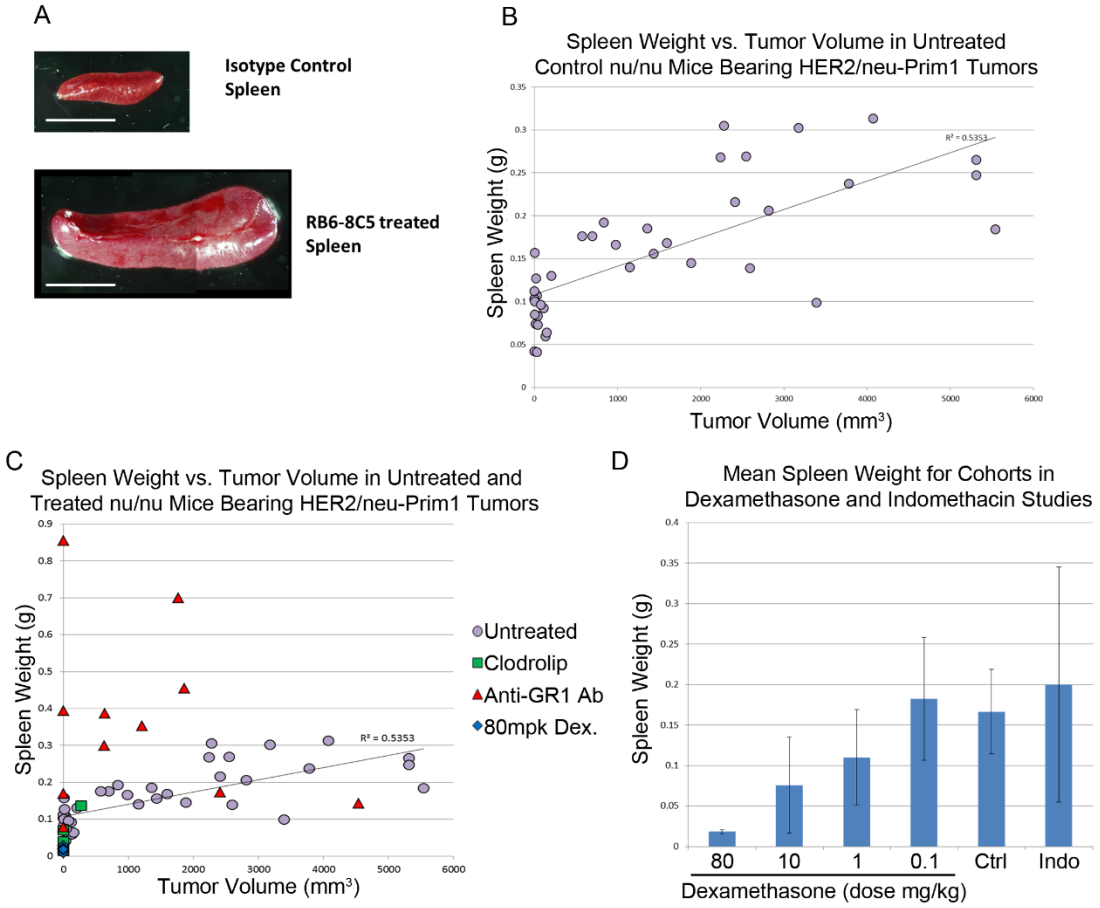

E

Dex. dose (mg/kg) or Indomethacin	p-values vs. Ctrl
80mpk	8.69E-5
10mpk	0.0043
1mpk	0.900
0.1mpk	0.66
Indomethacin	0.72

(A) Images showing representative spleens from mice treated with either isotype control antibody or anti-GR1 antibody RB6-8C5. (B) Dot plot showing correlation between spleen weight (g) and tumor volume (mm^3). (C) Dot plot showing spleen weight vs tumor volume for mice treated with

anti-GR1 antibody, dexamethasone, clodrolip, or untreated control mice data from (A). (D) Bar plot showing spleen weight for mice treated with different doses of dexamethasone, control IP injections of saline, or indomethacin in drinking water. (E) p-values for bar graphs in (D), vs control. Scale bars 1cm for (A).

Figure 4.11. c-fms-dependent Macrophage Ablation Results in a Small Delay in Tumor Recurrence

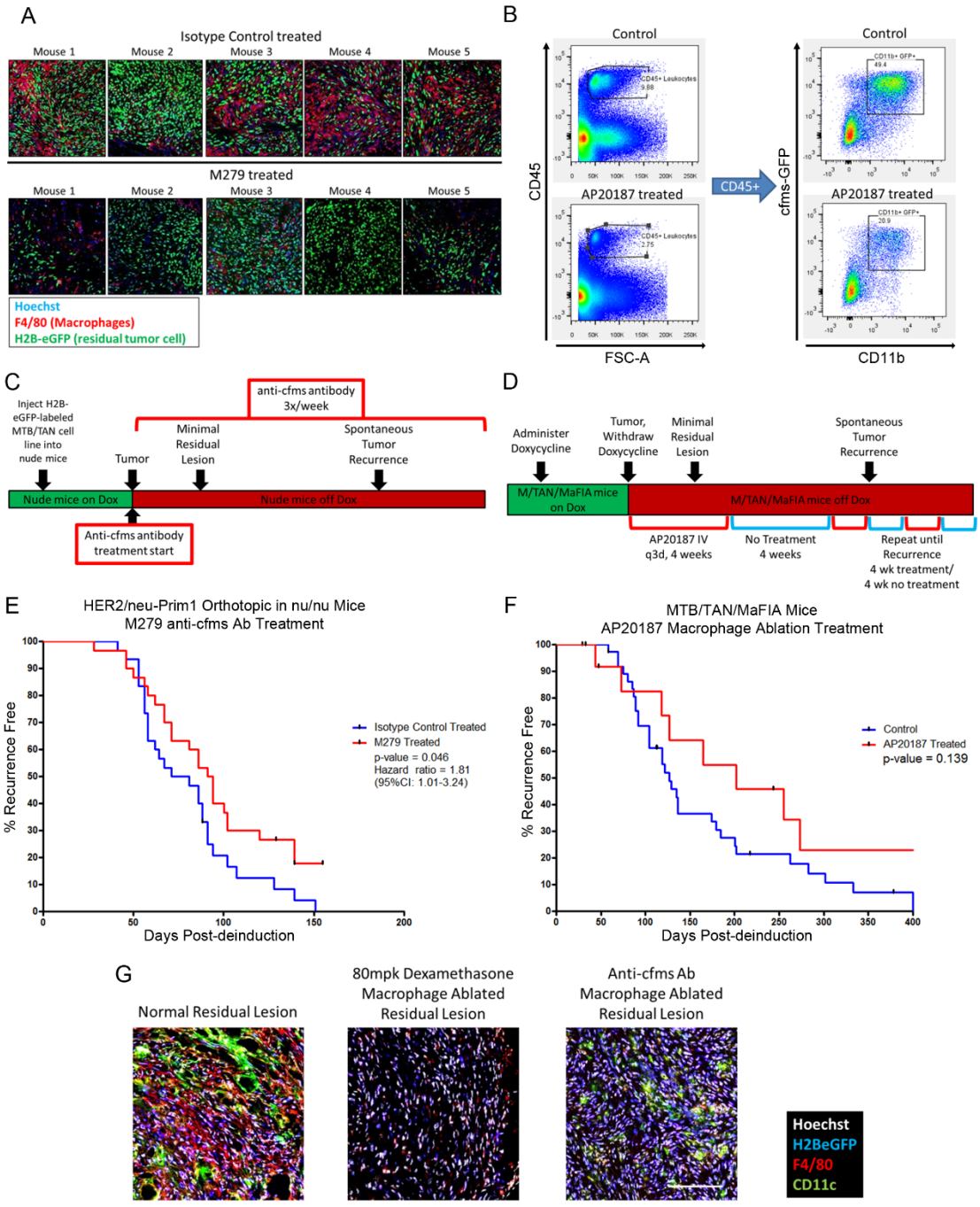

(A) IF for Hoechst (blue), H2B-eGFP (green), or F4/80 (red) on tissue sections of H2B-eGFP-labeled *HER2/neu-Prim1* orthotopic residual lesions in *nu/nu* mice treated either with isotype control antibody or with anti-c-fms antibody. (B) Flow cytometry on residual disease-bearing

mammary glands 4 weeks after doxycycline withdrawal in *MTB/TAN/Mafia* mice after 4 weeks of treatment with either vehicle or AP20187. (C) Experimental schematic showing timing of anti-c-fms antibody administration to *nu/nu* mice bearing *HER2/neu-Prim1* tumors following doxycycline withdrawal. (D) Experimental schematic showing timing of administration of AP20187 dimerizing agent to *MTB/TAN/Mafia* mice following doxycycline withdrawal. (E) Kaplan-Meier curves displaying RFS for (C). (F) Kaplan-Meier curves displaying RFS for (D). (G) IF for Hoechst (blue), H2BeGFP (blue), F4/80 (red), or CD11c (green). Scale bars 100μm for (A, G).

Figure 4.12. Chronic Intramammary Saline Injections Increase Residual Lesion IL6 and Promote Recurrence

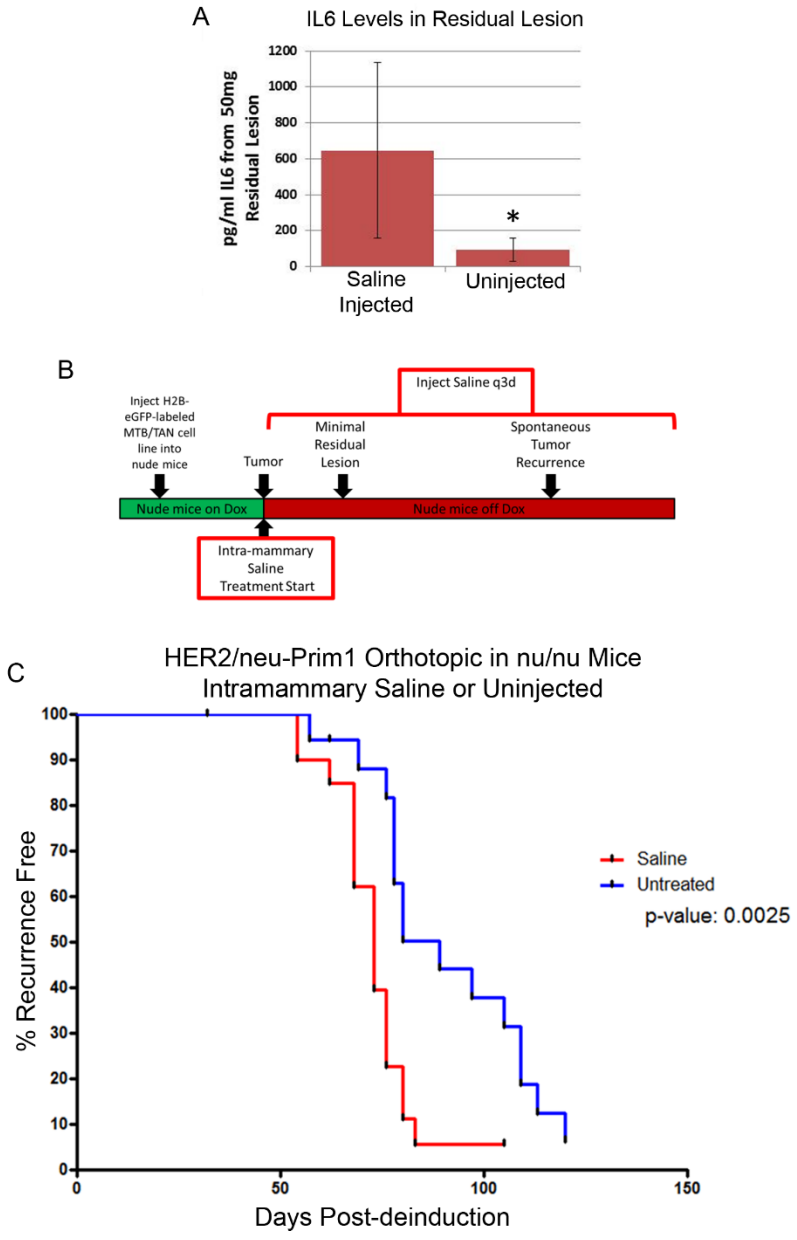

(A) Bar graph showing quantification of ELISA for IL6 from residual lesions either injected every 3 days (q3d) with saline or uninjected, 28 days after doxycycline withdrawal. (B) Experimental schematic showing timing of chronic saline injection. (C) Kaplan-Meier curves displaying RFS in *HER2/neu-Prim1* tumors in *nu/nu* mice either injected into residual lesion with q3d saline or uninjected. * = p-value<0.05

Methods

Statistics

Unless otherwise noted, all statistical analyses providing a p-value were conducted using student's two-sided T-test assuming homoscedastic variance, performed in Excel (Microsoft). p-values for survival analyses of Kaplan-Meier curves were analyzed attained with Wilcoxon rank-sum test, performed in Prism 5 (Graphpad).

Mice

Animal care and experiments were performed with the approval of, and in accordance with, guidelines of the University of Pennsylvania IACUC. Bitransgenic and nude mice were generated and tumors were induced, deinduced, monitored for tumor recurrence, and sacrificed as described [108, 121, 126]. Mafia mice were previously described [163].

Tissue Culture and Reagents

Primary tumor cells were cultured, and stable H2B-eGFP expression was achieved as described [108, 126].

Orthotopic Recurrence Assay

Recurrence assays were performed as described [108]. Recurrence-free survival curves were displayed as Kaplan-Meier survival curves using Prism 5.03 (Graph Pad Software, Inc).

Immunofluorescence and Direct Fluorescence

Normal mammary glands or mammary glands bearing MRLs were harvested, embedded in OCT compound, and frozen. 8μm tissue sections were either fixed and permeabilized in dehydrated acetone at -20°C for 10 min, or fixed in 4% paraformaldehyde for 10 min at room temperature (RT) and permeabilized in 0.1% Triton-X-100 in PBS for 20 min. Following fixation and permeabilization, sections were washed 2x5 min in PBS, blocked for 1 hr with 10% normal goat serum with 3% BSA in PBS and incubated overnight (O/N) at 4°C with primary antibody diluted in blocking buffer. Primary antibodies used to stain tissues fixed in paraformaldehyde were: F4/80 (1:50, AB6640, Abcam), GFP (1:1000, NB100-1770, Novus Biologicals), CD3 (1:100, ab5690, Abcam). Primary antibodies used to stain tissues fixed in acetone were: F4/80 (1:500, AB6640, Abcam), GFP (1:1000, NB100-1770, Novus Biologicals), CD3 (1:100, ab5690, Abcam), CD163

(1:50, SC-33560, Santa Cruz), CD206 (1:500, MCA2235, AbD Serotec), RELMa (1:20, ab39626, Abcam), Ym1 (1:20, 1404, StemCell Technologies), CD40 (1:50, sc-16933, Santa Cruz), Collagen-I (1:250, AB34710, Abcam), CK8 (1:50, , Developmental Studies Hybridoma Bank Uuniversity of Iowa), COX2 (1:500, ab15191, Abcam), CD11c (1:10, 550283, BD Pharmingen). Slides were imaged with a Leica TCS SP5 (Leica Microsystems) confocal microscope using Leica Application Suite Advanced Fluorescence (LAS AF, Leica Microsystems) software.

Flow Cytometry

Immediately following harvest, tissues from mice were digested enzymatically using collagenase/hyaluronidase (Stemcell Technologies) for 90 min at 37ºC, followed by pipetting vigorously in DNAse (Worthington Biochemical Corporation) and Dispase (Stemcell Technologies) for 5 min at 37C. Tissue digests were strained through a 40µm filter (BD Falcon). Single-cell suspensions were stained with fluorophore-conjugated antibodies for 30 min at 4ºC in 1%BSA and 5mM Ethylenediaminetetraacetic acid disodium salt (EDTA) in PBS. Antibodies used were: CD45 (1:200, 560510, BD Biosciences), CD11b (1:500, 101241, BioLegend), Ly6C (1:100, 128029, BioLegend), Ly6G (1:250, 562700, BD Biosciences), CD115 (1:50, 46-1152, eBioscience), F4/80 (1:50, 25-4801, eBioscience), CD40 (1:50, 553791, BD Biosciences), IgG Isotype control (1:50, 553989, BD Biosciences), CD86 (1:50, 553692, BD Biosciences), MHC-II (1:1000, 558593, BD Biosciences). Cells were washed twice in FACS diluent (PBS with 1% bovine serum albumin (BSA, Sigma) and 5mM EDTA (Sigma)), and resuspended in FACS diluent with 1µg/ml DAPI (Sigma-Aldrich Co.) for identifying viable cells. Compensation was performed using AbC™ anti-mouse bead kit (A10344, Life Technologies Corporation) and anti-rat/hamster bead kit (A10389, Life Technologies Corporation), according to manufacturer's instructions. Flow cytometry was performed on a BD FACSCanto™ system using BD FACSDiva™ software (BD Biosciences).

Data were analyzed using FlowJo. Dead cells, debris, and doublets were removed by sequentially analyzing gates for DAPI, SSC-A vs. FSC-A, SSC-W vs. SSC-H and FSC-W vs. FSC-H staining, respectively.

With the exception of enzymatic digest at 37ºC, all steps for flow cytometry, FACS, and limiting

dilution experiments were performed at 4ºC.

CHAPTER 5

Summary and Future Directions

Summary

Breast cancer is the second leading cause of cancer-related mortality among women worldwide, and breast cancer recurrence represents the final step in breast cancer progression for the majority of breast cancer patients. In spite of the paramount importance of preventing breast cancer recurrence, little is known about the biology of residual disease that gives rise to recurrence. Due to the increasingly widespread use of targeted therapies in the clinic, the need to define the phenotype of residual disease that gives rise to recurrence following targeted therapy is increasingly urgent. Simultaneously, the advent of immuno-oncology therapies in the clinic has had a major impact across multiple cancer types, however the relationship between the immune system and residual disease following targeted therapy remains poorly understood. In this thesis, we identify novel biological aspects of tumor cells that survive targeted therapy, and identify possible roles for targeted macrophage ablation in preventing tumor recurrence. The advances presented here represent a step towards a more complete understanding of residual disease that survives oncogenic pathway inhibition, however significant work remains before these findings can be said to be of importance to human breast cancer

Future directions for characterizing residual disease

While our finding of dormancy in residual disease argues that dormant residual disease may be an attractive therapeutic target because it is a conserved response across multiple models of oncogenic inhibition in GEMMs, several key questions remain. These can be divided into two main areas: clinical validation and functional validation.

Clinical validation

Replicating our finding – that residual tumor cells surviving oncogenic pathway inhibition exhibit cellular dormancy – in humans, is a critical step that if successful, would justify the investment of

greater time and resources into the use of these models to study dormancy with the goals of developing methods to identify and eliminate dormant residual disease in humans. Validation would consist of both determining the proportion of residual disease in a typical patient that is dormant, and evaluating these dormant tumor cells in order to determine whether dormant tumor cells in humans have similar biological qualities to dormant residual disease in out mouse models.

What tumor tissue would be used for clinical validation? Ideally, this should be performed on the residual tumor cells that give rise to recurrence in patients, though as it is unclear how to prospectively identify this population of tumor cells in a patient, it should then be accomplished in a manner that systematically evaluates all residual disease in a given patient. Again, it is unclear how to do this, as the only residual disease that can be identified in patients with no evidence of disease is typically DTCs in bone marrow or CTCs in blood. While these tumor cell populations are correlated with poor outcomes, it is unclear that they give rise to recurrent tumors in patients, or that they generally represent all residual disease in a patient. Nonetheless, as they represent an identifiable manifestation of MRD in patients, DTCs or CTCs are one of the best available options for clinical validation of our findings. An alternative tissue source for residual disease to validate findings is residual disease, local or metastatic, that shows complete and sustained regression upon neoadjuvant or adjuvant systemic targeted therapy. Given that residual tumor cells at local or metastatic sites show cellular dormancy in our models, it would be useful to identify patients receiving combination targeted therapy to maximally inhibit an oncogenic pathway, who also have surgically resectable residual disease following systemic therapy. Any source of residual disease would need to be compared to control tumor tissue, preferably both primary disease and any available metastases. Following identification of sources of tumor cells for analysis, tumor cells should be isolated to ensure that stromal cells do not contaminate the tumor cell samples.

Residual disease would subsequently need to be evaluated for whether it was dormant, and if it was dormant, whether it shared qualities of dormant residual disease with the mouse models

discussed here. Some approaches that were taken to conclusively demonstrate dormancy in these mouse models would not be feasible in human disease, such as 2 week BrdU uptake. However, gene expression profiling of dormant tumor cells in our models conclusively demonstrated dormancy through broad down-regulation of families of genes associated with mitosis and biosynthesis. Thus, an attractive approach would be to perform gene expression profiling on residual tumor cells to both determine whether they were dormant and, if dormant, provide a basis for comparison of dormancy in human to mouse models. Unfortunately this would only work well if the population of tumor cells analyzed is predominantly dormant prior to performing gene expression profiling, which would be difficult to evaluate due to the lack of markers available to identify dormant tumor cells in humans.

Identification of reproducible protein markers for dormant tumor cells in these mouse models could facilitate development of immunohistochemical or flow cytometric approaches to evaluate dormancy of human tumor cells on a per-cell basis in a high-throughput manner, thus permitting comparison between dormancy in human tumor cells and dormant in mouse tumor cells. Genes that are repeatedly up-regulated in residual tumor cells across models would be suitable candidates to evaluate for protein expression in residual tumor cells compared to other tumor cells.

To begin making progress towards these ends, we have developed partnerships with clinical collaborators to evaluate isolated residual tumor cells from breast cancer patients, and compare these cells to primary or metastatic tumor cells from the same patients.

Functional validation

Functional validation is also crucial in order to identify keystone genes and pathways that regulate both dormancy and survival of dormant tumor cells, and ultimately to provide conclusive evidence for the functional relevance of dormancy. While we observe that the vast majority of residual tumor cells are dormant, it remains possible that a small subpopulation of residual tumor cells have biological properties distinct from the majority dormant population, and that it is this small subpopulation that is responsible for recurrence, and not the dormant tumor cells. Thus, methods

that specifically eliminate dormant tumor cells are necessary to definitively demonstrate that dormant tumor cells contribute to recurrence.

Knockdown of genes recurrently up-regulated in dormant tumor cells, such as *Dec2*, and subsequent evaluation of the impact of knockdown on recurrence latency, should provide a reproducible approach to evaluating the role of particular genes in dormancy and recurrence. Beyond *Dec2*, transcription factors or kinases that are associated with families of up-regulated genes identified in residual tumor cells compared to proliferative tumor cells will also be key targets to investigate through evaluation of the impact of knockdown of a gene of interest on tumor recurrence latency.

High-throughput screening with an in vitro model of dormancy could help identify strategies to eliminate dormant tumor cells. To facilitate in vitro work, we are currently evaluating the similarity between an in vitro dormancy model developed in our lab, and in vivo dormancy in residual tumor cells.

Following both clinical and functional validation, therapies targeting dormant tumor cells that also have an impact on tumor recurrence in these preclinical mouse models could serve as candidates to be used to target dormant tumor cells in the clinic.

Future directions for studying immune response associated with dormant residual disease

Our findings surrounding the role of inflammation and macrophages in dormant residual disease similarly require clinical and functional validation. However, the first step to take is to determine whether CD11c+F4/80+ macrophages promote tumor recurrence.

Role for CD11c+F4/80+ macrophages in recurrence

To evaluate whether these leukocytes are necessary for tumor recurrence, we plan to perform bone marrow transplant from *CD11c-DTR* mice into *nu/nu* mice. The resulting *nu/nu;CD11c-DTR* chimeras will be able to be ablated of all CD11c+ cells upon administration of diphtheria toxin, thus permitting functional evaluation of the role of CD11c+F4/80+ macrophages in tumor

dormancy and recurrence. This study should involve four arms: a control treatment arm, an anti-c-fms antibody alone arm, a diphtheria toxin (to ablate CD11c+F4/80+ macrophages) alone arm, and a combined anti-c-fms plus diphtheria toxin arm, to ablate both non-inflammatory macrophages and inflammatory macrophages in the residual lesion.

Beyond this study, it would be useful to identify pharmacological targets that could be used to eliminate CD11c+F4/80+ macrophages from residual disease, which would also spare CD11c+ dendritic cells. Presumably the presence of dendritic cells near tumor cells has a positive impact on tumor progression due to the role of dendritic cells as antigen presenting cells, and this possibility is supported by the positive prognostic impact of increased CD11c expression levels in primary breast cancers (Figure 4.2). A possible approach to specifically therapeutically target inflammatory macrophages would be to inhibit cytokine receptors necessary to recruit these leukocytes to residual lesions, or to eliminate cells using antibodies targeting as-yet-unidentified specific markers for these immune cells.

Clinical validation

If we functionally demonstrate that CD11c+F4/80+ leukocytes potentiate tumor recurrence, validating this finding in samples from breast cancer patients would be an important next step. Due to the small spatial scale of residual disease, and the potential for leukocyte populations surrounding, but not juxtaposed with, residual tumor cells (such as CD163+ macrophages in the *HER2/neu-Prim1* orthotopic residual lesion or CD3+ T-cells in the intact *MTB/TAN/TTC/rYFP* residual lesion), it would be necessary to use tissue sections to determine the organization of leukocyte populations relative to tumor cells. This may best be achieved by analysis of local residual disease following neoadjuvant therapy, as it is not feasible to acquire tissue sections containing CTCs or DTCs from living patients. Evaluation of this tissue for the presence of CD11c+F4/80+ leukocytes would be an important first step, however it is possible that the functional role that these inflammatory leukocytes play in murine residual disease is filled in by alternate pro-inflammatory actors. Given the clinical evidence from the Nurses' Health Study

suggesting a role for inflammation in breast cancer recurrence, further evaluation of leukocyte populations present in residual disease should remain a priority for breast cancer research.

BIBIOLOGRAPHY

1. GLOBOCAN 2012: Estimated Cancer Incidence, Mortality and Prevalence Worldwide in 2012 http://globocan.iarc.fr/Pages/fact_sheets_cancer.aspx. IARC 2014
2. Siegel R, Naishadham D, Jemal A. Cancer statistics, 2013. CA Cancer J Clin. 2013;63(1):11-30.
3. Tevaarwerk AJ, Gray RJ, Schneider BP, et al. Survival in patients with metastatic recurrent breast cancer after adjuvant chemotherapy: little evidence of improvement over the past 30 years. Cancer. 2013 Mar 15;119(6):1140-8
4. Siegel R, DeSantis C, Virgo K, et al. Cancer treatment and survivorship statistics, 2012. CA Cancer J Clin. 2012;62(4):220.
5. Jemal A, Siegel R, Xu J, Ward E. Cancer statistics, 2010. CA Cancer J Clin. 2010 Sep-Oct;60(5):277-300.
6. Maruti SS, Willett WC, Feskanich D, Rosner B, Colditz GA. A prospective study of age-specific physical activity and premenopausal breast cancer. J Natl Cancer Inst. 2008 May 21;100(10):728-37.
7. Hamajima N. et al. Alcohol, tobacco and breast cancer--collaborative reanalysis of individual data from 53 epidemiological studies, including 58,515 women with breast cancer and 95,067 women without the disease. Br J Cancer. 2002 Nov 18;87(11):1234-45.
8. Boyd NF, Stone J, Vogt KN, Connelly BS, Martin LJ, Minkin S. Dietary fat and breast cancer risk revisited: a meta-analysis of the published literature. Br J Cancer. 2003 Nov 3;89(9):1672-85.
9. Pharoah, P. D., Day, N. E., Duffy, S., Easton, D. F. & Ponder, B. A. Family history and the risk of breast cancer: a systematic review and meta-analysis. Int. J. Cancer 71, 800–9 (1997).
10. Chen, S. & Parmigiani, G. Meta-analysis of BRCA1 and BRCA2 penetrance. J. Clin. Oncol. 25, 1329–33 (2007).
11. American Joint Committee on Cancer. *AJCC Cancer Staging Manual*. 7th ed. New York, NY: Springer; 2010

12. Breast. In: Edge SB, Byrd DR, Compton CC, et al., eds.: AJCC Cancer Staging Manual. 7th ed. New York, NY: Springer, 2010, pp 347-76.
13. Hanahan D, Weinberg RA. Hallmarks of cancer: the next generation. Cell. 2011 Mar 4;144(5):646-74.
14. Sorlie T, Tibshirani R, Parker J. Repeated observation of breast tumor subtypes in independent gene expression data sets. Proc Natl Acad Sci U S A. 2003 Jul 8;100(14):8418-23.
15. Rouzier R, Perou CM, Symmans WF. Breast cancer molecular subtypes respond differently to preoperative chemotherapy. Clin Cancer Res. 2005 Aug 15;11(16):5678-85.
16. S. Paik, S. Shak, G. Tang, C. Kim, et al. A multigene assay to predict recurrence of tamoxifen-treated, node-negative breast cancer. New England Journal of Medicine. 2004; 351(27):2817-2826
17. Banerji S, Cibulskis K, Rangel-Escareno C, et al. Sequence analysis of mutations and translocations across breast cancer subtypes. Nature. 2012 Jun 20;486(7403):405-9.
18. Farber S, Diamond LK, Mercer RD, et al. Temporary remissions in acute leukemia in children produced by folic acid antagonist, 4-Aminopteroyl-glutamic acid (Aminopterin). *N Engl J Med*. 1948; 238 (787): 787–93
19. Slamon D, Eiermann W, Robert N, et al. for the Breast Cancer International Research Group. Adjuvant trastuzumab in HER2-positive breast cancer. N Engl J Med. 365(14):1273-83, 2011.
20. Perez EA, Romond EH, Suman VJ, et al. Four-year follow-up of trastuzumab plus adjuvant chemotherapy for operable human epidermal growth factor receptor 2-positive breast cancer: joint analysis of data from NCCTG N9831 and NSABP B-31. J Clin Oncol. 2011 Sep 1;29(25):3366-73.
21. Winter JN, Li S, Aurora V et al. Expression of p21 protein predicts clinical outcome in DLBCL patients older than 60 years treated with R-CHOP but not CHOP: a prospective ECOG and Southwest Oncology Group correlative study on E4494. Clin Cancer Res. 2010 Apr 15;16(8):2435-42.

22. Ghosh R, Narasanna A, Wang SE, et al. Trastuzumab has preferential activity against breast cancers driven by HER2 homodimers. Cancer Res. 2011 Mar 1;71(5):1871-82.
23. Baselga J, Cortés J, Kim SB. Pertuzumab plus trastuzumab plus docetaxel for metastatic breast cancer. N Engl J Med. 2012 Jan 12;366(2):109-19.
24. Cortes JE, Kantarjian H, Shah NP, et al. Ponatinib in refractory Philadelphia chromosome-positive leukemias. N Engl J Med. 2012 Nov 29;367(22):2075-88
25. Rexer BN, Arteaga CL. Intrinsic and acquired resistance to HER2-targeted therapies in HER2 gene-amplified breast cancer: mechanisms and clinical implications. Crit Rev Oncog. 2012;17(1):1-16.
26. Doroshow JH. Overcoming resistance to targeted anticancer drugs. N Engl J Med. 2013 Nov 7;369(19):1852-3.
27. Anido J, Scaltriti M, Bech Serra JJ, et al. Biosynthesis of tumorigenic HER2 C-terminal fragments by alternative initiation of translation. EMBO J. 2006 Jul 12;25(13):3234–3244.
28. Scaltriti M, Rojo F, Ocaña A, et al. Expression of p95HER2, a truncated form of the HER2 receptor, and response to anti-HER2 therapies in breast cancer. J Natl Cancer Inst. 2007 May 18;99(8):628–638
29. Motoyama AB, Hynes NE, Lane HA. The efficacy of ErbB receptor-targeted anticancer therapeutics is influenced by the availability of epidermal growth factor-related peptides. Cancer Res. 2002 Jul 01;62(11):3151–3158.
30. Moulder SL, Yakes FM, Muthuswamy SK, et al. Epidermal growth factor receptor (HER1) tyrosine kinase inhibitor ZD1839 (Iressa) inhibits HER2/neu (erbB2)-overexpressing breast cancer cells in vitro and in vivo. Cancer Res. 2001 Dec 15;61(24):8887–8895.
31. Lu Y, Zi X, Zhao Y, Mascarenhas D, Pollak M. Insulin-like growth factor-I receptor signaling and resistance to trastuzumab (Herceptin) J Natl Cancer Inst. 2001 Dec 19;93(24):1852–1857
32. Shattuck DL, Miller JK, Carraway KL, Sweeney C. Met receptor contributes to trastuzumab resistance of Her2-overexpressing breast cancer cells. Cancer Res. 2008 Apr 01;68(5):1471–1477

33. Scaltriti M, Eichhorn PJ, Cortes J, et al. Cyclin E amplification/over-expression is a mechanism of trastuzumab resistance in HER2+ breast cancer patients. Proc Natl Acad Sci U S A. 2011 Apr 01;108(9):3761–3766.
34. Nahta R, Takahashi T, Ueno NT, et al. P27(kip1) down-regulation is associated with trastuzumab resistance in breast cancer cells. Cancer Res. 2004 Jul 01;64(11):3981–3986
35. Sequist LV, Waltman BA, Dias-Santagata D. Genotypic and histological evolution of lung cancers acquiring resistance to EGFR inhibitors. Sci Transl Med. 2011 Mar 23;3(75):75ra26.
36. Ahmad A. Pathways to breast cancer recurrence. ISRN Oncol. 2013;2013:290568.
37. Creighton CJ, Li X, Landis M, et al. Residual breast cancers after conventional therapy display mesenchymal as well as tumor-initiating features. Proc Natl Acad Sci U S A. 2009 Aug 18;106(33):13820-5.
38. Yu M, Bardia A, Wittner BS. Circulating breast tumor cells exhibit dynamic changes in epithelial and mesenchymal composition. Science. 2013 Feb 1;339(6119):580-4.
39. Topalian SL, Hodi FS, Brahmer JR. Safety, activity, and immune correlates of anti-PD-1 antibody in cancer. N Engl J Med. 2012 Jun 28;366(26):2443-54.
40. Hodi FS, O'Day SJ, McDermott D. Improved survival with ipilimumab in patients with metastatic melanoma. N Engl J Med. 2010 Aug 19;363(8):711-23.
41. Arnould L, Gelly M, Penault-Llorca F. Trastuzumab-based treatment of HER2-positive breast cancer: an antibody-dependent cellular cytotoxicity mechanism?Br J Cancer. 2006 Jan 30;94(2):259-67.
42. Holmes MD, Chen WY, Li L, Hertzmark E, Spiegelman D, Hankinson SE. Aspirin intake and survival after breast cancer. J Clin Oncol. 2010 Mar 20;28(9):1467-72.
43. Hayes DF. Systemic treatment for metastatic breast cancer: General principles. eds Dizon DS. UpToDate, Topic 767 Version 22.0, July 2014
44. Hirsch A, Kachnic LA, Sabel MS, Hayes DF. Management of locoregional recurrence of breast cancer after mastectomy. eds Gralow JR, Dizon DS, Duda RB. UpToDate, Topic 772 Version 22.0, July 2014

45. Tevaarwerk AJ, Gray RJ, Schneider BP. Survival in patients with metastatic recurrent breast cancer after adjuvant chemotherapy: little evidence of improvement over the past 30 years. Cancer. 2013 Mar 15;119(6):1140-8.
46. Dafni U, Grimani I, Xyrafas A, Eleftheraki AG, Fountzilas G. Fifteen-year trends in metastatic breast cancer survival in Greece. Breast Cancer Res Treat. 2010 Feb;119(3):621-31.
47. Breast cancer survival rates by stage. http://www.cancer.org/cancer/breastcancer/detailedguide/breast-cancer-survival-by-stage American Cancer Society, Inc. Jan 31, 2014
48. Esserman LJ, Moore DH, Tsing PJ. Biologic markers determine both the risk and the timing of recurrence in breast cancer. Breast Cancer Res Treat. 2011 Sep;129(2):607-16.
49. CellSearch™ Epithelial Cell Kit / CellSpotter™ Analyzer - K031588 http://www.fda.gov/MedicalDevices/ProductsandMedicalProcedures/DeviceApprovalsandClearances/Recently-ApprovedDevices/ucm081239.htm, U.S. Food and Drug Administration, Sept 4, 2013
50. Pantel K, Brakenhoff RH, Brandt B. Detection, clinical relevance and specific biological properties of disseminating tumour cells. Nat Rev Cancer. 2008 May;8(5):329-40.
51. Cristofanilli M, Budd GT, Ellis MJ. Circulating tumor cells, disease progression, and survival in metastatic breast cancer. N Engl J Med. 2004 Aug 19;351(8):781-91.
52. Steinert G, Schölch S, Koch M, Weitz J. Biology and significance of circulating and disseminated tumour cells in colorectal cancer. Langenbecks Arch Surg. 2012 Apr; 397(4):535-42.
53. Seeberg LT, Waage A, Brunborg C, Hugenschmidt H, Renolen A, Stav I, Bjørnbeth BA, Brudvik KW, Borgen EF, Naume B, Wiedswang G. Circulating Tumor Cells in Patients With Colorectal Liver Metastasis Predict Impaired Survival. Ann Surg. 2014 Feb 6.
54. Coello MC, Luketich JD, Litle VR, Godfrey TE. Prognostic significance of micrometastasis in nonsmall-cell lung cancer. Clin Lung Cancer 2004; 5:214–25.
55. Morgan TM, Lange PH, Vessella RL. Detection and characterization of circulating and disseminated prostate cancer cells. Front Biosci 2007; 12:3000–9.

56. Wolfrum F, Vogel I, Fandrich F, Kalthoff H. Detection and clinical implications of minimal residual disease in gastro-intestinal cancer. Langenbecks Arch Surg 2005; 390:430–41.
57. Jiao X, Krasna MJ. Clinical significance of micrometastasis in lung and esophageal cancer: a new paradigm in thoracic oncology. Ann Thorac Surg 2002; 74:278–84.
58. Akagi Y, Kinugasa T, Adachi Y, Shirouzu K. Prognostic significance of isolated tumor cells in patients with colorectal cancer in recent 10-year studies. Mol Clin Oncol. 2013 Jul;1(4):582-592.
59. Ghossein RA, Carusone L, Bhattacharya S. Molecular detection of micrometastases and circulating tumor cells in melanoma prostatic and breast carcinomas. In Vivo 2000; 14:237–50.
60. Speer. J. F. Petrosky. V. Retsky, M., and Wardwel. R. H. A stochastic numeric model of breast cancer that simulates clinical data. Cancer Res. 1984; 4:4124-4130.
61. Demicheli R, Abbattista A, Miceli R, Valagussa P, Bonadonna G. Time distribution of the recurrence risk for breast cancer patients undergoing mastectomy: further support about the concept of tumor dormancy. Breast Cancer Res Treat. 1996;41(2):177-85.
62. Muller, V. et al. Circulating tumor cells in breast cancer: correlation to bone marrow micrometastases, heterogeneous response to systemic therapy and low proliferative activity. Clin. Cancer Res. 2005; 11, 3678–3685.
63. Pantel, K., Brakenhoff, R. H. & Brandt, B. Detection, clinical relevance and specific biological properties of disseminating tumour cells. Nat. Rev. Cancer 2008; 8, 329–340.
64. Hou, J. M. et al. Clinical significance and molecular characteristics of circulating tumor cells and circulating tumor microemboli in patients with small-cell lung cancer. J. Clin. Oncol. 2012; 5, 525–532.
65. Rameshwar, P. Breast cancer cell dormancy in bone marrow: potential therapeutic targets within the marrow microenvironment. Expert Rev. Anticancer Ther. 2010; 10, 129–132.
66. Faries MB, Steen S, Ye X, Sim M, Morton DL. Late recurrence in melanoma: clinical implications of lost dormancy. J Am Coll Surg. 2013 Jul;217(1):27-34; discussion 34-6.

67. Ficarra V, Novara G. Kidney cancer: Characterizing late recurrence of renal cell carcinoma. Nat Rev Urol. 2013 Dec;10(12):687-9.
68. Goss PE, Chambers AF. Does tumour dormancy offer a therapeutic target? Nat Rev Cancer. 2010 Dec;10(12):871-7
69. Malogolowkin M, Spreafico F, Dome JS, van Tinteren H, Pritchard-Jones K, van den Heuvel-Eibrink MM, Bergeron C, de Kraker J, Graf N; COG Renal Tumors Committee and the SIOP Renal Tumor Study Group. Incidence and outcomes of patients with late recurrence of Wilms' tumor. Pediatr Blood Cancer. 2013 Oct;60(10):1612-5.
70. Mathieu MC, Rouzier R, Llombart-Cussac A et al. The poor responsiveness of infiltrating lobular breast carcinomas to neoadjuvant chemotherapy can be explained by their biological profile. Eur J Cancer. 2004 Feb;40(3):342-51.
71. Zellweger T, Günther S, Zlobec I, et al. Tumour growth fraction measured by immunohistochemical staining of Ki67 is an independent prognostic factor in preoperative prostate biopsies with small-volume or low-grade prostate cancer. Int J Cancer. 2009 May 1;124(9):2116-23.
72. Frangioni JV. New technologies for human cancer imaging. J Clin Oncol. 2008 Aug 20;26(24):4012-21.
73. Aguirre-Ghiso JA. Models, mechanisms and clinical evidence for cancer dormancy. Nat Rev Cancer. 2007 Nov;7(11):834-46.
74. Glennie S, Soeiro I, Dyson PJ, Lam EW, Dazzi F. Bone marrow mesenchymal stem cells induce division arrest anergy of activated T cells. Blood. 2005 Apr 1; 105(7):2821-7.
75. Ono M, Kosaka N, Tominaga N, Yoshioka Y, Takeshita F, Takahashi RU, Yoshida M, Tsuda H, Tamura K, Ochiya T. Exosomes from bone marrow mesenchymal stem cells contain a microRNA that promotes dormancy in metastatic breast cancer cells. Sci Signal. 2014 Jul 1;7(332)
76. Ghajar CM, Peinado H, Mori H, Matei IR, Evason KJ, Brazier H, Almeida D, Koller A, Hajjar KA, Stainier DY, Chen EI, Lyden D, Bissell MJ. The perivascular niche regulates breast tumour dormancy. Nat Cell Biol. 2013 Jul;15(7):807-17.

77. Luzzi KJ, MacDonald IC, Schmidt EE, Kerkvliet N, Morris VL, Chambers AF, Groom AC. Multistep nature of metastatic inefficiency: dormancy of solitary cells after successful extravasation and limited survival of early micrometastases. Am J Pathol. 1998 Sep;153(3):865-73.
78. Cameron MD, Schmidt EE, Kerkvliet N, Nadkarni KV, Morris VL, Groom AC, Chambers AF, MacDonald IC. Temporal progression of metastasis in lung: cell survival, dormancy, and location dependence of metastatic inefficiency. Cancer Res. 2000 May 1;60(9):2541-6.
79. Gao H, Chakraborty G, Lee-Lim AP, Mo Q, Decker M, Vonica A, Shen R, Brogi E, Brivanlou AH, Giancotti FG. The BMP inhibitor Coco reactivates breast cancer cells at lung metastatic sites. Cell. 2012 Aug 17;150(4):764-79
80. Lu X, Mu E, Wei Y, Riethdorf S, Yang Q, Yuan M, Yan J, Hua Y, Tiede BJ, Lu X, Haffty BG, Pantel K, Massagué J, Kang Y. VCAM-1 promotes osteolytic expansion of indolent bone micrometastasis of breast cancer by engaging α4β1-positive osteoclast progenitors. Cancer Cell. 2011 Dec 13;20(6):701-14.
81. Aguirre Ghiso, J. A., Kovalski, K. & Ossowski, L. Tumor dormancy induced by downregulation of urokinase receptor in human carcinoma involves integrin and MAPK signaling. J. Cell Biol. 1999; 147, 89–104.
82. Aguirre Ghiso, J. A. Inhibition of FAK signaling activated by urokinase receptor induces dormancy in human carcinoma cells in vivo. Oncogene 21, 2513–2524 (2002).
83. Liu, D., Aguirre Ghiso, J., Estrada, Y. & Ossowski, L. EGFR is a transducer of the urokinase receptor initiated signal that is required for in vivo growth of a human carcinoma. Cancer Cell, 2002; 1, 445–457 .
84. Sosa MS, Avivar-Valderas A, Bragado P, Wen HC, Aguirre-Ghiso JA. ERK1/2 and p38α/β signaling in tumor cell quiescence: opportunities to control dormant residual disease. Clin Cancer Res. 2011 Sep 15;17(18):5850-7.
85. Dean M, Fojo T, Bates S. Tumour stem cells and drug resistance. Nat Rev Cancer. 2005 Apr;5(4):275-84.

86. Al-Hajj M, Wicha MS, Benito-Hernandez A, Morrison SJ, Clarke MF. Prospective identification of tumorigenic breast cancer cells. Proc Natl Acad Sci U S A. 2003 Apr 1;100(7):3983-8.
87. Mani SA, Guo W, Liao MJ, et al. The epithelial-mesenchymal transition generates cells with properties of stem cells. Cell. 2008 May 16;133(4):704-15.
88. Tsai JH, Yang J. Epithelial-mesenchymal plasticity in carcinoma metastasis. Genes Dev. 2013 Oct 15;27(20):2192-206.
89. Asks whether EMT induces dormancy: Kang Y, Pantel K. Tumor cell dissemination: emerging biological insights from animal models and cancer patients. Cancer Cell. 2013 May 13;23(5):573-81.
90. Balic M, Lin H, Young L. Most early disseminated cancer cells detected in bone marrow of breast cancer patients have a putative breast cancer stem cell phenotype. Clin Cancer Res. 2006 Oct 1;12(19):5615-21.
91. Hutchin ME, Kariapper MS, Grachtchouk M, et al. Sustained Hedgehog signaling is required for basal cell carcinoma proliferation and survival: conditional skin tumorigenesis recapitulates the hair growth cycle. Genes Dev. 2005 Jan 15;19(2):214-23.
92. Lin WC, Rajbhandari N, Liu C, et al. Dormant cancer cells contribute to residual disease in a model of reversible pancreatic cancer. Cancer Res. 2013 Mar 15;73(6):1821-30.
93. Barkan D, Kleinman H, Simmons JL, Asmussen H, Kamaraju AK, Hoenorhoff MJ, Liu ZY, Costes SV, Cho EH, Lockett S, Khanna C, Chambers AF, Green JE. Inhibition of metastatic outgrowth from single dormant tumor cells by targeting the cytoskeleton. Cancer Res. 2008 Aug 1;68(15):6241-50.
94. Endo H, Okuyama H, Ohue M, Inoue M. Dormancy of cancer cells with suppression of AKT activity contributes to survival in chronic hypoxia. PLoS One. 2014 Jun 6;9(6)
95. Pallis M, Burrows F, Whittall A, Boddy N, Seedhouse C, Russell N. Efficacy of RNA polymerase II inhibitors in targeting dormant leukaemia cells. BMC Pharmacol Toxicol. 2013 Jun 15;14:32.

96. Aguirre-Ghiso JA, Bragado P, Sosa MS. Metastasis awakening: targeting dormant cancer. Nat Med. 2013 Mar;19(3):276-7.

97. El Touny LH, Vieira A, Mendoza A, Khanna C, Hoenerhoff MJ, Green JE. Combined SFK/MEK inhibition prevents metastatic outgrowth of dormant tumor cells. J Clin Invest. 2014 Jan 2;124(1):156-68.

98. Stewart, T.A., Pattengale, P.K., Leder, P. Spontaneous mammary adenocarcinomas in transgenic mice that carry and express MTV/myc fusion genes. Cell, 1984; 38:627–637

99. Smith HW, Muller WJ. Transgenic Mouse Models—A Seminal Breakthrough in Oncogene Research, Ch1, Abate-Shen C, Politi K, Chodosh LA, Olive KP eds *Mouse Models of Cancer: A Laboratory Manual*. Cold Spring Harbor Laboratory Press, 2014

100. Gunther EJ, Belka GK, Wertheim GB, Wang J, Hartman JL, Boxer RB, Chodosh LA. A novel doxycycline-inducible system for the transgenic analysis of mammary gland biology. FASEB J. 2002 Mar;16(3):283-92.

101. Livshits G, Lowe SW. Accelerating Cancer Modeling with RNAi and Nongermline Genetically Engineered Mouse Models, Ch12, Abate-Shen C, Politi K, Chodosh LA, Olive KP eds *Mouse Models of Cancer: A Laboratory Manual*. Cold Spring Harbor Laboratory Press, 2014

102. Hemann, M. Chimeric Tumor and Organ Transplantation Models, Ch13, Abate-Shen C, Politi K, Chodosh LA, Olive KP eds *Mouse Models of Cancer: A Laboratory Manual*. Cold Spring Harbor Laboratory Press, 2014

103. Sacca et al. Genetically Engineered Mouse Models in Drug Discovery Research, Proetzel G Wiles MB eds *Mouse Models for Drug Discovery*, Methods in Molecular Biology 602, Humana Press 2010

104. Mouse Genome Sequencing Consortium1, Waterston RH, Lindblad-Toh K, et al. Initial sequencing and comparative analysis of the mouse genome. Nature. 2002 Dec 5;420(6915):520-62.

105. Lunardi A, Nardella C, Clohessy JG, Pandolfi PP. Of Model Pets and Cancer Models: An Introduction to Mouse Models of Cancer. Cold Spring Harb Protoc 2014

106. Akbay EA, Koyama S, Carretero J, et al. Activation of the PD-1 pathway contributes to immune escape in EGFR-driven lung tumors. Cancer Discov. 2013 Dec;3(12):1355-63.

107. Beatty GL, Chiorean EG, Fishman MP, et al. CD40 agonists alter tumor stroma and show efficacy against pancreatic carcinoma in mice and humans. Science. 2011 Mar 25;331(6024):1612-6.

108. Moody SE, Perez D, Pan TC, Sarkisian CJ, Portocarrero CP, Sterner CJ, Notorfrancesco KL, Cardiff RD, Chodosh LA. The transcriptional repressor Snail promotes mammary tumor recurrence. Cancer Cell. 2005 Sep;8(3):197-209.

109. Lowe SW, Ruley HE, Jacks T, Housman DE. p53-dependent apoptosis modulates the cytotoxicity of anticancer agents. Cell. 1993 Sep 24;74(6):957-67.

110. Lowe SW, Schmitt EM, Smith SW, Osborne BA, Jacks T. p53 is required for radiation-induced apoptosis in mouse thymocytes. Nature. 1993 Apr 29;362(6423):847-9.

111. Mellinghoff IK, Wang MY, Vivanco I, et al. Molecular determinants of the response of glioblastomas to EGFR kinase inhibitors. N Engl J Med. 2005 Nov 10;353(19):2012-24.

112. Chen J, Li Y, Yu TS, McKay RM, Burns DK, Kernie SG, Parada LF. A restricted cell population propagates glioblastoma growth after chemotherapy. Nature. 2012 Aug 23;488(7412):522-6.

113. Lunardi A, Ala U, Epping MT, et al. A co-clinical approach identifies mechanisms and potential therapies for androgen deprivation resistance in prostate cancer. Nat Genet. 2013 Jul;45(7):747-55.

114. Karrison TG, Ferguson DJ, Meier P. Dormancy of mammary carcinoma after mastectomy. *J Natl Cancer Inst* 1999;91:80-5.

115. Demicheli R, Retsky MW, Hrushesky WJ, Baum M. Tumor dormancy and surgery-driven interruption of dormancy in breast cancer: learning from failures. *Nat Clin Pract Oncol* 2007 Dec;4(12):699-710.

116. Aguirre-Ghiso JA. Models, mechanisms and clinical evidence for cancer dormancy. *Nat Rev Cancer*. 2007;7:834-46.

117. Wikman H, Vessella R, Pantel K. Cancer micrometastasis and tumour dormancy. *APMIS* 2008;116:754-70.

118. Pantel K, Schlimok G, Braun S, Kutter D, Lindemann F, Schaller G, Funke I, Izbicki JR, Riethmüller G. Differential expression of proliferation-associated molecules in individual micrometastatic carcinoma cells. *J Natl Cancer Inst*. 1993 Sep 1;85(17):1419-24.

119. Braun S, Kentenich C, Janni W, Hepp F, de Waal J, Willgeroth F, Sommer H, Pantel K. Lack of effect of adjuvant chemotherapy on the elimination of single dormant tumor cells in bone marrow of high-risk breast cancer patients. *J Clin Oncol*. 2000 Jan;18(1):80-6.

120. Muller V, Stahmann N, Riethdorf S, Rau T, Zabel T, Goetz A, Janicke F, Pantel K. Circulating tumor cells in breast cancer: correlation to bone marrow micrometastases, heterogeneous response to systemic therapy and low proliferative activity. *Clin Cancer Res* 2005;11:3678-85.

121. Gunther EJ, Moody SE, Belka GK, Hahn KT, Innocent N, Dugan KD, Cardiff RD, Chodosh LA. Impact of p53 loss on reversal and recurrence of conditional Wnt- induced tumorigenesis. *Genes Dev* 2003;17:488-501.

122. Boxer RB, Jang JW, Sintasath L, Chodosh LA. Lack of sustained regression of c-MYC-induced mammary adenocarcinomas following brief or prolonged MYC inactivation. Cancer Cell. 2004 Dec;6(6):577-86.

123. Hurley, J., et al., Docetaxel, cisplatin, and trastuzumab as primary systemic therapy for human epidermal growth factor receptor 2-positive locally advanced breast cancer. *J Clin Oncol* 2006; 24(12): 1831-8.

124. Sequist LV, Waltman BA, Dias-Santagata D. Genotypic and histological evolution of lung cancers acquiring resistance to EGFR inhibitors. Sci Transl Med. 2011 Mar 23;3(75):75ra26.

125. Feng Y, Pan TC, Pant DK, Chakrabarti KR, Alvarez JV, Ruth JR, Chodosh LA. SPSB1 Promotes Breast Cancer Recurrence by Potentiating c-MET Signaling. Cancer Discov. 2014 Jul;4(7):790-803.

126. Alvarez JV, Pan TC, Ruth J, Feng Y, Zhou A, Pant D, Grimley JS, Wandless TJ, Demichele A; I-SPY 1 TRIAL Investigators, Chodosh LA. Par-4 downregulation promotes breast cancer recurrence by preventing multinucleation following targeted therapy. Cancer Cell. 2013 Jul 8;24(1):30-44.

127. Moody SE, Sarkisian CJ, Hahn KT, et al. Conditional activation of Neu in the mammary epithelium of transgenic mice results in reversible pulmonary metastasis. Cancer Cell. 2002 Dec;2(6):451-61.

128. Rakhra K, Bachireddy P, Zabuawala T, Zeiser R, Xu L, Kopelman A, Fan AC, Yang Q, Braunstein L, Crosby E, Ryeom S, Felsher DW. CD4(+) T cells contribute to the remodeling of the microenvironment required for sustained tumor regression upon oncogene inactivation. *Cancer Cell*. 2010 Nov 16;18(5):485-98.

129. Folkman J, Ryeom S. Is oncogene addiction angiogenesis-dependent? *Cold Spring Harb Symp Quant Biol*. 2005;70:389-97.

130. Giuriato S, Ryeom S, Fan AC, Bachireddy P, Lynch RC, Rioth MJ, van Riggelen J, Kopelman AM, Passegué E, Tang F, Folkman J, Felsher DW. Sustained regression of tumors upon MYC inactivation requires p53 or thrombospondin-1 to reverse the angiogenic switch. *Proc Natl Acad Sci U S A*. 2006 Oct 31;103(44):16266-71.

131. Holmgren L, O'Reilly MS, Folkman J. Dormancy of micrometastases: balanced proliferation and apoptosis in the presence of angiogenesis suppression. *Nat Med*. 1995 Feb;1(2):149-53.

132. Arteel GE, Thurman RG, Yates JM, Raleigh JA. Evidence that hypoxia markers detect oxygen gradients in liver: pimonidazole and retrograde perfusion of rat liver. Br J Cancer. 1995 Oct;72(4):889-95.

133. Olive KP, Jacobetz MA, Davidson CJ, et al. Inhibition of Hedgehog signaling enhances delivery of chemotherapy in a mouse model of pancreatic cancer. *Science*. 2009 Jun 12;324(5933):1457-61.

134. Wilson TR, Fridlyand J, Yan Y, et al. Widespread potential for growth-factor-driven resistance to anticancer kinase inhibitors. Nature. 2012 Jul 26;487(7408):505-9.

135. Mayer C, Grummt I. Ribosome biogenesis and cell growth: mTOR coordinates transcription by all three classes of nuclear RNA polymerases. Oncogene. 2006 Oct 16;25(48):6384-91.

136. Wertheim GBW et al. The Snf1-related kinase, Hunk, is essential for mammary tumor metastasis. Proc Natl Acad Sci U S A. 2009;106(37):15855–60.

137. Ghajar CM, Peinado H, Mori H, Matei IR, Evason KJ, Brazier H, Almeida D, Koller A, Hajjar KA, Stainier DY, Chen EI, Lyden D, Bissell MJ. The perivascular niche regulates breast tumour dormancy. *Nat Cell Biol.* 2013 Jul;15(7):807-17.

138. Bragado P, Estrada Y, Parikh F, Krause S, Capobianco C, Farina HG, Schewe DM, Aguirre-Ghiso JA. TGF-β2 dictates disseminated tumour cell fate in target organs through TGF-β-RIII and p38α/β signalling. *Nat Cell Biol*. 2013 Nov;15(11):1351-61.

139. Kim RS, Avivar-Valderas A, Estrada Y, Bragado P, Sosa MS, Aguirre-Ghiso JA, Segall JE. Dormancy signatures and metastasis in estrogen receptor positive and negative breast cancer. PLoS One. 2012;7(4):e35569.

140. Mani SA, Guo W, Liao MJ, Eaton EN, Ayyanan A, Zhou AY, Brooks M, Reinhard F, Zhang CC, Shipitsin M, Campbell LL, Polyak K, Brisken C, Yang J, Weinberg RA. The

epithelial-mesenchymal transition generates cells with properties of stem cells. *Cell*. 2008 May 16;133(4):704-15

141. Dontu G, Abdallah WM, Foley JM, Jackson KW, Clarke MF, Kawamura MJ, Wicha MS. In vitro propagation and transcriptional profiling of human mammary stem/progenitor cells. *Genes Dev*. 2003 May 15;17(10):1253-70.

142. Maguer-Satta V, Chapellier M, Delay E, Bachelard-Cascales E. CD10: a tool to crack the role of stem cells in breast cancer. Proc Natl Acad Sci U S A. 2011 Dec 6;108(49):E1264

143. Liu S, Cong Y, Wang D, Sun Y, Deng L, Liu Y, Martin-Trevino R, Shang L, McDermott SP, Landis MD, Hong S, Adams A, D'Angelo R, Ginestier C, Charafe-Jauffret E, Clouthier SG, Birnbaum D, Wong ST, Zhan M, Chang JC, Wicha MS. Breast Cancer Stem Cells Transition between Epithelial and Mesenchymal States Reflective of their Normal Counterparts. Stem Cell Reports. 2013 Dec 27;2(1):78-91.

144. Shimono Y, Zabala M, Cho RW, Lobo N, Dalerba P, Qian D, Diehn M, Liu H, Panula SP, Chiao E, Dirbas FM, Somlo G, Pera RA, Lao K, Clarke MF. Downregulation of miRNA-200c links breast cancer stem cells with normal stem cells. Cell. 2009 Aug 7;138(3):592-603

145. Gupta PB, Onder TT, Jiang G, Tao K, Kuperwasser C, Weinberg RA, Lander ES. Identification of selective inhibitors of cancer stem cells by high-throughput screening. Cell. 2009 Aug 21;138(4):645-59.

146. Marcato P, Dean CA, Pan D, Araslanova R, Gillis M, Joshi M, Helyer L, Pan L, Leidal A, Gujar S, Giacomantonio CA, Lee PW. Aldehyde dehydrogenase activity of breast cancer stem cells is primarily due to isoform ALDH1A3 and its expression is predictive of metastasis. Stem Cells. 2011 Jan;29(1):32-45

147. Lapidot T, Sirard C, Vormoor J, Murdoch B, Hoang T, Caceres-Cortes J, Minden M, Paterson B, Caligiuri M, Dick J(1994) Nature 17:645–648.

148. Lin T, Meng L, Li Y, Tsai RY. Tumor-initiating function of nucleostemin-enriched mammary

tumor cells. Cancer Res. 2010 Nov 15;70(22):9444-52.

149. Cho RW, Wang X, Diehn M, Shedden K, Chen GY, Sherlock G, Gurney A, Lewicki J, Clarke MF. Isolation and molecular characterization of cancer stem cells in MMTV-Wnt-1 murine breast tumors. Stem Cells. 2008 Feb;26(2):364-71.

150. Sharma SV, Lee DY, Li B, et al. A chromatin-mediated reversible drug-tolerant state in cancer cell subpopulations. Cell. 2010 Apr 2;141(1):69-80.

151. DeNardo DG, Brennan DJ, Rexhepaj E, et al. Leukocyte complexity predicts breast cancer survival and functionally regulates response to chemotherapy. Cancer Discov. 2011 Jun;1(1):54-67.

152. Shabo I, Stål O, Olsson H, Doré S, Svanvik J. Breast cancer expression of CD163, a macrophage scavenger receptor, is related to early distant recurrence and reduced patient survival. Int J Cancer. 2008 Aug 15;123(4):780-6.

153. Medrek C, Pontén F, Jirström K, Leandersson K. The presence of tumor associated macrophages in tumor stroma as a prognostic marker for breast cancer patients. BMC Cancer. 2012 Jul 23;12:306.

154. Swierczak A, Cook AD, Lenzo JC, et al. The Promotion of Breast Cancer Metastasis Caused by Inhibition of CSF-1R/CSF-1 Signaling Is Blocked by Targeting the G-CSF Receptor. Cancer Immunol Res. 2014 Aug;2(8):765-76.

155. Mantovani A, Sozzani S, Locati M, Allavena P, Sica A. Macrophage polarization: tumor-associated macrophages as a paradigm for polarized M2 mononuclear phagocytes. Trends Immunol. 2002 Nov;23(11):549-55.

156. Beatty GL, Chiorean EG, Fishman MP, Saboury B, Teitelbaum UR, Sun W, Huhn RD, Song W, Li D, Sharp LL, Torigian DA, O'Dwyer PJ, Vonderheide RH. CD40 agonists alter tumor stroma and show efficacy against pancreatic carcinoma in mice and humans. Science. 2011 Mar 25;331(6024):1612-6.

157. Holmes MD, Chen WY, Li L, Hertzmark E, Spiegelman D, Hankinson SE. Aspirin intake and survival after breast cancer. J Clin Oncol. 2010 Mar 20;28(9):1467-72

158. Terry MB, Gammon MD, Zhang FF, et al. Association of frequency and duration of aspirin use and hormone receptor status with breast cancer risk. JAMA. 2004 May 26;291(20):2433-40.

159. DuBois RN. Aspirin and breast cancer prevention: the estrogen connection. JAMA. 2004 May 26;291(20):2488-9.

160. Ali B, Kaur S. Mammalian tissue acetylsalicylic acid esterase(s): identification, distribution and discrimination from other esterases. J Pharmacol Exp Ther. 1983 Aug;226(2):589-94.

161. Stairs DB, Bayne LJ, Rhoades B, Vega ME, Waldron TJ, Kalabis J, Klein-Szanto A, Lee JS, Katz JP, Diehl JA, Reynolds AB, Vonderheide RH, Rustgi AK. Deletion of p120-catenin results in a tumor microenvironment with inflammation and cancer that establishes it as a tumor suppressor gene. Cancer Cell. 2011 Apr 12;19(4):470-83.

162. van Rooijen N, van Nieuwmegen R. Elimination of phagocytic cells in the spleen after intravenous injection of liposome-encapsulated dichloromethylene diphosphonate. An enzyme-histochemical study. Cell Tissue Res. 1984;238(2):355-8.

163. Burnett SH, Kershen EJ, Zhang J, Zeng L, Straley SC, Kaplan AM, Cohen DA. Conditional macrophage ablation in transgenic mice expressing a Fas-based suicide gene. J Leukoc Biol. 2004 Apr;75(4):612-23.

164. MacDonald KP, Palmer JS, Cronau S, Seppanen E, Olver S, Raffelt NC, Kuns R, Pettit AR, Clouston A, Wainwright B, Branstetter D, Smith J, Paxton RJ, Cerretti DP, Bonham L, Hill GR, Hume DA. An antibody against the colony-stimulating factor 1 receptor depletes the resident subset of monocytes and tissue- and tumor-associated macrophages but does not inhibit inflammation. Blood. 2010 Nov 11;116(19):3955-63.

165. Zitvogel L, Apetoh L, Ghiringhelli F, Kroemer G. Immunological aspects of cancer chemotherapy. Nat Rev Immunol. 2008 Jan;8(1):59-73.

166. Weiskopf K, Ring AM, Ho CC, Volkmer JP, Levin AM, Volkmer AK, Ozkan E, Fernhoff NB, van de Rijn M, Weissman IL, Garcia KC. Engineered SIRPα variants as

immunotherapeutic adjuvants to anticancer antibodies. Science. 2013 Jul 5;341(6141):88-91.